



SEISMIC DESIGN OF MONOLITHIC BRIDGE ABUTMENTS

Prepared under:
NATIONAL SCIENCE FOUNDATION
GRANT ECE-8316976

Prepared by:
THE EARTH TECHNOLOGY CORPORATION
LONG BEACH, CALIFORNIA

REPRODUCED BY
NATIONAL TECHNICAL
INFORMATION SERVICE
U.S. DEPARTMENT OF COMMERCE
SPRINGFIELD, VA. 22161

JULY, 1986

REPORT DOCUMENTATION PAGE		1. REPORT NO. NSF/ENG-86062	2.	3. Recipient's Accession No. PB88 235643/AS													
4. Title and Subtitle Seismic Design of Monolithic Bridge Abutments				5. Report Date July 1986													
7. Author(s) G.R. Martin; C.B. Crouse; G. Liang; B. Hushmand; J. Wood				6.													
9. Performing Organization Name and Address The Earth Technology Corporation 3777 Long Beach Boulevard Long Beach, CA 90807				8. Performing Organization Rept. No.													
12. Sponsoring Organization Name and Address Directorate for Engineering (ENG) National Science Foundation 1800 G Street, N.W. Washington, DC 20550				10. Project/Task/Work Unit No.													
				11. Contract(C) or Grant(G) No. (C) (G) ECE8316976													
15. Supplementary Notes				13. Type of Report & Period Covered													
				14.													
16. Abstract (Limit: 200 words) The objective of the research was to investigate the soil-structure interaction characteristics between monolithic bridge abutments and the surrounding soil. The investigation consisted of: (1) vibration tests on the Horsethief Bridge, a single span structure with monolithic abutments, located near Corona, California, and (2) static and dynamic tests on a 1/100 scale model of this bridge in the centrifuge at the California Institute of Technology. The test results, which revealed significant soil-structure interaction, were predicted reasonably well by finite element models of both bridge-soil systems. Further research would be helpful to: (1) complete the understanding of the behavior of monolithic abutments during lateral seismic loading, and (2) translate the results into a design guide suitable for direct use by the bridge engineer.																	
17. Document Analysis a. Descriptors <table border="0" style="width: 100%;"> <tr> <td>Bridge abutments</td> <td>Dynamic tests</td> <td>Design</td> </tr> <tr> <td>Highway bridges</td> <td>Dynamic loads</td> <td>Earthquakes</td> </tr> <tr> <td>Bridges (structures)</td> <td>Static tests</td> <td>Vibration</td> </tr> <tr> <td>Earthquake resistant structures</td> <td>Model tests</td> <td>Models</td> </tr> </table> b. Identifiers/Open-Ended Terms Earthquake engineering c. COSATI Field/Group						Bridge abutments	Dynamic tests	Design	Highway bridges	Dynamic loads	Earthquakes	Bridges (structures)	Static tests	Vibration	Earthquake resistant structures	Model tests	Models
Bridge abutments	Dynamic tests	Design															
Highway bridges	Dynamic loads	Earthquakes															
Bridges (structures)	Static tests	Vibration															
Earthquake resistant structures	Model tests	Models															
18. Availability Statement NTIS			19. Security Class (This Report)		21. No. of Pages 127												
			20. Security Class (This Page)		22. Price												

DYNAMIC RESPONSE OF BRIDGE - ABUTMENT - BACKFILL SYSTEMS

Any opinions, findings, conclusions
or recommendations expressed in this
publication are those of the author(s)
and do not necessarily reflect the views
of the National Science Foundation.

C. B. Crouse
Senior Engineer
Earth Technology

B. Hushmand
Staff Engineer
Earth Technology

G. Liang
Senior Engineer
Earth Technology

G. Martin
Vice President of Engineering
Earth Technology

J. Wood
Laboratory Services Engineer
Ministry of Works & Development, New Zealand

INTRODUCTION

The numerous case histories of damage or failure to bridges induced by abutment failure or displacement during earthquakes (1,2,3) have clearly demonstrated the need for careful attention to abutment design and detailing in seismic areas. In addition, the interaction between the bridge and the abutment-backfill soils can have a significant influence on the dynamic characteristics of the entire system. For example, previous analytical studies (4,5,6,7,8) have shown the potential for monolithic abutments to contribute significantly to the stiffness and damping of the overall bridge system in the longitudinal mode of vibration, and affect the distribution of load to structural elements on the bridge. Thus, proper characterization of the stiffness, damping and the allowable passive resistance of the abutment-backfill system and the foundation soils will lead to more realistic estimates of the dynamic response of the bridge during seismic loading, and hence, lead to a better design.

As a result of a 1979 Applied Technology Council Workshop, which was sponsored by the U.S. National Science Foundation (NSF), a NSF research program was initiated by Earth Technology to investigate the dynamic interaction of bridge-abutment-backfill systems. The program consists of:

- (1) vibration testing of a single-span bridge with a monolithic abutment,
- (2) static, cyclic and dynamic testing of a model bridge in a centrifuge,
- (3) analytical modeling studies based on the experimental data, and
- (4) developing recommendations for analysis and design procedures.

The experimental testing and data reduction has been completed and some preliminary results have been obtained. This paper presents the details of the testing program and some of the observations from both sets of experiments.

EXPERIMENTAL TEST PROGRAM

Field Tests. Ambient, quick-release, and forced vibration tests were conducted on the Horsethief Rd. Undercrossing bridge, located on Interstate

Highway 15 approximately 15 miles south of Corona, California. These tests were conducted mainly by personnel from Earth Technology and ANCO engineers, although Professor G. Pardoen of the University of California at Irvine conducted some limited ambient surveys at the beginning of the program. The bridge (Figure 1) is a single span, monolithic, prestressed-concrete, box-girder bridge. Vertical support is provided by a rectangular concrete footing beneath each abutment. The footing is not structurally tied to the abutment wall; rather a thin neoprene strip separates the bottom of the abutment from the top of the footing. This sliding-bearing design is typical of monolithic abutments on California bridges. The shear key on top of the footing (Figure 1) in back of the abutment is designed to resist lateral movements of the abutment. The footings rest on sandy soil with some coarse gravel content. The average shear-wave velocity, V_s , of the upper ten feet of soil beneath the footings was about 850 fps⁽⁹⁾. The backfill soil consisted of similar material except the average V_s was about 700 fps.

During the testing, the response of the bridge was measured with 30 accelerometers (Endevco Model 5241) placed at various locations on the bridge deck, abutment walls and footings. In addition, two displacement transducers (Schaevitz Model 250 HCD) were placed near the bottom of one abutment wall to measure the relative displacement between the abutment and footing resulting from any sliding or deformation of the neoprene bearing strip.

Ambient vibration tests were conducted at the beginning, middle and end of the field testing program. Three types of recording techniques were used: (1) an 8-channel, Kinometrics, ranger seismometer system, which was installed by University of California at Irvine personnel prior to the forced vibration tests, (2) the 32-channel (30 accelerometers, 2 displacement gauges) system, which recorded time-history response data of 41 sec and 82 sec durations, and (3) a 2-channel spectrum analyzer, which obtained the frequency response of time-history samples recorded on various channels of the 32-channel array. Only the results of (3) have been analyzed to date, and they are reported in the next section.

The quick-release tests were conducted in the middle stages of the test program and consisted of applying a 10 kip tension force to a steel cable attached to two reaction frames, one attached to the bridge deck and the other attached to the concrete approach slab. The cable was aligned parallel to the traffic flow near the centerline of the bridge. The quick release of the cable tension set the bridge into free vibration. The results of these tests are currently being analyzed.

Most of the experimental testing consisted of forced vibration tests using a large eccentric mass shaker. The shaker was bolted to the top of the bridge deck midway between the two abutments at point approximately 15 ft from the longitudinal centerline of the bridge. The two counter rotating weights of the shaker were adjusted to apply unidirectional harmonic shaking in the longitudinal and transverse directions. Because of the slight skew of each abutment, these shaking directions were not quite parallel and perpendicular to the centerline of the bridge deck. The excitation frequencies ranged between 5 and 15 Hz and the applied loads varied between 2 and 100 kips, or approximately 0.1 to 5 percent of the weight of the bridge. During any one test, the loads varied by an order of magnitude from the smallest to largest

frequencies. Although this was a large variation, the loads were still small and did not appear to induce any significant non-linear response.

Centrifuge Tests. Centrifuge modeling is a useful approach to the solution of complex geotechnical problems, such as static and dynamic soil-structure interaction of bridge abutments and foundations. Most soil properties strongly depend upon the confining pressure, which is largely gravity induced. Thus, in soils, for the model and prototype to behave similarly, the confining stress must be identical in both systems at homologous points. Under the increased gravity field in a centrifuge, it is possible to test small scale models of soil-structure systems and achieve similarity with the full scale prototypes. If a model, N times smaller than its prototype and constructed from the same material as the prototype, is placed in a centrifuge-acceleration field that is N times normal terrestrial gravity, then the strains and stresses at homologous points of the model and prototype will be the same. A detailed discussion of static and dynamic centrifuge modeling techniques and scaling relationships can be found elsewhere (11, 12).

Centrifuge model tests were performed at California Institute of Technology (Caltech) by the Earth Technology personnel under supervision of Professor Ronald F. Scott. Earthquake simulated shaking, quick-release, forced-vibration and quasi-static cyclic push-pull tests were conducted on a 1/100 scale model of a bridge similar to the Horsethief Rd. Undercrossing bridge (Figure 2). Experiments were performed at three different scaling ratios of 50g, 87g, and 100g. These tests provided a broad range of information on behavior of different sizes of prototype bridge-abutment-foundation soil systems. Some of these data will be compared to the results of field tests on the Horsethief Bridge. The model bridge was constructed of aluminum; its moment of inertia and flexural stiffness values were scaled properly to simulate the Horsethief bridge. The model bridge was placed in a rectangular soil container 22"x 7"x 10" with a front glass wall at the end of the centrifuge arm (Figure 3). The type of soil used was Nevada 120 silica sand (Nevada Fine Sand-NFS). This sand in its well compacted condition (medium dense to dense) has a behavior comparable to the prototype frictionless soil material at the Horsethief bridge abutment and foundation. Shear-wave velocities (V_s) in the range of 690 ft/sec to 810 ft/sec for NFS in its dense condition (dry unit weight of 105 pcf) at a confining pressure of 8.0 psi to 12.0 psi were measured by the resonant column technique (13). The above confining pressure range represents a soil depth around 10 feet.

The response of the bridge model during the testing was measured with 6 strain gages (Micromeasurements, Model CEA-13-062UW-350), 6 miniature pressure transducers (Entran Devices, Inc., Model EPB6-125U-50A), 2 to 4 miniature accelerometers (Entran Devices, Inc., Model EGA-125F-500D), and one photo diode displacement transducer (United Detector Technology, Inc. Model PIN-SC110D). The locations of the transducers are shown in Figures 2 and 3. On each abutment wall and at the center of the bridge deck, two strain gages were mounted to measure the flexural deformation of the abutments and the deck. Pressure transducers were mounted along the height at the center of the abutments. Accelerometers were located on the bucket floor, on the road way under the bridge, and at different locations on the bridge. One displacement transducer was mounted at the center of bridge deck to measure horizontal movement of the bridge.

Earthquake simulated shaking of the soil container and the model bridge was done by the continuous earthquake generating mechanism developed at Caltech. This is an electro-hydraulic system capable of generating any desired type of random shaking of the bucket in the frequency range of real earthquake produced vibrations. A micro-computer, MTS controller, and servo-valve control the shaking process by sending the earthquake simulated signal from the computer to the MTS controller and then to the servo-valve which controls the flow of highly pressurized oil to the piston under the bucket.

Quick-release (snap) tests were conducted by applying a tension force to a copper cable attached to two reaction frames, one attached to the model deck at its center and the other attached to the stationary frame which holds the soil container. The cable was aligned parallel to the centerline of the model and was attached to a block mounted to the bridge deck. The applied tension was measured by a load cell. The quick cutting of the cable by a sharp knife released the cable tension and set the bridge model into free vibration.

Steady-state forced vibration tests were performed using a miniature air-driven eccentric mass shaker designed and constructed at Caltech (13). The shaker was mounted on the bridge model deck at its center and its eccentric masses were oriented such that it applied harmonic forces in the longitudinal direction parallel to the model deck. The excitation frequency varied between 2 and 12 Hz at prototype scale.

Cyclic push-pull tests of the model bridge against the abutment-backfill soil was performed by applying a horizontal force parallel to the centerline of the bridge deck. The soil container was moved relative to the frame which resulted in a push-pull force on the model through a rigid rod, which was attached at one end to the bridge deck and at the other end to the stationary frame at the end of centrifuge arm holding the soil container. The applied force was measured by a load cell.

PRELIMINARY RESULTS

Field Tests. The amplitude data obtained from each accelerometer during the forced vibration tests were converted to displacements by dividing by ω^2 . The displacements were in turn normalized by the applied shaker force. These normalized displacements and their associated phase angles, which were computed with respect to the maximum positive shaker force, were plotted as a function of frequency for each vibration test. The natural frequencies of the bridge system were identified from these plots. The amplitude data from the spectrum analyzer, which was used in the third ambient survey, also gave an indication of the natural frequencies. The natural frequencies identified from both tests are listed below.

Test	Natural Frequencies - Hz										
Ambient (0-25 Hz)	3.2	4.7	5.7(?)	6.7	7.5(?)	-	9.7	11.2	15.5	20.7	24.2
Force Vib. (2-14 Hz)	3.2(?)	4.7	-	6.2	-	8.2	-	10.6	14+	-	-

The frequencies with a question mark(?) may not be natural frequencies because peaks or 90° phase angles at these frequencies were not consistently observed in the response data. On the other hand, they may be natural frequencies corresponding to heavily damped modes involving considerable interaction with the backfill and foundation soils. The natural frequencies without the question mark are frequencies associated with considerable vertical vibration of the deck. With the exception of the one at 8.2 Hz, these modes are lightly damped (i.e. $\zeta < 10\%$). The mode at 8.2 Hz is moderately damped (i.e. $\zeta = 15\%$) and appears to be associated with significant soil-structure interaction in the transverse direction.

The normalized displacement amplitudes from the forced vibration tests at the natural frequencies of 4.7, 6.2, 8.2, 10.6 and 14+ Hz were plotted at the corresponding accelerometer locations on the bridge. These plots provided some indication of the mode shapes at these frequencies. A preliminary interpretation of the mode shapes are shown in Figure 4. The modes at 4.7, 6.2 and 10.6 Hz correspond to classical modes of vibration for a rectangular, isotropic plate (10), which is either simply supported or clamped at the two opposite sides along the width of the plate. The mode at 14+ Hz may also correspond to a classical plate mode as suggested in Figure 4, but further analysis will be required to verify this. The mode at 8.2 Hz is similar to the one at 6.2 Hz except the deck motion is smaller and its direction reversed. These characteristics together with the relatively large transverse motion of the footing at 8.2 Hz further support the earlier conclusion that this mode is predominately one of soil-structure interaction.

Because the deck displacements comprising the mode shapes in Figure 4 represent classical vibrational modes of a plate, a comparison was made between: (1) the experimental mode shapes and the frequencies at which they occur, and (2) the corresponding natural frequencies and mode shapes of a rectangular isotropic plate with the same length/width ratio as the bridge. The first natural frequency observed during the vibration tests (4.7 Hz) was assumed to be the fundamental natural frequency of the plate in vertical vibration. The higher natural frequencies were scaled from the results in Reference (10) for the two types of support conditions (simple and clamped) along the width of the plate. The theoretical results are shown in Figure 5. The first three natural frequencies (4.7, 6.5 and 13.0 Hz) and mode shapes for the clamped support condition correspond reasonably well to the experimental results at 4.7, 6.2, and 14+ Hz shown in Figure 4. The saddle-shaped experimental mode at 10.6 Hz is influenced significantly by soil-structure interaction in the vertical direction, and this interaction may have been partly responsible for lowering the frequency from the theoretical value of 15.0 Hz to 10.6 Hz.

In addition to the deformations observed for the deck, acceleration measurements made on the abutment wall and footing during the vibration test revealed some deformation of the wall. However, the LVDT measurements generally indicated little or no relative movement between the bottom of the abutment and top of footing. Deformation of the wall may have a significant effect on the effective stiffness characteristics of the abutment-soil interaction phenomenon. Subsequent analytical studies, using finite element models, will investigate the importance of the abutment-wall flexibility.

Centrifuge Tests. The transducer signals generated during each test were passed through a high speed, 16 channel, analog-to-digital converter (ADC). The digital signals were accessed by a microcomputer and transmitted to a main-frame computer for subsequent analyses.

Fourier transforms and amplitude spectra were computed from the transient data recorded during the quick-release and earthquake simulated shaking tests. Figure 6 presents a selected number of Fourier Amplitude Spectra (FAS) for two different quick-release tests at centrifugal accelerations of 50 g and 100 g. The FAS plots are for the translational acceleration and flexural strain of the bridge deck and the pressure and flexural strain near the center of the right abutment wall. Comparison of the FAS for each test illustrates an obvious similarity and consistency in the number and relative location of each resonant peak. The peaks occur at different frequencies in the 50 g and 100 g tests, because each test simulates a different prototype condition. The 50 g tests simulate a smaller bridge with a higher rigidity and lower mass, which results in higher frequencies compared to those from the 100 g tests. Generally, the ratio between the natural frequencies in the 50 g and 100 g tests is 2:1. The lightly damped fundamental mode observed at 10 Hz (50 g) and 5 Hz (100 g) involves considerable flexure of the bridge deck. This mode probably corresponds to the 4.7 Hz fundamental mode obtained from the field tests (recall that the model at 100 g was intended to simulate the Horsethief bridge). The higher damped resonant peaks at 12.5 Hz (50 g) and 7 Hz (100 g) probably represent the primary translational soil-structure interaction mode. This mode is observed in the FAS plots for the deck acceleration and for the pressure and strain in the wall; it is not observed in the FAS for the deck strain. However, based on the similarity in frequencies between the 100 g test (7 Hz) and the field test (6.2 Hz), this mode may be, instead, associated with a saddle-shaped deck response, which would also exhibit little or no flexural strain in the center of the deck. Unfortunately, the transducer data by themselves may not be adequate to resolve this and other modes without the aid to analytical modeling studies, which will be conducted in the near future.

The data derived from earthquake simulated shaking tests provide valuable information on the behavior of bridge during a moderate to severe ground shaking. Accelerograms recorded on the soil bucket and the bridge deck during the 87 g test are shown in Figure 7. Note that the bucket acceleration contains the salient features of actual ground-motion accelerograms, i.e., an initial high frequency part simulating the P-wave arrival, followed by a large amplitude lower frequency part simulating the S-wave arrival, and finally a longer period tail. Maximum input acceleration of the bucket was equal to 0.11 g which was amplified to 0.22 g on the bridge deck.

Figure 8 illustrates the force-displacement response of the bridge during cyclic loading in the longitudinal direction. Five consecutive loading cycles are plotted in the figure. Note that a large permanent deformation occurs at the end of the first cycle while in the next four cycles practically no permanent deformation happens. The backfill soil appears to have densified gradually under the applied cyclic force and the hysteretic energy loss decreased considerably. The stiffness of the backfill soil increases slightly from cycle 1 to 5. As expected, the slope of the force-displacement curve, in pushing, is higher than in pulling. It should be noted that this destructive

loading on the specimen was applied after many non-destructive lower amplitude load cycles. Stiffness and damping characteristics of abutment wall - backfill soil system will be derived from the results of these tests.

FUTURE RESEARCH

Although the comparisons between the results of the field experiment and simple plate vibration theory offered useful insights, more analyses, using finite element models and systems-identification techniques, will be conducted to better understand the dynamic characteristics of the bridge-abutment-soil system during the vibration tests. Once this understanding is gained, more reliable models for studying the seismic response will be established. Parametric studies will then be conducted to determine the key system parameters affecting the seismic response.

A preliminary study of all the time history records and FAS collected during the centrifuge tests also suggested a great need for detailed investigations of different features of the results by incorporating a finite element modeling of the centrifuge tests. This will help to identify the observed resonant frequencies and modes of vibration. In addition, further data processing, such as the derivation of phase spectra, will be helpful in the discrimination of resonant peaks. Some containment effects of the soil bucket were observed in the form of resonant frequencies of the whole soil-bridge-bucket system. This effect will be isolated in the results by determining exact values of these resonant frequencies using FAS and results derived from finite element modeling. The quasi-static cyclic tests will also be modeled by the finite element technique using non-linear constitutive soil models. This will illustrate the usefulness of finite element modeling in deriving stiffness and damping characteristics of the abutment-backfill soil.

REFERENCES

1. Fung, G. G., LeBeau, R. J., Klein, E.D., Belvedere, J., and Goldsmith, A. F., 1971. "Field Investigation of Bridge Damages in the San Fernando Earthquake," Preliminary Report, State of California Business and Transportation Agency, Department of Public Works, Division of Highways, Bridge Department.
2. Gates, J. H., 1979, "Factors Considered in the Development of the California Seismic Design Criteria for Bridges," Applied Technology Council Workshop of the Research Needs of Seismic Problems Related to Bridges, January.
3. Elms, D. G., and Martin, G. R., 1979. "Factors Involved in the Seismic Design of Bridge Abutments," Applied Technology Council Workshop of the Research Needs of Seismic Problems Related to Bridges, January.
4. Chen, M. C., and Penzien, J., 1979. "Soil-Structure Interaction of Short Highway Bridges," Applied Technology Council Workshop of the Research Needs of Seismic Problems Related to Bridges, January.
5. Chen, M. C., and Penzien, J., 1975. "Analytical Investigation of Seismic Response of Short, Single or Multiple Span Highway Bridges," EERC 75-4, Earthquake Engineering Research Center, University of California, Berkeley.
6. Chen, M. C., and Penzien, J., 1977. "Nonlinear Soil-Structure Interaction of Skew Highway Bridges," EERC-77/24, Earthquake Engineering Research Center, University of California, Berkeley.
7. Tseng, W. C., and Penzien, J., 1973. "Analytical Investigation of the Seismic Response of Long Multiple Span Highway Bridges," EERC-73/12, Earthquake Engineering Research Center, University of California, Berkeley.
8. Richards, R., Jr., and Elms, D., 1977. "Seismic Behavior of Retaining Walls and Bridge Abutments," Civil Engineering Research Report No. 77-10, Dept. of C.E., University of Canterbury, Christchurch, New Zealand, June.
9. Nazarian, S., and Stokoe, K. H., 1984, "In-Situ Wave Velocities by Surface Wave Method, Horse-Thief Overpass, Interstate 15, California," Report prepared for Earth Technology, December.
10. Blevins, R. D., 1979, Formula for Natural Frequency and Mode Shape, Van Nostrand Reinhold Company.
11. Scott, R. F., 1975, "The Centrifuge Technique in Geotechnology, Selected Papers," Soil Mechanics Laboratory, California Institute of Technology, November.

12. Schofield, A. N., 1981, "Dynamic and Earthquake Geotechnical Centrifuge Modeling," Proc. Int. Conf. Recent Advances in Geotech Eng. and Soil Dynamics, St. Louis, Missouri, p. 1-18.
13. Hushmand, B., 1983, "Experimental Studies of Dynamic Response of Foundations," Report SML 83-02, Soil Mechanics Laboratory, California Institute of Technology, November.

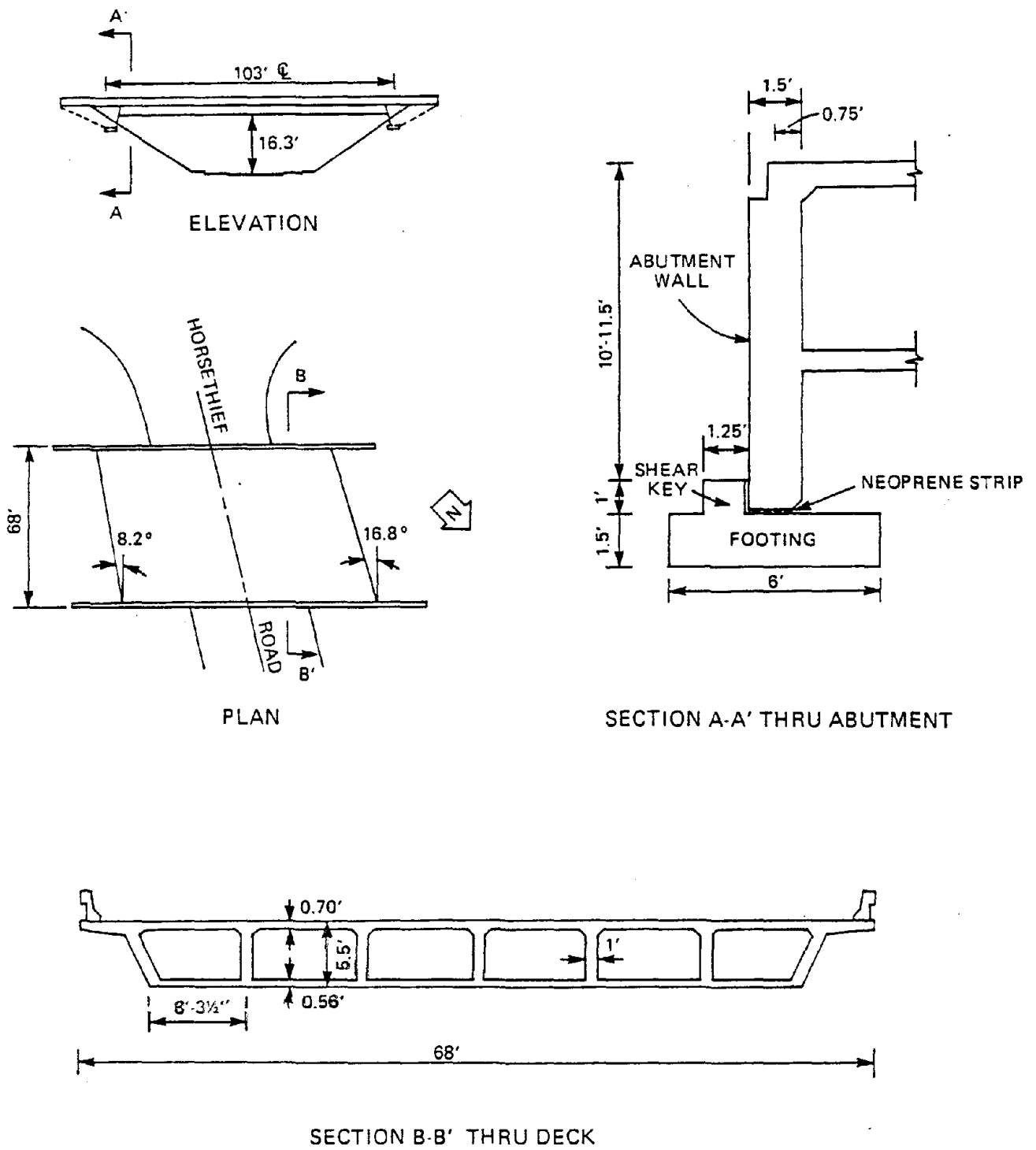


FIGURE 1 HORSETHIEF ROAD UNDERCROSSING BRIDGE

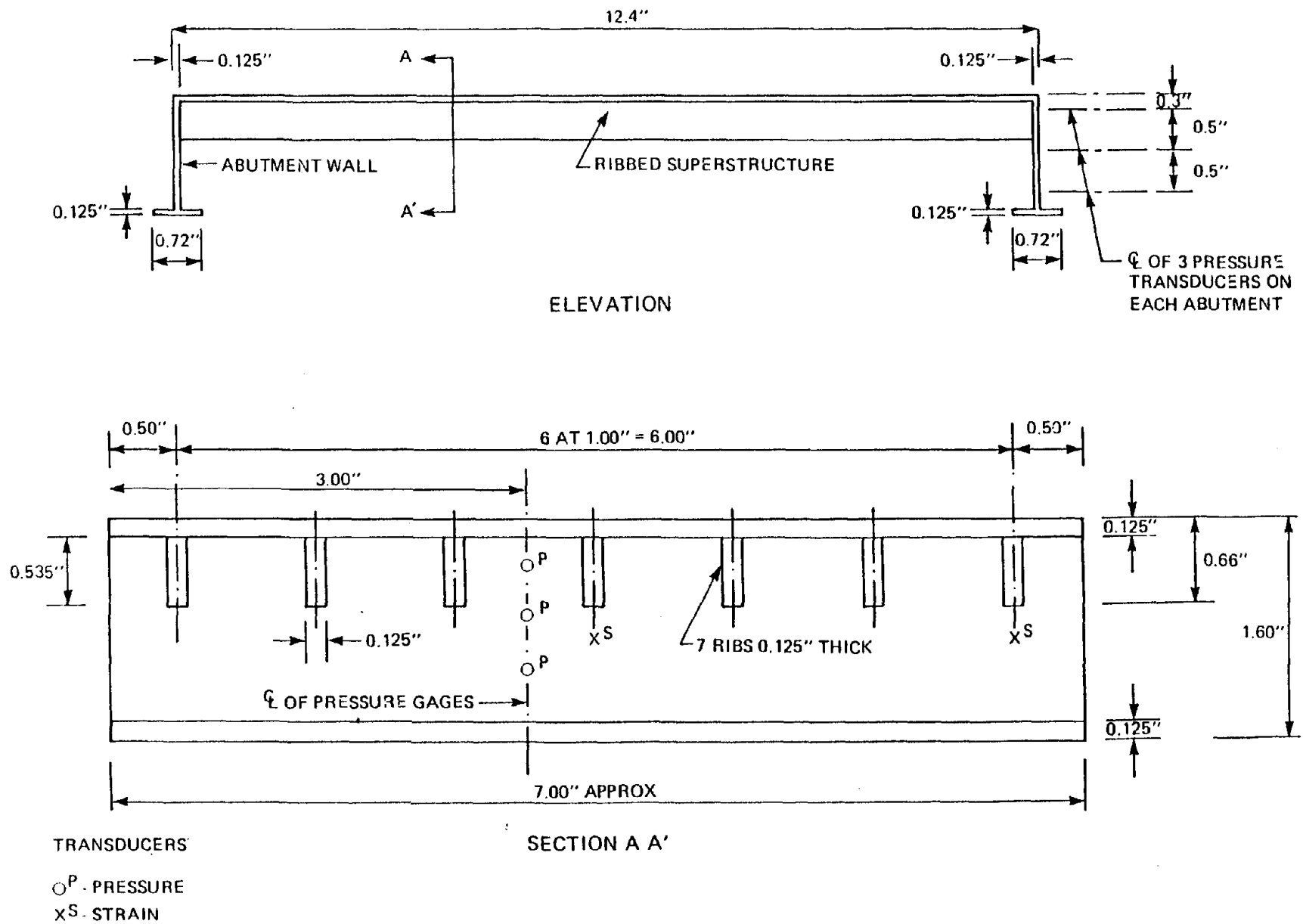
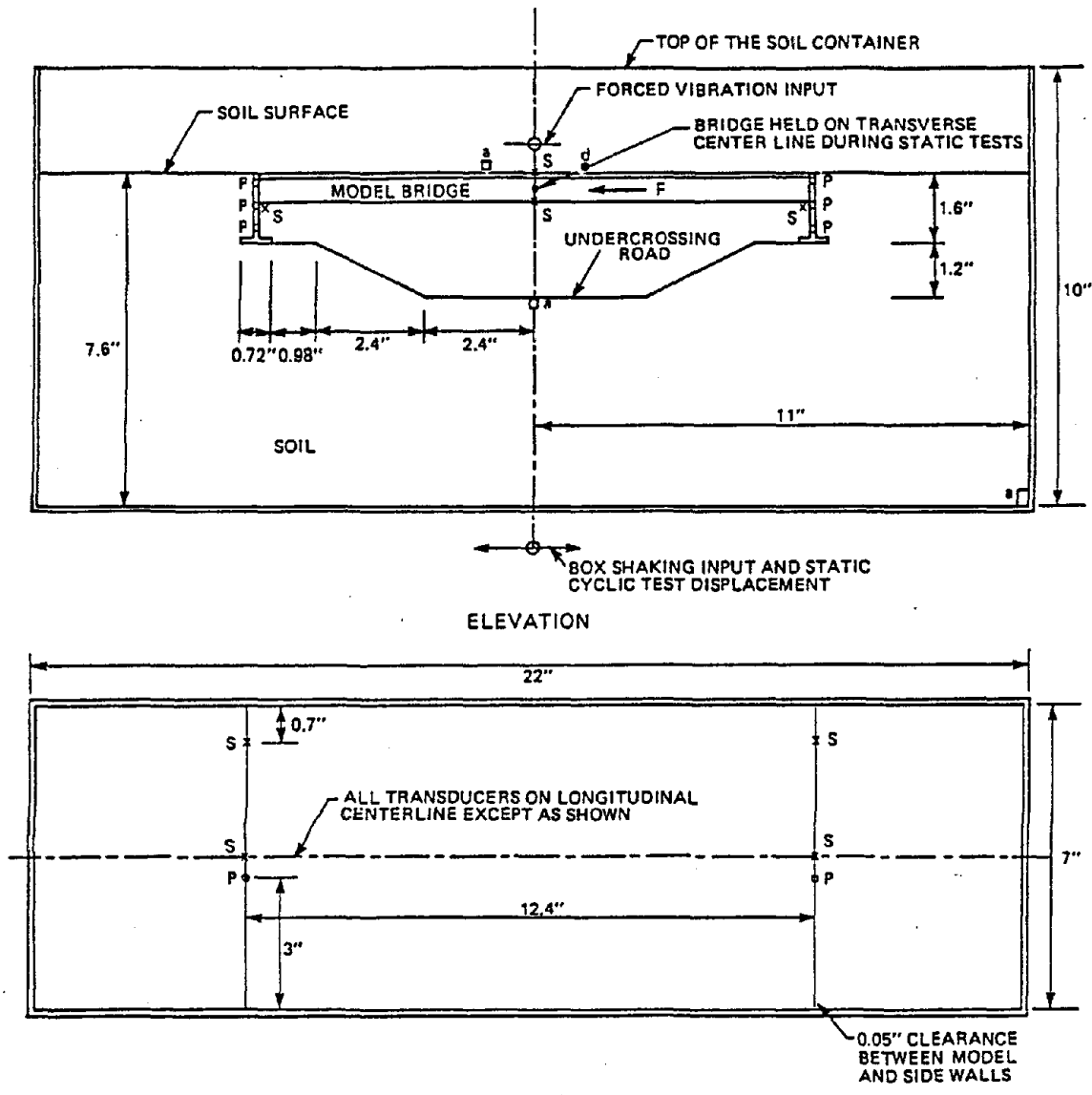


FIGURE 2. HORSETHIEF ROAD BRIDGE MODEL FOR CENTRIFUGE TESTS



- TRANSDUCERS**
- a □ - ACCELERATION
 - d ● - DISPLACEMENT
 - p ○ - PRESSURE
 - s x - STRAIN
 - F - FORCE

FIGURE 3 BRIDGE MODEL, SOIL CONTAINER, AND TRANSDUCER DIAGRAM FOR CENTRIFUGE TESTS

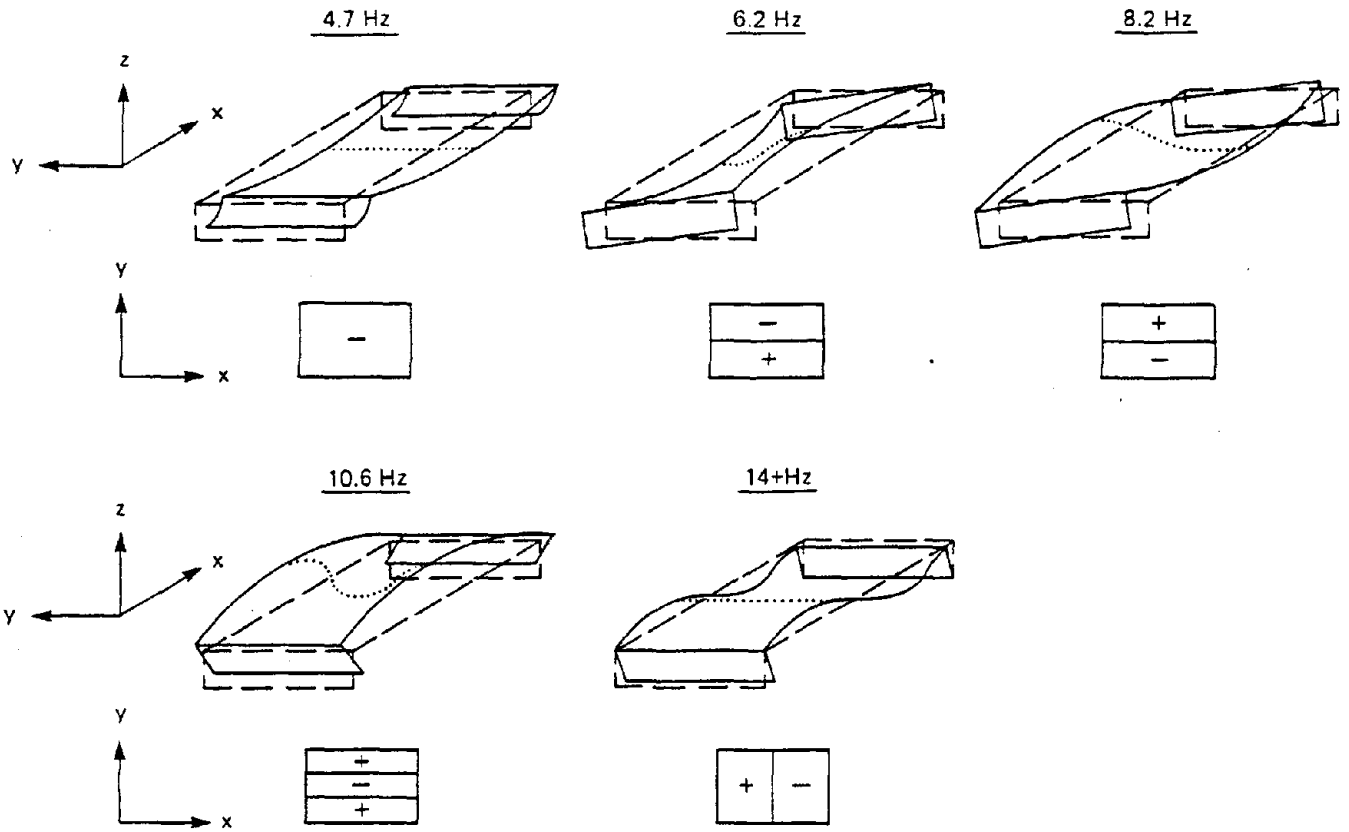
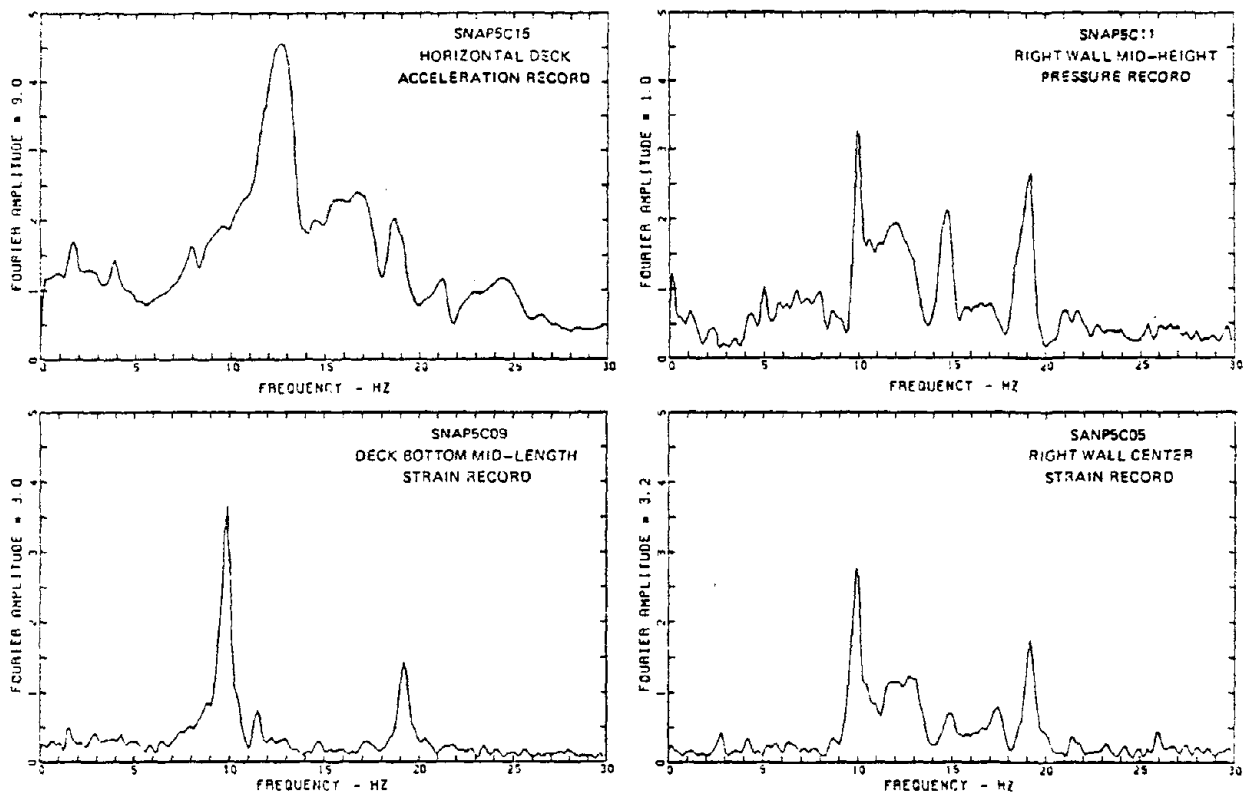


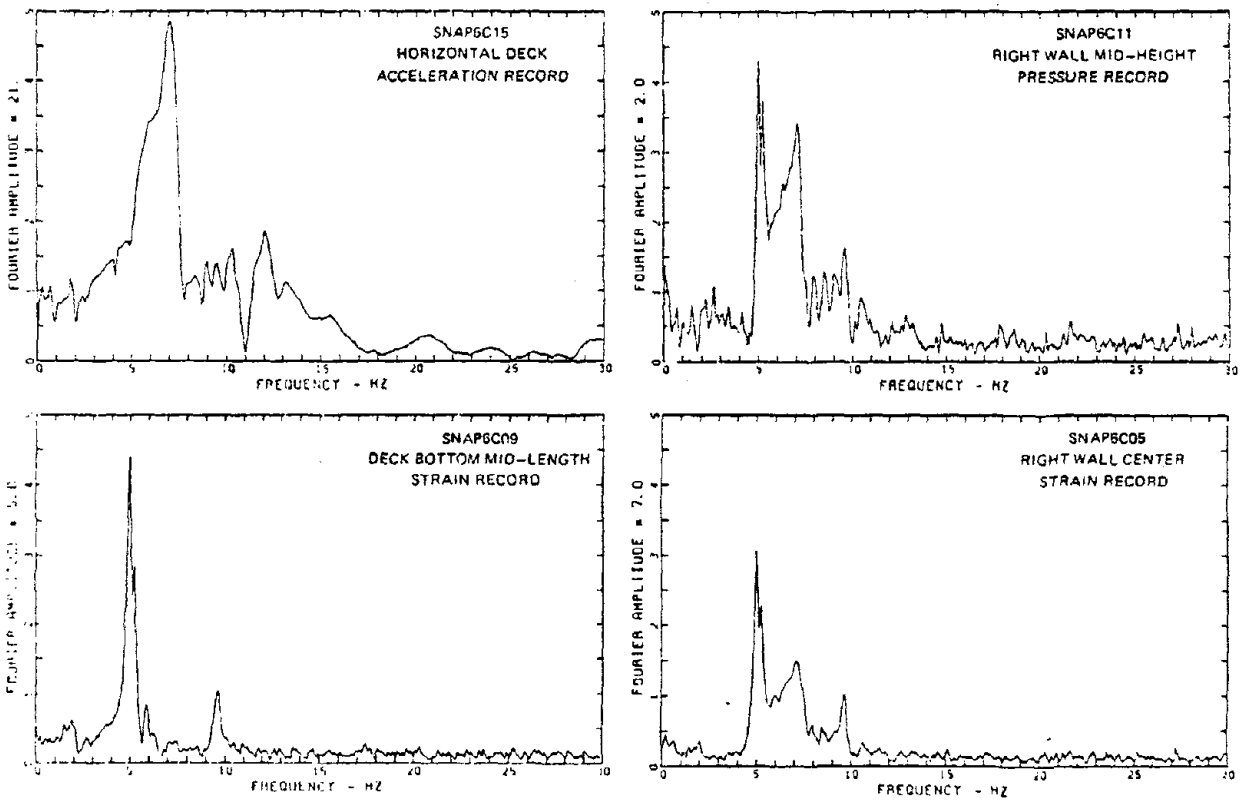
FIGURE 4. EXPERIMENTAL NATURAL FREQUENCIES AND APPARENT MODE SHAPES

		NATURAL FREQUENCY - Hz							
SUPPORT CONDITION		<u>4.7</u>	<u>10.6</u>	<u>19.0</u>	<u>26.9</u>	<u>32.3</u>	<u>43.1</u>		
S	F								
		<u>4.7</u>	<u>6.5</u>	<u>13.0</u>	<u>15.0</u>	<u>15.7</u>	<u>25</u>		
		C	F						
				<u>4.7</u>	<u>6.5</u>	<u>13.0</u>	<u>15.0</u>	<u>15.7</u>	<u>25</u>

FIGURE 5 VIBRATIONAL MODES OF A RECTANGULAR PLATE



(a) 50 g



(b) 100 g

FIGURE 6 FOURIER SPECTRUM OF ACCELERATION, PRESSURE, AND STRAIN SIGNALS IN 50g AND 100g (CENTRIFUGAL ACCELERATION) TESTS (PROTOTYPE SCALE)

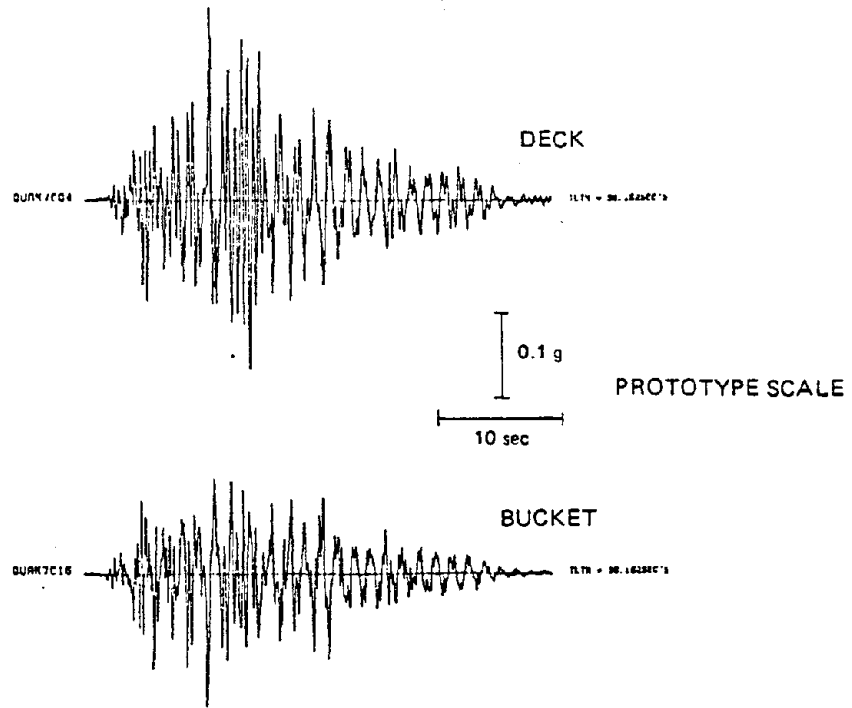


FIGURE 7 ACCELEROGRAMS RECORDED DURING EARTHQUAKE SIMULATED SHAKING TEST
(CENTRIFUGAL ACCELERATION = 87g)

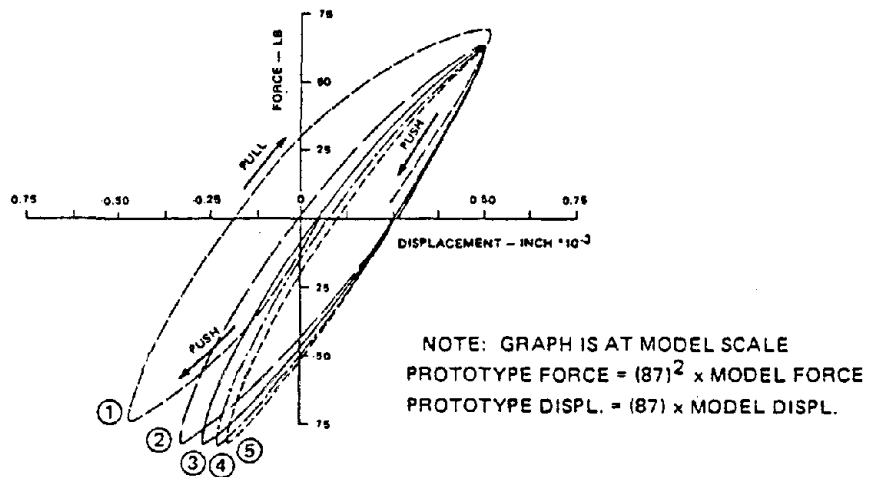


FIGURE 8 FORCE-DISPLACEMENT CURVES FROM QUASI-STATIC CYCLIC PUSH-PULL TEST
(CENTRIFUGAL ACCELERATION = 87g)

DYNAMIC SOIL-STRUCTURE INTERACTION OF A
SINGLE SPAN BRIDGE

C. B. CROUSE, B. HUSHMAND AND G. R. MARTIN

EARTH TECHNOLOGY CORPORATION
3777 LONG BEACH BLVD., LONG BEACH, CALIFORNIA, U.S.A.

SUMMARY

Experimental and analytical studies were conducted to determine dynamic soil-structure interaction characteristics of a single-span, prestressed-concrete bridge with monolithic abutments supported by spread footings. The experimental program, consisting of harmonic forced-vibration excitation of the bridge in the transverse and longitudinal directions, revealed the presence of four modes in the frequency band, 0 to 11 Hz, and the onset of a fifth mode at 14 Hz, the highest frequency attained during the tests. The fundamental mode at 4.7 Hz was the primary longitudinal bending mode of the deck and had a relatively low damping ratio, (ζ_1), that was approximately 0.025 of critical. The second and third modes at 6.4 Hz and 8.2 Hz were the primary twisting modes of the deck which involved substantial transverse rocking, transverse translation and torsion of the footings. As expected, the damping ratios associated with these two modes, $\zeta_2 = 0.035$ and $\zeta_3 = 0.15$, were directly related to the relative amounts of deck and footing motion. The fourth mode at 10.6 Hz was the second twisting mode of the deck and involved relatively little motion of the footings and abutment walls, which was consistent with the low damping, $\zeta_4 = 0.02$, observed in this mode. The response data at 14 Hz suggested that the fifth mode beyond

this frequency was the second longitudinal bending mode of the deck involving longitudinal translation and bending of the abutment walls.

A three-dimensional finite element model of the bridge, with Winkler springs attached to the footings and walls to represent the soil-structure interaction, was able to reproduce the experimental data (natural frequencies, mode shapes and bridge response) reasonably well. Although the stiffnesses assigned to the Winkler springs were based largely on the application of a form of Rayleigh's Principle to the experimental data, these stiffnesses were similar to theoretical foundation stiffnesses of the same size footings on a linearly elastic half space and theoretical lateral stiffnesses of a rigid retaining wall against a linearly elastic backfill.

INTRODUCTION

The numerous case histories of bridge damage¹ during major 20th century earthquakes in Japan concerned many civil engineers in that country for a long time. However, relatively little attention was given to the seismic behavior of bridges in the United States until the 1971 San Fernando earthquake in Southern California. The poor performance of bridges^{2,3} in the epicentral region of that earthquake led to a considerable amount of research in the United States on the seismic response and design of different types of bridges and their various structural components such as abutment walls, footings, superstructure, wingwalls, columns and piers, and the connections between these components. Among the many analytical studies conducted, several examined the interaction between the bridge and the surrounding soil. For example, theoretical studies by Penzien and co-workers^{4,5,6,7} and Agbabian Associates⁸ demonstrated that the interaction between the bridge and abutment-backfill soils can have a significant influence on the dynamic characteristics of the entire system, and thus, can affect the distribution of loads to structural elements comprising the bridge. Efforts at quantifying this interaction during the San Fernando earthquake were hampered because the bridges were not instrumented. As a result,

the California Department of Transportation (Caltrans) and the U.S. Geological Survey instrumented selected bridges in seismic areas of California. Since that time, a few of these bridges have recorded strong ground motion^{9,10,11,12}. The accelerograms recorded by a relatively large number of accelerometers at various locations on two of these bridges (the San Juan Bautista 156/101 Separation Bridge and the Meloland Road Overpass) and in the nearby free field, have permitted fairly detailed analytical studies on their dynamic behavior^{13,14,15,16,17}, including pier-foundation and abutment-backfill interaction. However, the instrumentation on the abutment walls and foundation elements of these structures was insufficient or lacking altogether to provide an accurate indication of the stiffness and damping characteristics of these components.

During quick-release tests, measurements of transient translation and rocking responses of one of the pier foundations supported on piles enabled Douglas and co-workers^{18,19} to make reliable estimates of the transverse translational and rotational stiffnesses of the pier foundations of the Rose Creek Interchange Bridge in Nevada. The transverse stiffness of the neoprene elastomeric bearings, supporting the bridge deck at each abutment, were also estimated from the vibration data. Other experimental studies have been performed on many types of bridges, but

the soil-structure interaction phenomenon at the abutments has been largely ignored.

The experimental and analytical studies reported in this paper focus on the dynamic interaction between the monolithic abutments and support footings of a single span bridge and the surrounding soil, a topic that has not been studied in any detail. The first portion of this paper describes the structural characteristics of the bridge and the vibrational testing program. The important data collected during the tests are presented and interpreted. The remainder of the paper discusses the results of finite-element modeling of the bridge, aimed at simulating the vibrational tests, and presents conclusions regarding the foundation stiffnesses and their effect on the overall dynamic behavior of the bridge system.

FIELD TESTING PROGRAM

Ambient, quick-release and forced vibration tests were conducted on the Horsethief Road Undercrossing Bridge, located approximately 24 km south of Corona, California. The bridge (Figure 1) is a single span, monolithic, prestressed-concrete, box-girder bridge. Vertical support is provided by a rectangular concrete footing beneath each abutment. The footing is not structurally tied to the abutment wall; rather, a thin neoprene strip separates the bottom of the abutment from the top of the footing. This sliding-bearing design is typical of monolithic abutments on California bridges. The shear key on top of the footing (Figure 1) in back of the abutment is designed to resist lateral movements of the abutment. The abutment and box comprising the bridge deck are cast together - hence the term, monolithic. Longitudinal and transverse reinforcing steel are present in the top deck slab and bottom soffit to control shrinkage and provide transverse bending strength between the girders. The 32-day concrete compression strength, f_c' , as determined from standard cylinder compression tests performed during construction of the bridge in 1979, was approximately 41 MPa (6,000 psi). Such high strength is typical of prestressed bridges in California and prestressed concrete structures in general.

The footings rest on sandy soil with some coarse gravel content. The average shear-wave velocity, V_s , of the upper 3 m (10 ft) of soil beneath the footings is about 260 mps (850 fps). The backfill soil consists of similar material except the average V_s is about 210 mps (700 fps). Both estimates were obtained by spectral analysis of surface waves, excited by a vertical impulse load applied near each abutment²⁰.

During the testing, the response of the bridge was measured with 30 accelerometers (Endevco Model 5241) placed at various locations on the bridge deck, abutment walls and the top of the footings near the inside edges of the abutment walls. The locations of these accelerometers are shown in Figure 2. The number of locations (37) exceeds the number of accelerometers because during some tests, certain accelerometers were moved to different locations on the bridge. The accelerometers were positioned so that the rigid body and flexural motions of the footing, abutment and deck could be determined. In addition, two displacement transducers (Schaevitz Model 250 HCD) were placed near the bottom of one abutment wall to measure the relative displacement between the abutment wall and footing resulting from any sliding or deformation of the neoprene bearing strip. However, measurements from these transducers did not reveal any relative displacement, and thus, in the sub-

sequent finite element analyses, a perfectly bonded contact between the footings and abutment walls was assumed.

Signals from the transducers were passed through a STI differential amplifier and antialias filter, which removed frequencies greater than 42.6 Hz. The output was passed through an analog-to-digital converter and stored on a Data General Nova 3 Computer. A Hewlett Packard HP 3582A Spectrum Analyzer and a terminal screen were used to visually examine the response of each transducer during and after a particular vibration test.

Although ambient-vibration and quick-release tests were performed, these tests corroborated the results of the more comprehensive forced vibration tests, which are reported in this paper. The forced vibration tests were conducted by ANCO engineers with their large MK-15 eccentric mass shaker, which was bolted to the top of the bridge deck midway between the two abutments at a point approximately 4.6 m (15 ft) from the longitudinal centerline of the bridge (see Figure 2). The two counter-rotating buckets of the shaker, each one containing a variable number of 11.3 kg (25 lb) lead bricks, were adjusted to apply unidirectional harmonic shaking in the longitudinal or transverse directions. Because of the slight skew of each abutment, these shaking directions were not quite parallel and per-

pendicular to the centerline of the bridge deck. The transverse direction of shaking was skewed approximately 12.5 degrees, the average of the skew angles of each abutment as shown in Figure 1. The longitudinal direction of shaking was perpendicular to this direction. The excitation frequencies ranged between 2 and 14 Hz, and the applied loads varied between 8.9 and 445 kN (2 and 100 kips), or approximately 0.1 to 4 percent of the weight of the bridge. Many tests, each one over a preselected frequency band, were conducted in each direction as shown in Figure 3. For a given frequency, the applied load varied by as much as an order of magnitude between the smallest and largest load test. During a given test, the load varied by up to an order of magnitude between the smallest and largest frequencies. Although these were large variations, the applied loads were still small and did not appear to induce any significant nonlinear response.

During a particular test sequence (e.g., Test 9 Run 2), the excitation frequencies were incremented such that each succeeding frequency was one to two percent larger than the preceding frequency. When a steady-state condition was reached at each frequency, the acceleration amplitudes and phases of the acceleration-time histories recorded by the accelerometers were determined by Fourier analysis. The modulus was taken as the

amplitude of the steady-state acceleration and the phase angle was computed from the real and imaginary parts. The phase angle (p) was defined with respect to the applied force; i.e., if the shaker force was $F = F_0 \sin(\omega t)$, the response measured by a particular accelerometer was $a = a_0 \sin(\omega t + p)$. To time the application of the harmonic force, a sensor was placed on the rotating shaft of the shaker. This sensor recorded the times at which the shaker force reached its maximum positive value during each revolution.

DATA ANALYSIS

The amplitude data obtained from each accelerometer during the forced vibration tests were converted to displacements by dividing by ω^2 where ω is circular frequency. The displacements were in turn normalized by the applied shaker force. These normalized displacements and their associated phase angles were plotted as a function of frequency for each vibration test. The natural frequencies and modal damping ratios of each mode of vibration, which could be positively identified, were estimated from these data. A sample of representative amplitude and phase data, showing the natural frequencies, is presented in Figures 4 a & b. Figure 4a shows the response data for the three vertical accelerometers located in the middle of the deck during two transverse shaking tests. Figure 4b shows the response data from one triaxial accelerometer package located on a footing during the same tests. Four natural frequencies, and the onset of the fifth one, are visible. These frequencies are approximately 4.7, 6.4, 8.2, 10.6 and 14+ Hz. Response peaks at 11.0 Hz were observed for Test 13, when the shaker force was in the longitudinal direction. This mode is probably the same one noted at 10.6 Hz in the transverse-direction tests, which produced higher amplitudes at this frequency. This interpretation

is supported by the amplitude and phase data recorded by the three vertical accelerometers on the deck during this test. However, the possibility of a closely spaced mode, which was excited more by the longitudinal shaking, cannot be totally discounted.

With the exception of the one at 8.2 Hz, all modes positively identified from the response data are lightly damped. As determined by the half-power method, the modal damping ratios, ζ , corresponding to the natural frequencies of 4.7, 6.4, 10.6 (or 11.0) Hz, are approximately 0.025, 0.035, and 0.020 (0.025), respectively. As will become apparent when the experimental and theoretical mode shapes are examined below and in the next section, these modes involve considerable vertical vibration of the bridge deck and relatively little vibration of the abutment walls and the footings. On the other hand, the mode at 8.2 Hz, which is only visible in the response data for accelerometer 19 in Figure 4b and in other transverse-direction response data not shown in the figure, is moderately damped ($\zeta \approx 0.15$), and appears to be associated with significant soil-structure interaction in the transverse direction.

To obtain some indication of the mode shapes, the normalized displacement amplitudes from the forced vibration tests

at frequencies near the natural frequencies were plotted at the corresponding accelerometer locations on the bridge. The tests which best displayed the character of the mode shapes were selected and the results are shown in Figure 5. The appropriate directions (positive or negative) of the displacement vectors were determined from the phase angles. In a few instances, usually for the smaller amplitudes, the phase angles did not suggest any preferred direction.

The mode in Figure 5 associated with the fundamental frequency of 4.7 Hz is interpreted as the primary longitudinal bending mode of the bridge deck. The relatively large longitudinal (i.e., x direction in Figure 2) displacements of the bridge are the result of: (1) the shaker force being applied in that direction during Test 17-Run 1, and (2) possible interference from a higher mode (possibly the fifth one), having significant modal displacements in that direction. As will be shown in the next section, these longitudinal displacements are not representative of the theoretical mode shape, which primarily consists of vertical deformation of the bridge deck.

The second mode at 6.4 Hz (response data in Figure 5 shown at 6.2 Hz to preserve the amplitude scale) is the primary torsional or twisting mode of the deck. In this mode, the longitu-

dinal centerline of the deck represents the approximate location of the nodal line; the halves of the deck on either side are displacing vertically in opposite directions. Another interesting observation in this mode is the transverse shearing deformation of the deck, which is apparent by comparing the larger transverse displacements in the middle of the deck along each side with the smaller transverse displacements at the corners of the deck. The flexure and twisting of the abutment walls are also obvious by comparing the longitudinal displacements at the corners of the deck with those toward the bottom of the walls and top of the footings. A significant amount of rigid-body transverse displacements and torsional and rocking rotations of the footings is also indicated in this second mode. Nonetheless, the maximum footing displacements are about a factor of 5 to 10 less than the maximum vertical displacement of the deck, which accounts for the relatively low damping in this mode.

On the other hand, the third mode at 8.2 Hz shows a relatively high ratio of transverse footing displacement to vertical deck displacement, which explains the higher damping observed in this mode. The type of deck deformation is similar to that observed in the second mode, except the sense of motion is reversed and the vertical displacements are smaller.

The mode at 10.6 Hz appears to be the second twisting mode of the deck because the vertical displacements of the middle of the deck along the sides are in the same direction and are approximately the same amplitude, whereas the displacement near the center of gravity of the deck is in the opposite direction.

The mode near 14 Hz (shown in Figure 5 at 13.9 Hz) may be the second longitudinal bending mode of the deck. The limited number of vertical responses measured on the deck are consistent with this interpretation. Furthermore, if the influence of the walls and footings and their interaction with the soil is neglected, and if the deck is assumed to be a uniform, linearly elastic, isotropic plate of similar dimensions and fundamental frequency as the bridge, then the second longitudinal bending mode is at 13.0 Hz provided the plate is clamped at opposite edges along the abutments and free along the sides²¹.

FINITE ELEMENT MODELING

A three-dimensional (3-D) finite element model of the Horsethief bridge was constructed in an attempt to predict the observations of the forced vibration tests. The model is shown in Figure 6 and consists of linearly elastic, isotropic plate elements capable of simulating in-plane and out-of-plane deformations. Such elements, which are part of the element library in the DYNAFLOW computer program used in this study²², are essential to properly model the torsional and in-plane bending stiffnesses of the girders. As shown in Figure 6, the geometry of the bridge, including the box section and the abutment skews, is accurately represented. The footings, which are the bottom row of elements along the abutment walls, were modeled as plate elements similar to the abutment-wall elements but with a larger mass density to compensate for the fact that the width of the footing elements was much less than the 1.83-m (6-ft) width of the the actual footings at the Horsethief bridge. This approximate modeling of the footing was considered sufficient for this application.

The interaction between the footings and the soil was modeled by a set of three mutually perpendicular translational springs (not shown in Figure 6) attached to each node at the

bottom of the footing. The two lateral springs were parallel and perpendicular to the principal horizontal axes of the footings; the other spring was vertical. The interaction between the abutment wall and backfill soil was modeled by one set of lateral springs perpendicular to the face of the wall. The other two springs parallel to the face of the wall were omitted because the frictional forces between the wall and soil were assumed to be negligible. This Winkler-spring arrangement is known to be an approximate representation of the interaction phenomenon; however, it was considered to be a reasonable choice, and is one often adopted for finite element models of soil-structure interaction.

Generally, each node of the elements in Figure 6 has three translational and three rotational degrees of freedom. The total number of elements is 236 and the number of nodes is 234. The total number of degrees of freedom of the system is 1,109. The point in common to the four triangular elements in the middle of the deck between two girders is the location of the shaker force.

The unknown parameters of the finite element model were the two elastic moduli (Young's modulus and Poisson's ratio) of the plate elements and the stiffnesses of the Winkler springs. A Young's modulus for concrete (E_c) of 3.4×10^7 kPa (7.2×10^8 psf)

was computed using the standard ACI formula, $E_c = 57,500 \sqrt{f'_c}$ (in psi). Before substituting into this formula, the value of f'_c , measured from the cylinder compression tests, was increased by 25 percent to account for the increase in concrete strength with age. A Poisson's ratio for concrete of 0.17 was assumed.

Values of the spring stiffnesses for the footings were estimated by: (1) applying a variational form of Rayleigh's Principle (see Appendix for details) to an approximate deformation shape assumed for the second mode of vibration at 6.4 Hz, and (2) using information in references 23 and 24 for the theoretical response of a surface footing on an elastic half space. The footings were assumed to be rigid rectangular foundations with a length-to-width ratio of 11. The elastic half space was assumed to have a shear-wave velocity of 260 mps (850 fps) and a Poisson's ratio of 1/3. Stiffness estimates of the springs attached to the abutment walls were obtained from the application of the same form of Rayleigh's Principle to the fifth mode near 13.9 Hz and from 2-D finite element solutions of the pressure distribution along the height of rigid retaining walls subjected to lateral movement²⁵. Estimates of the spring stiffnesses for each footing and wall based on Rayleigh's Principle and theory are shown in Table I. Note that these two sets of stiffnesses are remarkably similar.

The well-known modal superposition procedure²⁶ was used to compute the responses at various points on the structure corresponding to the locations of accelerometers that measured the accelerations generated during a particular forced vibration test. Because the excitation was harmonic, the solution was easily obtained in the frequency domain. The specification of the proper force and moment applied to the node representing the shaker location was straight-forward for excitation in the transverse direction. However, for shaking forces in the longitudinal direction, an additional moment about a vertical axis through the node had to be incorporated. This moment results from the phasing between the two counter-rotating weights of the shaker that is required to produce the longitudinal force, F . The moment has an amplitude, $Fd/2$, where d is the distance between the counter-rotating shafts in the shaker. The moment is also $\pi/2$ radians out-of-phase with respect to the shaker force.

Five modes were used in the superposition; the modal damping ratios that were used were obtained from the experimental response data. The size of the finite-element model and the storage capacity and CPU time required on the Harris 800 computer limited the solution of the eigenvalue problem to this number of modes. However, these modes covered the frequency range 0 to 12 Hz, and thus, were considered sufficient for the purposes of estimating the response in this frequency band.

A trial-and-error method was used to determine the stiffnesses of the interaction springs that: (1) yielded natural frequencies and mode shapes consistent with the experimental data and (2) provided a reasonable match between the responses measured during the vibration tests and those predicted by the model. Using estimates of the stiffnesses based on either the variational form of Rayleigh's Principle or theory (Table I) initially produced a satisfactory fit to the data. By making small adjustments to some stiffnesses, an improved fit was obtained. The final stiffness values are shown in Table I. Because a reasonable fit was achieved with these final interaction stiffnesses, modifications to the initial estimates of the elastic moduli of the plate elements representing the bridge were not considered necessary.

The first five natural frequencies and mode shapes computed for the finite element model are shown in Figure 7. Note that the computed and experimental natural frequencies are within 2 percent of each other for the first, second and fourth modes. The computed third natural frequency of 9.3 Hz is approximately 13 percent greater than the corresponding experimental one at 8.2 Hz. The computed fifth natural frequency at 11.9 Hz is probably slightly more than 15 percent less than the experimental natural frequency, which was believed to be just beyond 14 Hz.

The computed mode shapes in Figure 7 are similar to the deformation patterns observed during the vibration testing (Figure 5), which provides a measure of confidence to the finite element model. The predominant vertical deformation of the deck in the first, second and fourth modes is consistent with the relatively low damping ratios observed in the experimental data. Conversely, the predominant transverse translations of the footings in the third mode are consistent with the much higher damping ratio observed in this mode.

Comparisons between the computed and observed responses of selected accelerometers are shown in Figures 8 and 9. The top half of Figure 8 shows the responses of accelerometers in the middle of the bridge deck in the frequency band 0 to 8 Hz during Test 9 Run 2, a transverse shaking test. Both the computed and observed responses (amplitude and phase) are similar. Reasonable agreement is also observed between the computed and observed responses on the wall and footing (bottom half of Figure 8) in the same frequency band during the same test, although the computed amplitude response of the footing in the transverse direction (accelerometer 27) is larger than the observed response by 50 to 100 percent.

Representative comparisons in the frequency band 5 to 14 Hz for Test 11 Run 1 are shown in the top half of Figure 9. The

vertical response in the middle of the deck (accelerometer 15) observed during the test is similar to the computed response for frequencies less than 13 Hz. The divergence in the two responses beyond this frequency may reflect the limited number of modes used in the superposition. The increase in the observed amplitude indicates the presence of another mode beyond 14 Hz, which was mentioned earlier. However, this mode may be different from the second bending mode, which was interpreted from the response data obtained during Test 13 Run 1, a longitudinal shaking test. The vertical deformation shape for this mode has a transverse nodal line which passes near accelerometer 15. Thus, the rapidly increasing response of this accelerometer for frequencies greater than 13 Hz is inconsistent with this mode shape. Natural frequencies computed for a simpler model of the bridge involving fewer degrees of freedom indicated a number of closely spaced modes, other than the second bending mode, at frequencies greater than 14 Hz. Possibly one of these modes is responsible for the large amplitude response near 14 Hz observed for accelerometer 15.

The computed and observed responses for the other two accelerometers (18 and 19) on the footing are similar except in the frequency band from 7 to 10 Hz, where the third mode is governing the response. Much better agreement could have been

obtained in this frequency band by simply increasing the damping in the third mode from 0.15 to about 0.3. Such high damping might be justifiable on the basis of the experimental and computed mode shapes which indicate that the transverse-footing and vertical-deck motions are not greatly different. For this case, the large radiation damping associated with translational motions of a footing on soil ²⁴ would be the dominant factor contributing to the higher damping ratio around 0.3. However, the half-power method applied to the experimental data consistently showed damping ratios around 0.15. Furthermore, when applied to the experimental mode shape in Figure 5, the method of computing the modal damping ratio based on the strain energy stored in various elements with different damping ratios²⁷ (e.g., the bridge deck which has low damping and the footing-Winkler spring system which has much higher damping), yielded a damping ratio closer to 0.15. Regardless of the actual damping ratio, the experimental response data and the computed mode shape clearly demonstrate that a damping ratio in this mode much higher than the usual 2 to 5 percent damping, observed in most field tests of bridges or assigned to computer models of these structures, is required.

A comparison of the computed and observed responses in the frequency band 3 to 11 Hz during Test 3 Run 2, a longitudinal

shaking test, is presented in the bottom half of Figure 9. The vertical amplitude response computed for accelerometer 15 is somewhat greater than the observed response but the salient features are reproduced. Again, the larger response computed in the transverse direction (accelerometer 13) in the frequency band 7 to 10 Hz is observed for this test also and is the result of the third mode response discussed in the previous paragraph. The longitudinal amplitude-response curve computed for accelerometer 7 is of the same order as the observed curve although the shapes are somewhat different. The computed response is dominated by the fifth mode, which has a significant component of footing translation in the longitudinal direction and a substantial amount of bending of the abutment wall about the transverse axis as indicated in the fifth mode shape shown in Figure 7. The damping assigned to this mode (0.15) was required to produce a reasonable fit to the longitudinal data recorded during shaking in this direction. The wall flexibility is undoubtedly accounting for the lower than expected natural frequency computed for the fifth mode (11.9 Hz). However, there did not appear to be any rational basis for increasing the bending stiffness of the wall; the Young's modulus of 3.4×10^7 kPa (7.2×10^8 psf) that was used in the model was considered to be close to the upper limit of this parameter based on the concrete

cylinder strength obtained in the field. Possibly the attachment detail between the abutment wall and footing was not properly modeled or possibly the representation of the stiffness contribution of the backfill soils by linear springs of constant stiffness along the height of the wall needs revision. The abutment-footing detail (Figure 1) and the shear-wave velocity profile of the backfill soil, which indicated higher velocities near the ground surface, suggest that a more elaborate model of the abutment and its interaction with the backfill soil might have produced better results.

CONCLUSIONS

The presence of soil-structure interaction was clearly established by the forced vibration tests conducted on the Horsethief bridge. This interaction was most apparent for the footings, which exhibited substantial transverse translation and rocking about the longitudinal axis between 5 and 9 Hz. Large longitudinal translations of the footings and abutment walls were not observed for frequencies less than 14 Hz; the mode of vibration involving this response appeared to be at a slightly higher frequency which was not attained during the vibration tests.

One of the encouraging results of this study was the ability of a finite element model, based on reasonable estimates of the foundation and structural stiffness parameters, to reproduce the important vertical deformations of the deck observed during the vibration tests. These deformations produce the bending stresses in the girders which need to be considered in the design for heavy moving vehicular or seismic loads. In assessing the seismic response, the results of this and another recent study indicate the need to consider all three components of input excitation, which is not currently recommended in the AASHTO guidelines²⁸ for seismic design. These guidelines state that only the two horizontal components need to be considered in the

analysis. However, by including the vertical component of excitation in a seismic response analysis of the Horsethief bridge, for example, the participation factor in the first mode would substantially increase, thereby increasing the bending stresses in the girders in this mode and the vertical forces transmitted to the foundations. Foutch and Saadeghvaziri²⁹ recently demonstrated that vertical excitation during the 1971 San Fernando earthquake contributed to the damage observed at the mid-span columns of some concrete box-girder bridges in the epicentral region.

For single- or double-span bridges, finite element models, which incorporate the exact geometric and stiffness properties of the deck superstructure, are preferred over models that approximate this detail with a line of equivalent beam elements between spans. Such simplified models will not properly represent the twisting modes of the deck, which were dominant during the transverse vibration tests. These modes also would be quite apparent during transverse seismic excitation or vehicular loading.

In any finite-element or other structural model used in design, the selection of the proper input parameters is crucial if reasonably accurate estimates of the member stresses are to be obtained. For concrete bridges with foundation and abutment

details similar to those at the Horsetheif bridge, the results from the well-established theory of rigid surface footings on an elastic half space (e.g., references 23 and 24) appear to provide reasonable estimates of the footing-foundation stiffnesses provided the shear-wave velocity profile beneath the footing is known or can be reliably estimated from other in situ data.

Estimating Young's modulus of the concrete from the compressive strengths obtained during cylinder tests in the field (with suitable increases in strength with age) appears to be a reasonable procedure to specify the modulus of the elements comprising the superstructure. However, procedures to estimate the lateral stiffness associated with the interaction between the abutment wall and backfill soil could not be identified with any certainty from the results of this study because the mode containing a significant amount of longitudinal motion of the abutment wall was not fully identified during the vibration tests. The presence of such a mode beyond 14 Hz was inferred from the response data near 14 Hz, which showed increases the longitudinal abutment response with increasing frequency. However, a complete definition of this mode, including pressure measurements and more acceleration measurements along the height of the abutment wall, would have been needed to better address this problem.

Fortunately, the interaction between the abutment wall and back-

fill soil did not play a major role in the dynamic response of the Horsethief bridge for frequencies less than 12 Hz, and it may not affect the dynamic response of bridges with similar abutment details and backfill soils. However, this interaction may be important in the design of the abutment wall against lateral loads, and further studies should be undertaken to determine its significance.

The intuitive notion that greater modal damping will occur when the foundation motion increases relative to the superstructure motion, was verified by the vibration tests. For modes involving a greater proportion of structural response, damping ratios less than 5 percent appear to be appropriate for low strains. Much higher damping ratios are appropriate for those modes in which the foundation and structural responses are of the same order of magnitude.

Table I. Stiffnesses estimated for the springs representing the soil-structure interaction in the finite element model.

	(k_{1fbc})	EACH FOOTING (k_{2fbc})	(k_{3fbc})	EACH ABUTMENT WALL (k_{1wab})
Rayleigh's Principle ⁽¹⁾	--	2.2×10^9 N/m (1.5×10^8 lb/ft)	5.3×10^9 (3.6×10^8)	2.0×10^9 (1.4×10^8)
Theory ⁽²⁾	3.9×10^9 (2.7×10^8)	2.3×10^9 (1.6×10^8)	4.4×10^9 (3.0×10^8)	2.2×10^9 (1.5×10^8)
Final ⁽³⁾	3.9×10^9 (2.7×10^8)	2.5×10^9 (1.7×10^8)	5.3×10^9 (3.6×10^8)	2.8×10^9 (1.9×10^8)

(1) See Appendix for details

(2) Half-space theory^{23,24} for footing; retaining-wall theory²⁵ for abutment wall

(3) Based on reasonable fit between experimental and computed responses.

Notation: (k_{1fbc}) and (k_{1wab}) are longitudinal (~ x direction in Figure 2) stiffnesses; (k_{2fbc}) is the transverse (~ y direction) stiffness; and (k_{3fbc}) is the vertical stiffness. The constants b and c are the length and width of the footing, respectively, and the constant a is the height of the wall.

ACKNOWLEDGEMENTS

This study was supported by the National Science Foundation under grant ECE-8316976. Caltrans personnel, Jim Gates and Jack Christie, were instrumental in providing the Horsethief Road Undercrossing bridge for our vibration tests. The excellent field work of the following individuals was appreciated: Dan Chitty and Steve Keowen of ANCO Engineers, who performed the vibration tests, Soheil Nazarian and Ken Stokoe of the University of Texas, who performed an in situ velocity survey, and George Edmonds of Earth Technology, who conducted Cone Penetrometer Tests. Drs. John Wood of the Ministry of Works and Development in New Zealand and George Liang of Earth Technology assisted during the testing and data reduction phases of the project. Their help was also appreciated.

REFERENCES

1. T. Iwasaki, J. Penzien and R. Clough, "An investigation of the effectiveness of existing bridge design methodology in providing adequate structural resistance to seismic disturbance, Report No. FHWA-RD-73-13, Federal Highway Administration, Washington, D.C., 1972.
2. P. C. Jennings and J. H. Wood, "Earthquake damage to freeway structures", Engineering Features of the San Fernando Earthquake, February 9, 1971, P. C. Jennings (ed.) Earth Engng. Res. Lab., Calif. Inst. of Tech., 1971.
3. G. G. Fung, R. J. LeBeau, E. D. Klein, J. Belvedere and A. F. Goldsmith, "Field investigations of bridge damages in the San Fernando earthquake", Preliminary Report, State of California Business and Transportation Agency, Dept. of Public Works, Div. of Highways, 1971.
4. M. C. Chen and J. Penzien, "Soil-structure interaction of short highway bridges", Applied Tech. Council Workshop of the Research Needs of Seismic Problems Related to Bridges, 1979.
5. M. C. Chen and J. Penzien, "Analytical investigation of seismic response of short, single or multiple span highway bridges", EERC 75-4, Earthq. Engng. Res. Center, Univ. of Calif., Berkeley, 1975.
6. M. C. Chen and J. Penzien, "Nonlinear soil-structure interaction of skew highway bridges", EERC-77/24, Earthq. Engng. Res. Center, Univ. of Calif., Berkeley, 1977.
7. W. C. Tseng and J. Penzien, "Analytical investigation of the seismic response of long multiple span highway bridges", EERC-73/12, Earthq. Engng. Res. Center, Univ. of Calif., Berkeley, 1973.
8. Agbabian Associates, "A methodology for the dynamic analysis of bridge/abutment/backfill systems subjected to traveling seismic waves", Report R-8113-5470, 1983.
9. L. D. Porter, "Processed data from the strong-motion records of the Imperial Valley Earthquake of 15 October 1979", California Dept. of Conservation, Div. of Mines and Geology, Special Publication 65, 1983.

10. R. D. McJunkin and C. D. Turpen, "Strong-motion records recovered from the Trinidad-Offshore, California Earthquake of 8 November 1980", California Div. of Mines and Geology, Preliminary Report 80-11.1, 1980.
11. L. D. Porter, A. G. Brady, P. N. Mork, and V. Perez, "Processed data from the San Juan Bautista 101/156 Separation Bridge and the San Juan Bautista freefield records from the Coyote Lake Earthquake 6 August 1979", California Dept. of Conservation, Div. of Mines and Geology, Special Publication 64, 1983.
12. A. G. Brady, R. L. Porcella, G. N. Bycroft, E. C. Etheredge, P. N. Mork, B. Silverstein, and A. F. Shakal, "Strong-motion results from the main shock of April 24, 1984", The Morgan Hill, California Earthquake of April 24, 1984 (A Preliminary Report), U.S. Geological Survey Open-File Report 84-498A, 1984.
13. J. C. Wilson, "Analysis of the observed earthquake response of a multiple span bridge", Ph.D. Thesis, California Institute of Technology, Earthq. Engng. Res. Lab., Report EERL 84-01, 1984.
14. R. Shepherd and L. Lisiecki, "The response of a bridge to strong ground shaking", Proc. 7th European Conf. Earthq. Engng., Athens, Greece, 1982.
15. S. D. Werner, M. B. Levine and J. L. Beck, "Seismic response characteristics of Meloland Road Overpass during 1979 Imperial Valley Earthquake", Agbabian Associates, Report R-8222-5603, 1985.
16. S. D. Werner, J. L. Beck and M. B. Levine, "Seismic response evaluation of Meloland Road Overpass using 1979 Imperial Valley Earthquake records", submitted to J. Earthq. Engng. and Structural Dyn., 1985.
17. B. Douglas, G. Norris, L. Dodd and J. Richardson, "Behavior of the Meloland Road Overcrossing during the 1979-Imperial Valley Earthquake", Seismic Research for Highway Bridges (U.S. - Japan Program), Dept. Civil Engng., Univ. of Pittsburgh, Pittsburgh, Pennsylvania, 1984.
18. B. Douglas and J. A. Richardson, "Maximum amplitude dynamic tests of a highway bridge", Proc. 8th World Conf. Earthq. Engng., San Francisco, California, 1984.

19. B. M. Douglas and W. H. Reid, "Dynamic tests and system identification of bridges", J. Struct. Div., ASCE, 108, 2295-2312 (1982).
20. S. Nazarian and K. H. Stokoe, II, "In situ shear wave velocities from spectral analysis of surface waves", Proc. 8th World Conf. Earthq. Engng., San Francisco, California, 1984.
21. C. B. Crouse, B. Hushmand, G. Liang, G. Martin and J. Wood, "Dynamic response of bridge-abutment-backfill systems", Proc. Joint U.S. - New Zealand Workshop on Seismic Resistance of Highway Bridges, San Diego, California, 1985.
22. J. H. Prevost, "DYNAFLOW: A nonlinear transient finite element analysis program", Dept. of Civil Engng., Princeton, N. J., 1981.
23. H. L. Wong and J. E. Luco, "Tables of impedance functions and input motions for rectangular foundations", Report No. CE 78-15, Dept. of Civil Engng., Univ. of Southern California, 1978.
24. G. Gazetas, "Analysis of machine foundation vibrations: state-of-the-art", Soil Dyn. Earthq. Engng., 2, 2-42, (1983).
25. J. H. Wood, "Earthquake induced soil pressures on structures", Ph.D. Thesis, California Institute of Technology, Earthq. Engng. Res. Lab., Report EERL 73-05, 1973.
26. R. W. Clough and J. Penzien, Dynamics of Structures, McGraw-Hill Book Company, New York, 1975.
27. R. V. Whitman, "Soil-Structure interaction", Seismic Design for Nuclear Power Plants, R. J. Hansen (ed.), MIT Press, Cambridge, Massachusetts and London, England, 245-269, 1970.
28. The American Association of State Highway and Transportation Officials (AASHTO), "Guide specifications for the design of highway bridges, 1983", AASHTO, Washington, D.C., 1983.
29. D. A. Foutch and M. A. Saadeghvaziri, "The effects of vertical earthquake motions on the response of highway bridges", Dynamic Response of Structures, ASCE, New York, N.Y., 1986.

30. S. P. Timoshenko and S. Woinowsky-Krieger, Theory of Plates and Shells, McGraw-Hill Book Company, New York, 1959.

APPENDIX - Estimation of Foundation Stiffnesses
from Results of Forced Vibration Test.

A variational form of Rayleigh's Principle was used to estimate the stiffnesses of the Winkler springs that model the interaction between the footings and foundation soil and between the abutments and backfill soil. Equations were written representing the kinetic energy and potential energy in the main elements of the bridge soil-structure-interaction (SSI) model shown in Figure A-1 (the Winkler Springs attached to the abutment walls and footings are not shown). The elements consisting of the deck and two abutment walls were homogeneous, isotropic, linear-elastic rectangular plates of uniform thickness. The two footings were rigid rectangular blocks. The abutment skews were neglected in this model. Approximate expressions for the deflection of each element were developed from the deflections measured by the accelerometers at the second natural frequency ($f_2 = 6.4$ Hz) during a particular forced vibration test. This test was the one in which the shaker applied a harmonic force in the transverse direction ($\sim y$ direction). As indicated in the text, this test induced significant transverse displacement and rocking of both footings, and thus, is ideally suited for estimating the foundation stiffnesses associated with these two motions. Equations of motion corresponding to the assumed deflection shape were then derived from Lagrange's equations and the unknown

stiffnesses were estimated from these equations by substituting into them the values of the geometric and inertial properties of the bridge and the values of the displacement responses in the second mode.

The coordinate system and variables designating the deflection of each element are shown in Figure A-2. The motion of the footings' c.g. considered was transverse and vertical translations (v and w) and rotations about the X and Z axes (ϕ_x and ϕ_z). The other two components of rigid body motion were neglected. In addition to the motions in the abutment walls and deck arising from the rigid body motions of the footings, motions based on the deformation of these elements were also considered. The deformation of the abutment wall, shown in Figure A-2, is designated as u and is a function of y and z . Referring to the coordinate system through the c.g. of the wall, the deflection u was approximated as

$$u = - \left(\left(\frac{z}{a} - \frac{1}{2} \right) \right)^2 (\phi_z y) \quad (A-1)$$

This equation satisfies the boundary condition $\frac{\partial u}{\partial y} = -\phi_z$ at $z = -a/2$ imposed by the rigid body rotation (ϕ_z) of the footing. In developing equation (A-1), $\frac{\partial u}{\partial y} = 0$ at $z = a/2$ was assumed as well as a quadratic expression in z for the deflection shape at a given y . This deflection shape corresponds to twisting or torsion of the wall about the y axis and is consistent with the deflections measured during the forced vibration test.

The deformation of the deck, shown in Figure A-2, is a function of x and y . Two types of deformation were considered:

(1) the bending and twisting of the deck denoted by the displacement w_d in the z direction, and (2) the transverse shear of the deck denoted by the displacement v_d in the y direction.

Expressions for these two displacements were chosen as

$$w_d = -W_d \cos(\pi x/L) \sin(\pi y/b) \quad (A-2)$$

$$v_d = V_d \cos(\pi x/L) \quad (A-3)$$

where L and b are the length and width of the bridge, and w_d and v_d are displacement variables.

Kinetic Energy. The expression for the kinetic energy of the footing in Figure A-2a is simply

$$T_f = (1/2) (m_f \dot{v}^2 + 1/2 I_{zf} \dot{\phi}_z^2 + 1/2 I_{xf} \dot{\phi}_x^2 + 1/2 m_f \dot{w}^2) \quad (A-4)$$

where: The subscript f refers to the footing; m_f is the mass of the footing; and, I_{xf} and I_{zf} are the principal moments of inertia. The dot over the variable refers to differentiation with respect to time. Because of its deformation, the analogous expressions for the abutment walls and deck involve integration of the velocity over the area of these elements. For the wall in Figure A-2, the velocity of a differential volume element, $dx dy dz$, is

$$\dot{\underline{v}}_w = \dot{u} \underline{i} + (\dot{v} - h_w \dot{\phi}_x - z \dot{\phi}_x + x \dot{\phi}_z) \underline{j} + (\dot{w} + y \dot{\phi}_x) \underline{k} \quad (\text{A-5})$$

where: h_w is the height of the c.g. of the wall above the c.g. of the footing; y and z are coordinates of a system whose origin is fixed to the c.g. of the wall; and \underline{i} , \underline{j} and \underline{k} are unit vectors in the X, Y, Z coordinate system, which is fixed at the initial position of the footing c.g. Small displacements were assumed in the development of equation (A-5). Substituting the expression for u (equation (A-1)) into equation (A-5) and substituting equation (A-5) into the expression for kinetic energy,

$$T_w = (1/2) \iiint \rho \dot{\underline{v}}_w \cdot \dot{\underline{v}}_w \, dx dy dz \quad (\text{A-6})$$

the resulting equation for the kinetic energy of the wall is

$$T_w = (1/2) m_w [(\dot{v} - \dot{\phi}_x h_w)^2 + \dot{w}^2] + I_{xw} \dot{\phi}_x^2 + (1/2) m_w [(h_o^2/12) + (b^2/60) \dot{\phi}_z^2] \quad (\text{A-7})$$

where the subscript, w , refers to the wall. The first two terms represent the rigid body motion of the wall while the last term represents the wall deformation.

A similar procedure was followed for the deck. The velocity of a differential element of volume, $dx \, dy \, dz$, at position (x, y, z) in the deck is

$$\dot{\underline{v}}_d = (\dot{v} - \dot{\phi}_x h_d + \dot{v}_d - z \dot{\phi}_x) \underline{j} + (\dot{w} + \dot{v}_d + y \dot{\phi}_x) \underline{k} \quad (\text{A-8})$$

where h_d is the height of the deck c.g. above the footing c.g. Substituting equations (A-2) and (A-3) for w_d and v_d into equation (A-8) and substituting the resulting equation (A-8) into the expression for kinetic energy (analogous to equation (A-6)) and performing the integration over the volume of the deck element yields

$$\begin{aligned}
 T_d = & (1/2) m_d [(\dot{v} - \dot{\phi}_x h_d)^2 + \dot{w}^2] + (1/2) I_{xd} \dot{\phi}_x^2 & (A-9) \\
 & + (1/2) m_d [(4/\pi) \dot{v} \dot{V}_d - (4/\pi) h_d \dot{\phi}_x \dot{V}_d \\
 & - (8b/\pi^3) \dot{W}_d \dot{\phi}_x + (1/2) \dot{V}_d^2 + (1/4) \dot{W}_d^2]
 \end{aligned}$$

where the subscript, d, refers to the deck. The velocity terms in the first row of this equation are associated with rigid body motion of the deck; the velocity terms in the second and third rows are due to the deformation of the deck.

Potential Energy. The potential energy in the system is simply the strain energy in the Winkler foundation springs attached to the bottoms of both footings and the outside faces of the abutment walls, and the strain energy in the abutment walls and deck. Winkler springs in the x, y, z directions are attached to differential area elements of the footing and wall. For simplicity, the stiffness of a particular spring is assumed to be constant over the area of the footing or wall.

The displacement vector associated with the differential element on the bottom of the footing is

$$\underline{v}_f = (-\phi_z y)\underline{i} + (v + \frac{1}{2}h_f\phi_x + \phi_z x)\underline{j} + (\phi_x y + w)\underline{k} \quad (A-10)$$

The displacement components of this equation are substituted into the integral expression for potential energy

$$V_{fs} = (1/2) \iint (k_{1f} v_{1f}^2 + k_{2f} v_{2f}^2 + k_{3f} v_{3f}^2) dx dy \quad (A-11)$$

where k_{1f} , k_{2f} and k_{3f} are the stiffnesses associated with the springs in the x, y and z directions, and v_{1f} , v_{2f} , v_{3f} are the x, y, and z components of \underline{v}_f (i.e., $v_{1f} = -\phi_z y$, etc.). The integration of equation (A-11) gives

$$V_{fs} = (1/2) (k_{2f} bc)v^2 + (1/2) (k_{3f} bc)w^2 + (1/8) [h_f^2 (k_{2f} bc) + (b^3/3) (k_{3f} bc)] \phi_x^2 \quad (A-12)$$

$$+ (1/24) [b^2 (k_{1f} bc) + c^2 (k_{2f} bc)] \phi_z^2 + (1/2)h_f (k_{2f} bc)v\phi_x$$

The total potential energy, V_{ws} , in the Winkler springs attached to the abutment wall is derived following the same general procedure. The analogous expression for V_{ws} is

$$V_{ws} = (1/2)(k_{2w} ab)v^2 + (1/2)(k_{3w} ab)w^2 + [(1/2)(k_{2w} ab)(h_w^2 + (a^2/12)) + (b^2/24) (k_{3w} ab)] \phi_x^2 + (1/8) [(b^2/15) (k_{1w} ab) + (k_{2w} ab)h_o^2] \phi_z^2 - (k_{2w} ab)h_w v\phi_x - (h_o/2) (k_{2w} ab)v\phi_z + (h_o h_w/2) (k_{2w} ab)\phi_x \phi_z$$

(A-13)

Equations (A-12) and (A-13) apply to each footing and abutment.

The strain energy, dV_{we} , in a differential element of the abutment wall (see reference 30 - page 47) undergoing bending and twisting deformations is

$$dV_{we} = (1/2) D_w [[(\partial^2 u / \partial y^2) + (\partial^2 u / \partial z^2)]^2 - (1-\nu) [(\partial^2 u / \partial y^2) (\partial^2 u / \partial z^2) - (\partial^2 u / \partial y \partial z)^2]] dy dz \quad (A-14)$$

where $D_w = (Eh_o^3)/(12(1-\nu))$ is the flexural rigidity of the plate representing the wall (E = Young's modulus, h_o = wall thickness, ν = Poisson's ratio) and the deformation u is given by equation (A-1). Substituting equation (A-1) into equation (A-14) and integrating over the surface area of the wall gives

$$V_{we} = (D_w b / 3a) [(b^2 / 2a^2) + 4(1-\nu)] \phi_z^2 \quad (A-15)$$

The expression for the strain energy in a differential element of the deck undergoing bending and twisting deformation is similar to equation (A-14). Substituting the expression for w_d (equation (A-2)) into this analogous equation and integrating gives the total strain energy in the deck

$$V_{de} = (\pi^4 / 8) [(b^2 + L^2)^2 / (b^3 L^3)] D_d W_d^2 \quad (A-16)$$

where $D_d = (Et^3)/(12(1-\nu))$ is the flexural rigidity of the deck.

The other component of strain energy in the deck is due to the deformation, v_d , in the transverse direction given by equation (A-3). This deformation was assumed to be the result of transverse shear. The differential strain energy for this case is

$$dV_{de}^s = (1/2) AG (\partial v_d / \partial x)^2 dx \quad (A-17)$$

where $A = bt$ is the cross-sectional area of the deck plate in the y - z plane and G is the shear modulus. Substituting equation (A-3) into (A-17) and integrating gives

$$V_{de}^s = (\pi^2/4) (AG/L) v_d^2 \quad (A-18)$$

The above equations for kinetic and potential energies contain six variables: four associated with the rigid body motion of the footing (v , w , ϕ_x , ϕ_z) and two associated with the deformation of the deck (w_d and v_d).

The next step is to take the expressions for the total kinetic and potential energies of the footing-wall-deck system and substitute them into Lagrange's equations

$$(d/dt) (\partial T / \partial \dot{q}_i) - (\partial T / \partial q_i) + \partial V / \partial q_i = Q_i \quad (A-19)$$

where: $T = 2T_f + 2T_w + T_d$; $V = 2V_{fs} + 2V_{ws} + 2V_{we} + V_{de} + V_{de}^s$;
 q_i is one of the six displacement variables; and, Q_i is the

external applied force, which, in this example, is the force applied by the eccentric mass shaker. Because the expressions for the kinetic energies (equations (A-4), (A-7), and (A-9)) are in terms of \dot{q}_i only (not q_i), $\frac{\partial T}{\partial q_i} = 0$.

Although six equations can be derived from equation (A-19) by considering each displacement variable, only those derived for $q_1 = v$ and $q_2 = \phi_x$ were considered to be well-conditioned for determining the stiffness values of the footing Winkler springs, k_{2fbc} and k_{3fbc} . These two equations are

$$\begin{aligned}
 & 2(m_f + m_w + (m_d/2)) \ddot{v} - (2m_w h_w + m_d h_d) \ddot{\phi}_x \\
 & + (2/\pi) m_d \ddot{V}_d + 2 [(k_{2fbc}) + (k_{2w ab})] v \\
 & + [h_f (k_{2fbc}) - 2 h_w (k_{2w ab})] \phi_x - h_o (k_{2w ab}) \phi_z = 0 \quad (A-20)
 \end{aligned}$$

$$\begin{aligned}
 & 2 (I_{xf} + m_w h_w^2 + I_{xw} + (1/2) m_d h_d^2 + (1/2) I_{xd}) \ddot{\phi}_x \\
 & - (2 m_w h_w + m_d h_d) \ddot{v} - (2/\pi) m_d (h_d \ddot{V}_d + (2b/\pi^2) \ddot{W}_d) \\
 & + 2 [(h_f^2/4) (k_{2fbc}) + (b^2/12) (k_{3fbc}) + (h_w^2 + (a^2/12)) (k_{2w ab}) \\
 & \quad + (b^2/12) (k_{3w ab})] \phi_x \\
 & + [h_f (k_{2fbc}) - 2h_w (k_{2w ab})] v + h_o h_w (k_{2w ab}) \phi_z = 0 \quad (A-21)
 \end{aligned}$$

The right-hand sides of both equations are zero from theoretical considerations, because, at the natural frequency of a

lightly damped mode that is well separated from other modes, the applied force and system response are $\pi/2$ radians out-of-phase. This phase relationship was observed in the experimental data also. Note that the frictional shearing stiffnesses of the abutment wall, $(k_{2w} ab)$ and $(k_{3w} ab)$, were retained in the derivation. Equations similar to (A-20) and (A-21) were derived for the third-mode experimental response, which was similar to the deformation pattern observed for the second mode (See Figure 5 in text). Theoretically, these equations and equations (A-20) and (A-21) could have provided unique estimates of all stiffnesses. However, accurate estimates of some of the response variables for the third mode could not be obtained and thus, the equations were ill-conditioned to provide meaningful estimates of the stiffnesses. As indicated in the text the shearing stiffnesses of the wall are probably small, and so these terms were omitted from equations (A-20) and (A-21). Converting accelerations to displacements ($-\omega^2 v = \ddot{v}$, etc.), substituting the values of these displacements and the other parameters into the equations, and solving for the unknown footing stiffnesses yielded $(k_{2f} bc) = 2.2 \times 10^9$ N/m (1.5×10^8 lb/ft) and $(k_{3f} bc) = 5.3 \times 10^9$ N/m (3.6×10^8 lb/ft). These values are also listed in Table I in the text.

A similar procedure, involving the fifth mode shown in Figure 5, was followed to obtain an estimate of the wall stiff-

ness (k_{1w} ab) listed in Table I. The stiffness was computed assuming (k_{1f} bc) = 3.9×10^9 N/m (2.7×10^8 lb/ft).

Figure Captions

- Figure 1. Horsethief Road Undercrossing bridge.
- Figure 2. Location and orientation of the accelerometers and eccentric mass shaker. The arrows point in the direction of positive acceleration or positive shaker force.
- Figure 3. Shaker force versus frequency for the various longitudinal (x) and transverse (y) shaking tests.
- Figure 4a. Normalized displacement and phase responses observed on the deck during two transverse shaking tests. The circled numbers denote the accelerometers in Figure 2.
- Figure 4b. Normalized displacement and phase responses observed on one footing during two transverse shaking tests. The circled numbers denote the accelerometers in Figure 2.
- Figure 5. Normalized vector displacement responses of the Horsethief bridge observed during various tests at or near the natural frequencies. The numbers adjacent to the black dots denote the accelerometers;

values at the tips of some arrows denote the amount of displacement. The scale at the bottom of the figure is to be used for the arrows without the displacement values shown. A question mark (?) in the middle of a vector denotes an assumed, rather than measured, displacement.

Figure 6. Finite element model of the Horsethief bridge.

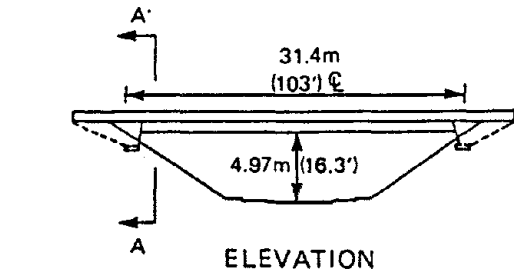
Figure 7. Natural frequencies and mode shapes computed by the finite element model. Selected mode numbers are identified in the top-left figure. Nodal translational displacements (x, y, z) are indicated in other figures.

Figure 8. Comparisons between observed (—) and computed (- - -) responses. The circled numbers denote the accelerometers in Figure 2.

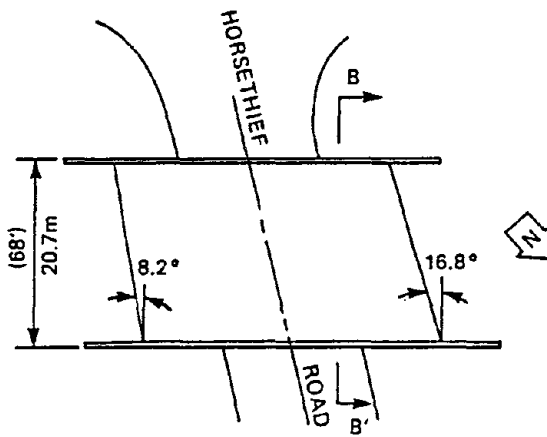
Figure 9. Comparisons between observed (—) and computed (- - -) responses. The circled numbers denote the accelerometers in Figure 2.

Figure A-1. Simplified model of Horsethief bridge.

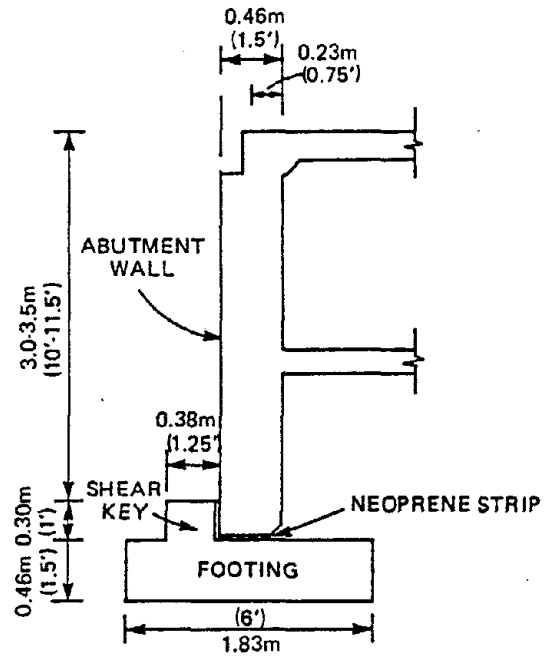
Figure A-2. Deformation shapes of the deck, wall, and footing assumed for the second mode of vibration.



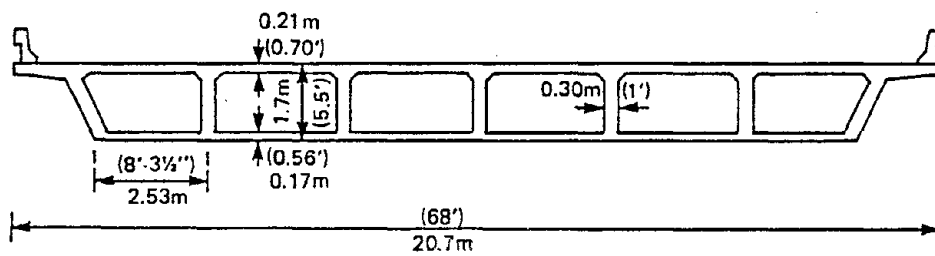
ELEVATION



PLAN



SECTION A-A' THRU ABUTMENT



SECTION B-B' THRU DECK

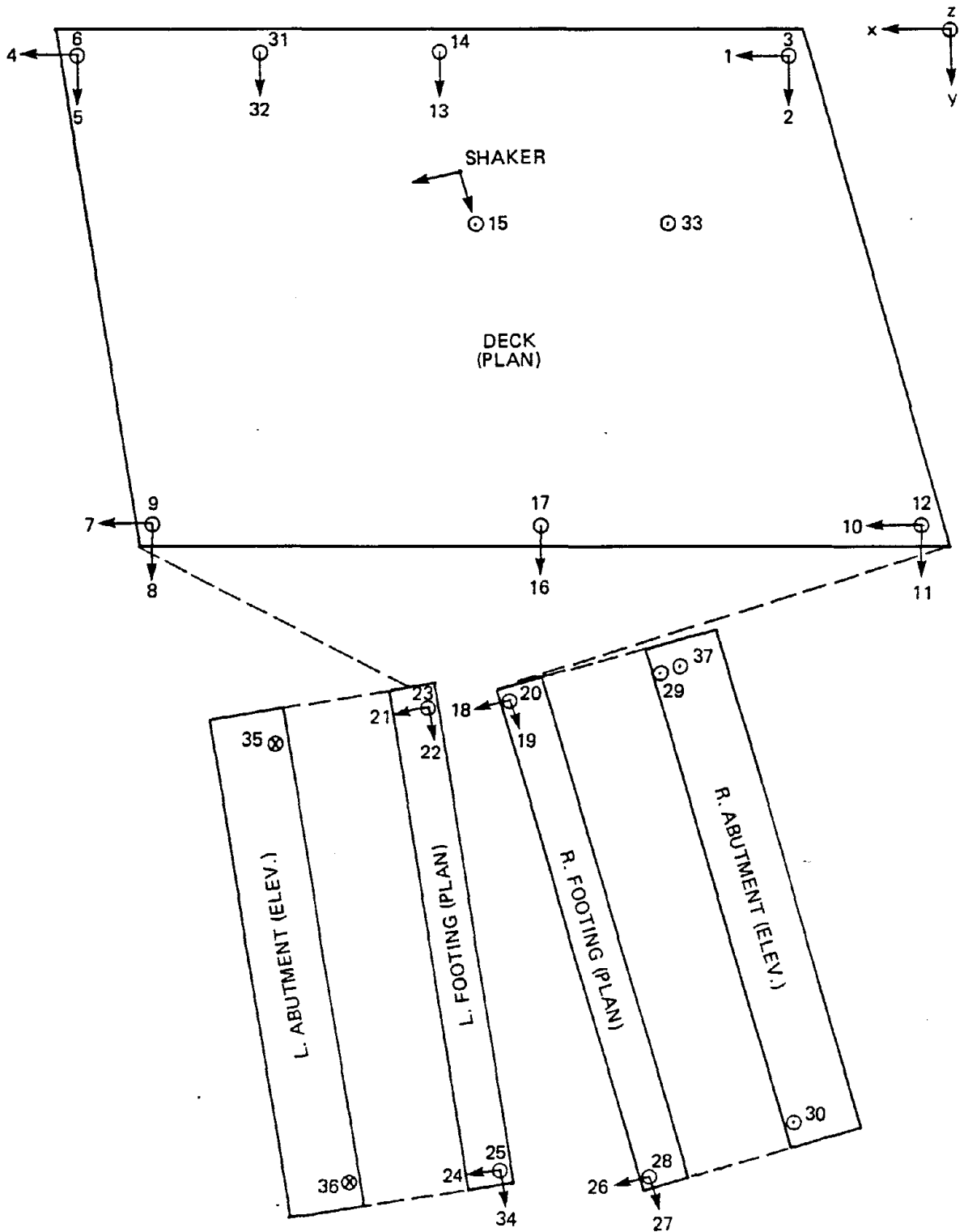


Fig. 2

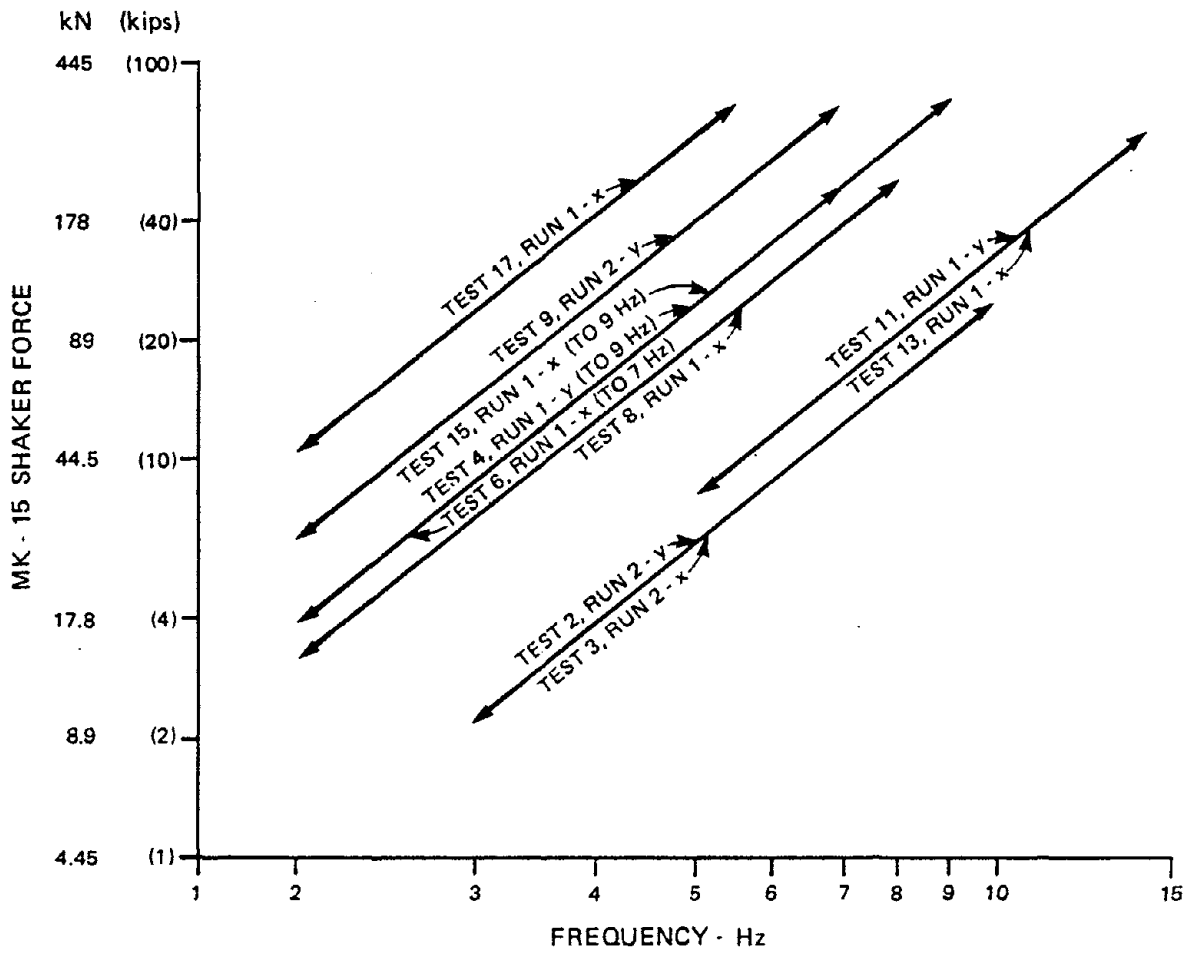


Fig. 3

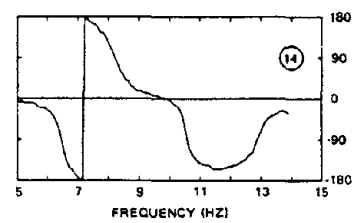
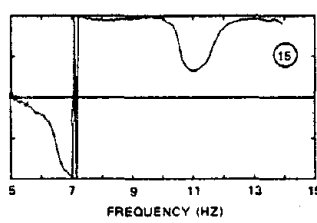
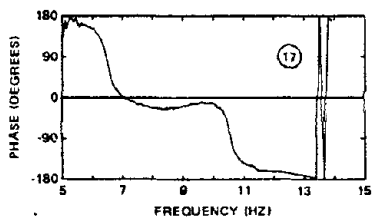
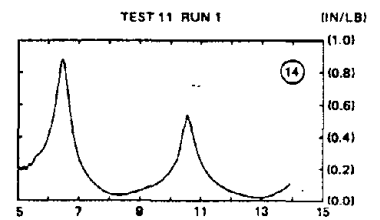
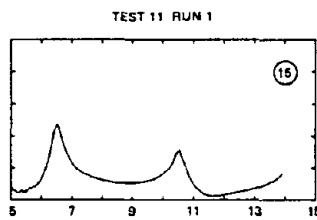
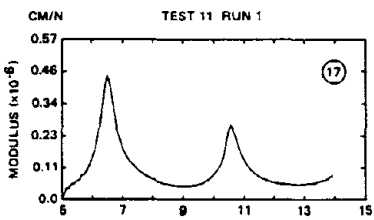
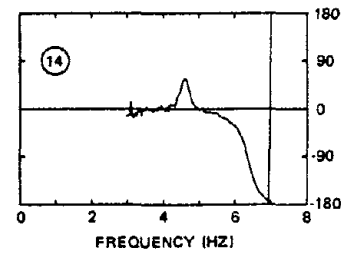
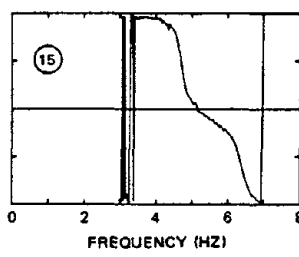
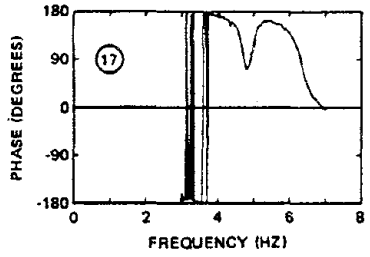
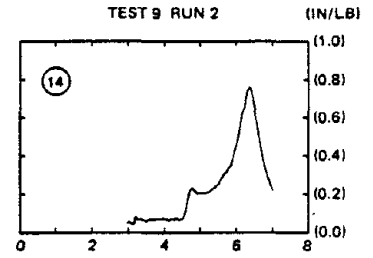
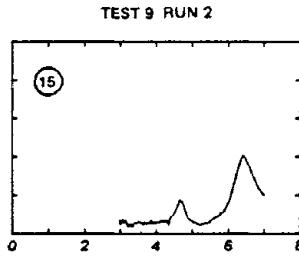
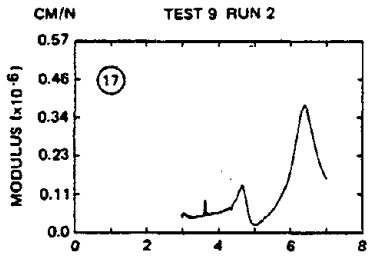
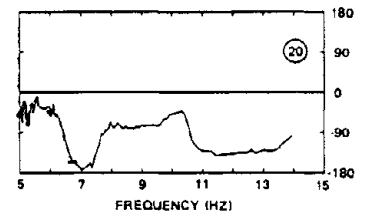
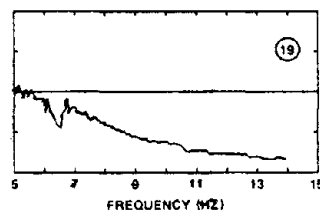
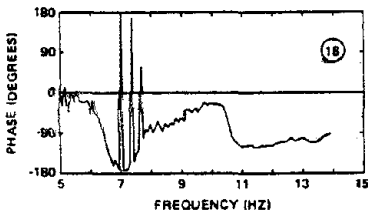
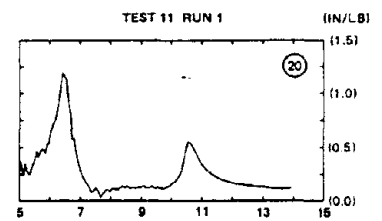
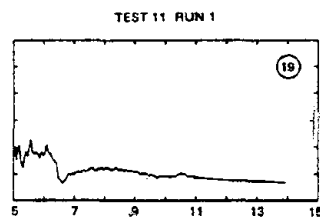
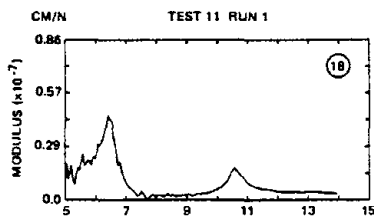
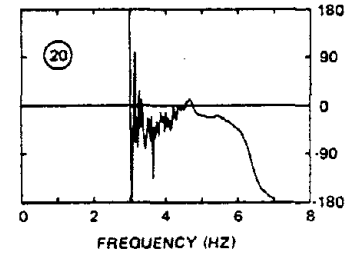
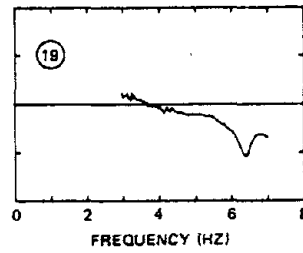
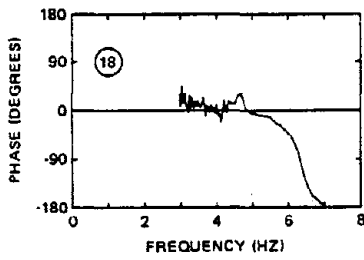
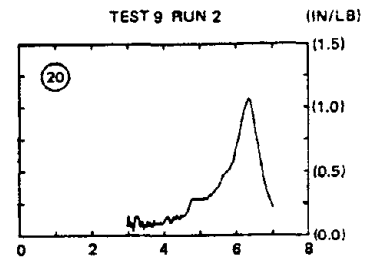
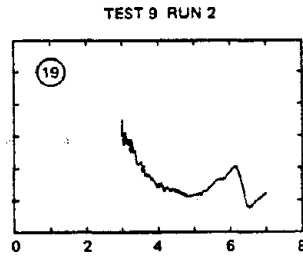
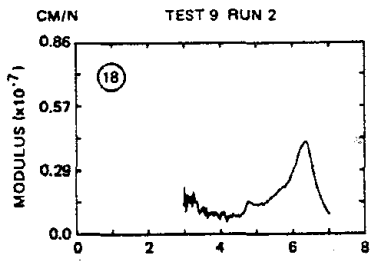


Fig 4a



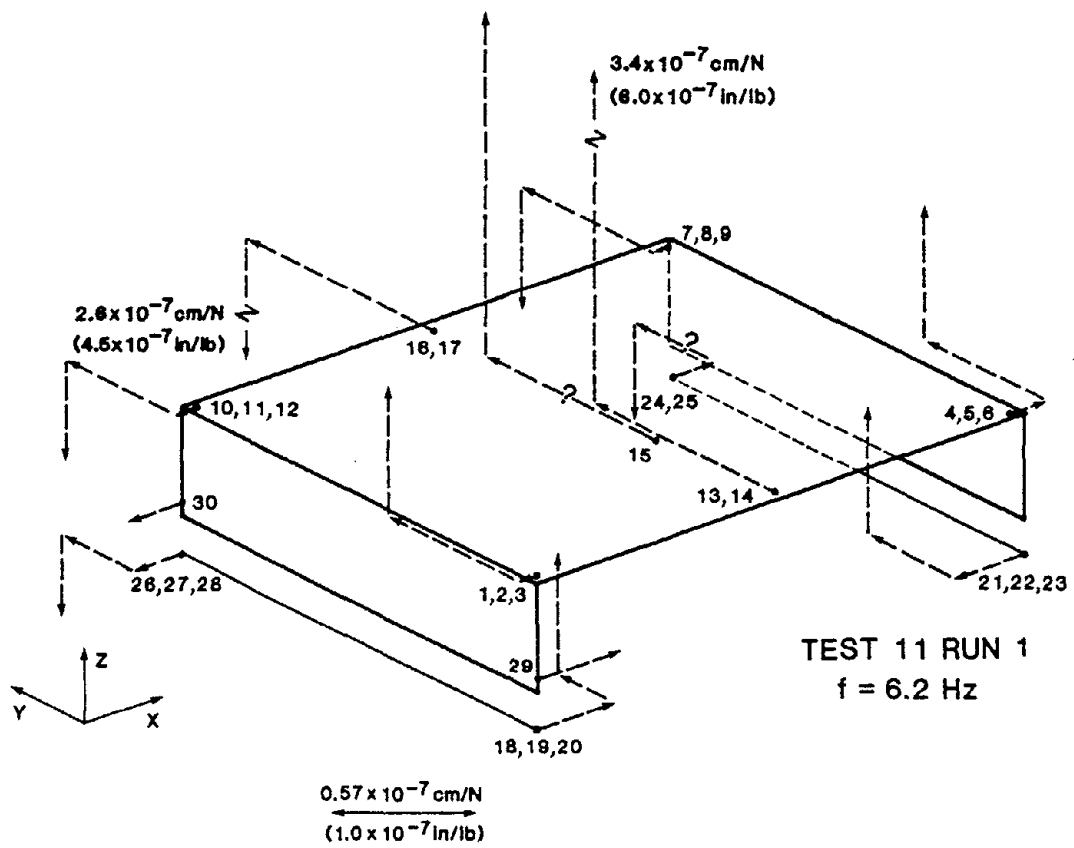
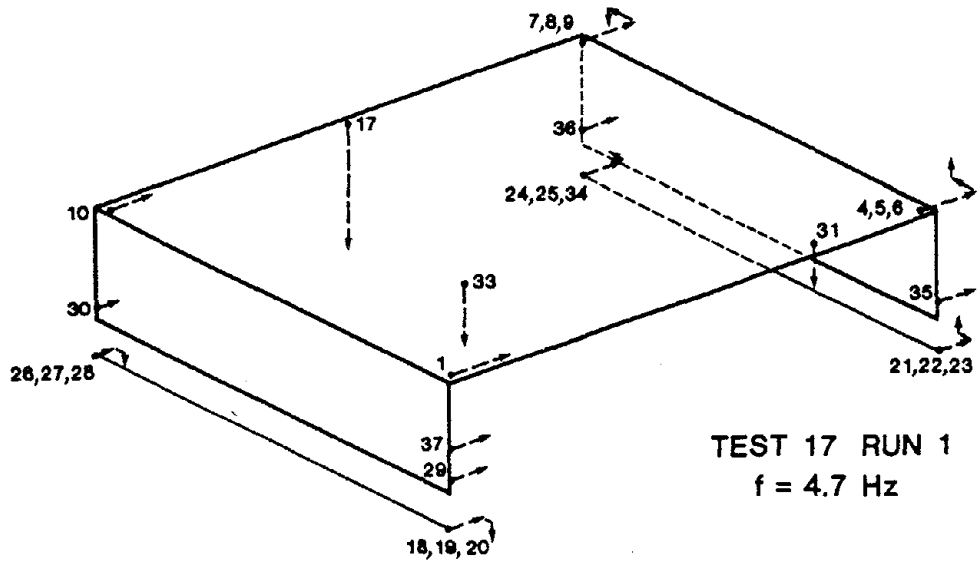
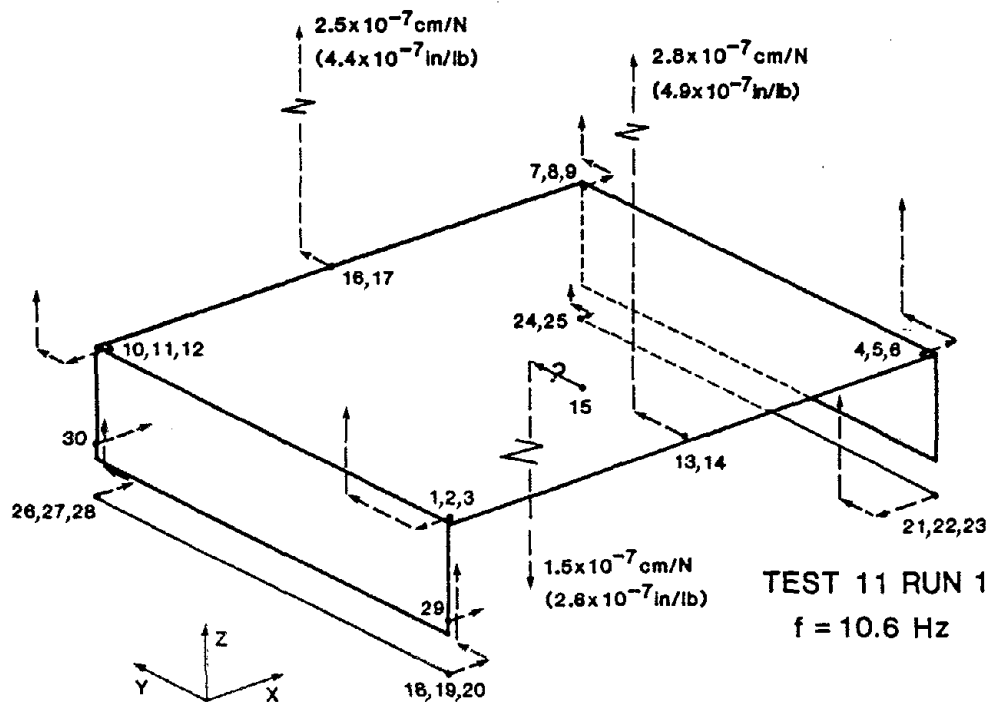
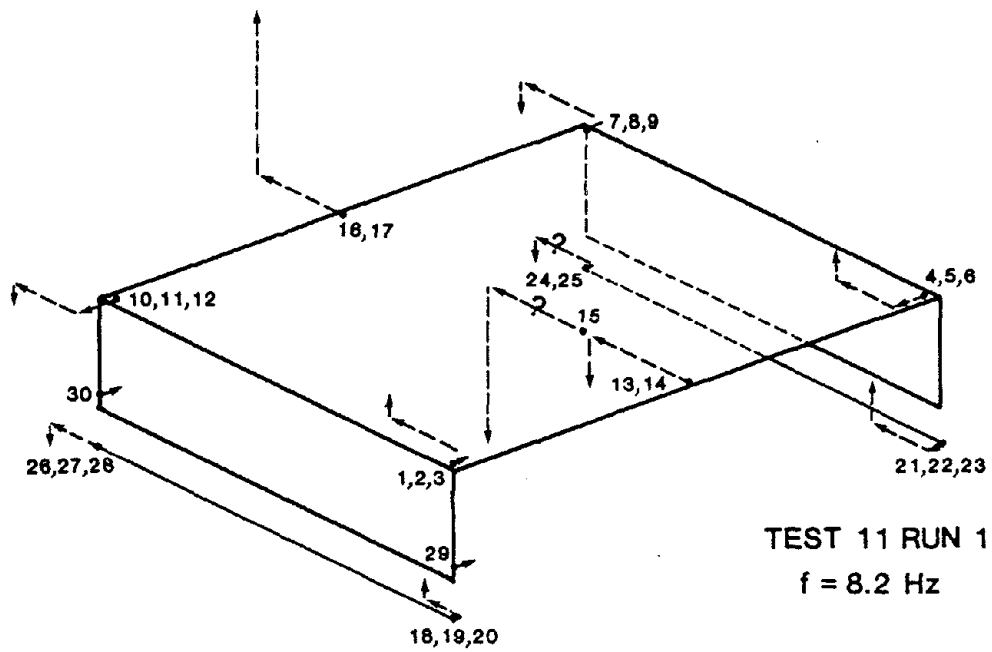
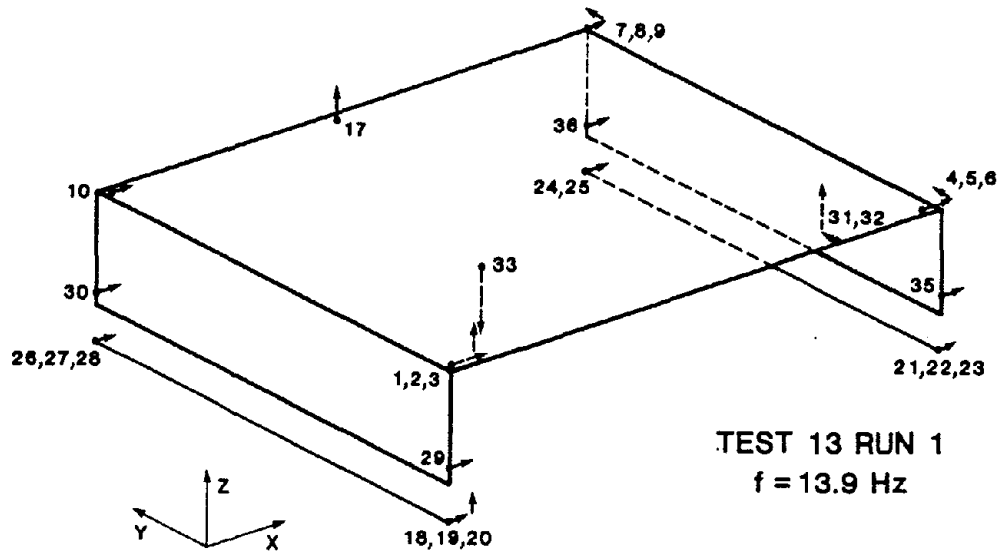


Fig 5



$0.57 \times 10^{-7} \text{ cm/N}$
 $(1.0 \times 10^{-7} \text{ in/lb})$

Fig. 5 (cont.)



$0.57 \times 10^{-7} \text{ cm/N}$
 $(1.0 \times 10^{-7} \text{ in/lb})$

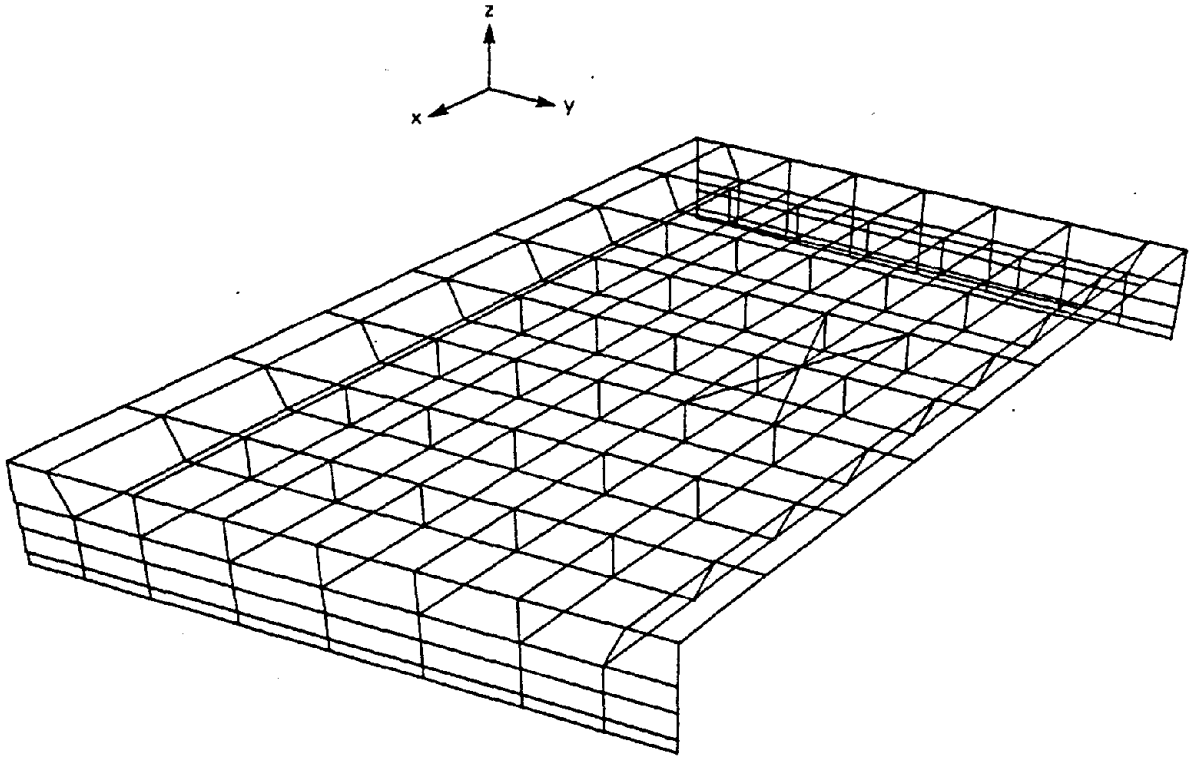


Fig. 6

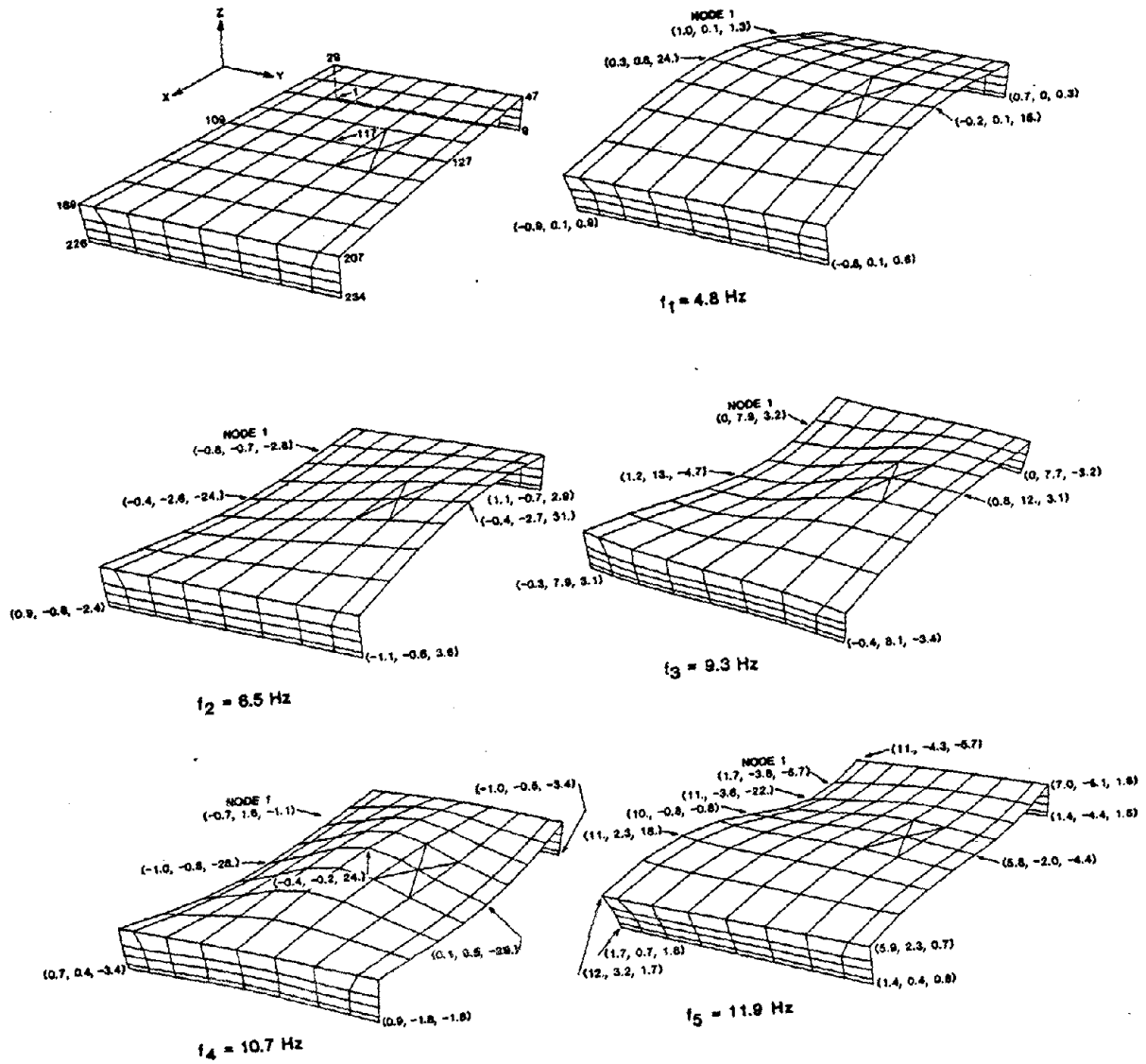


Fig. 7

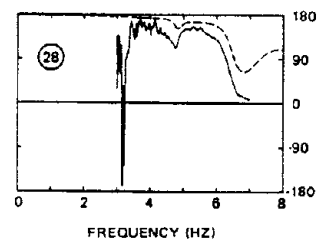
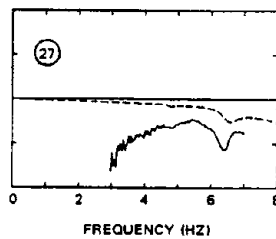
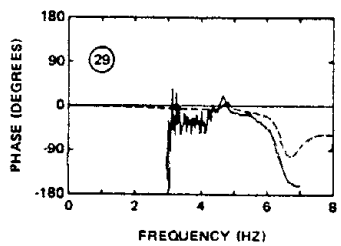
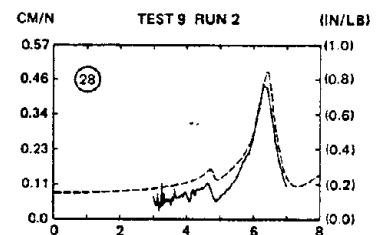
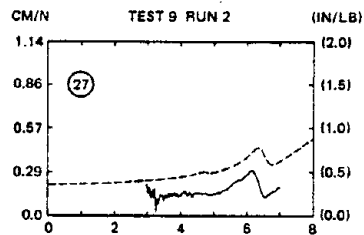
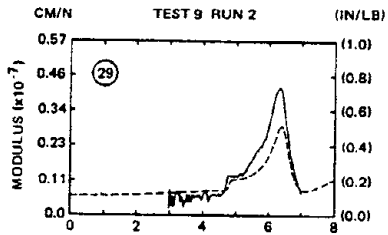
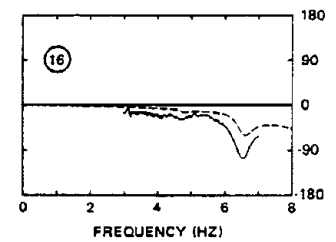
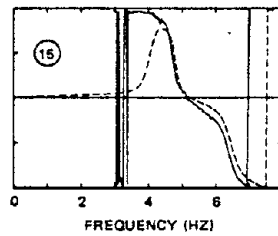
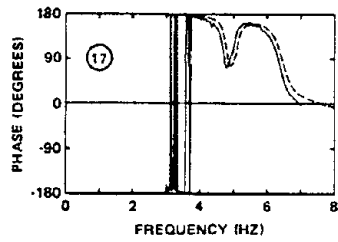
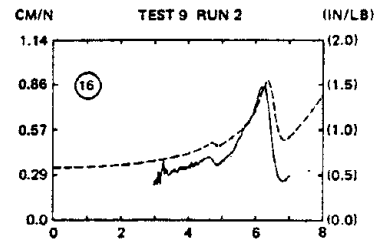
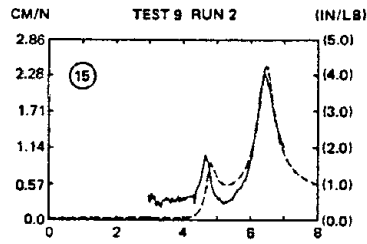
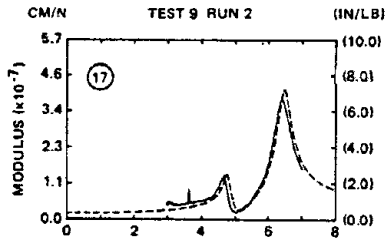


Fig. 8

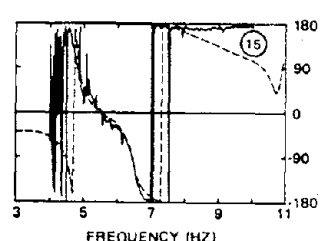
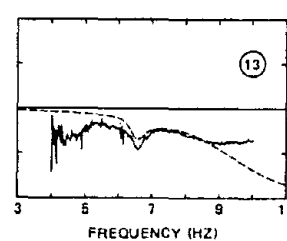
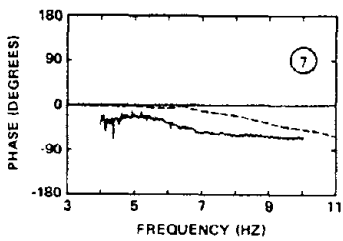
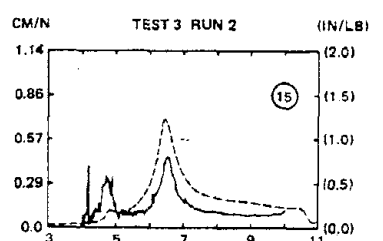
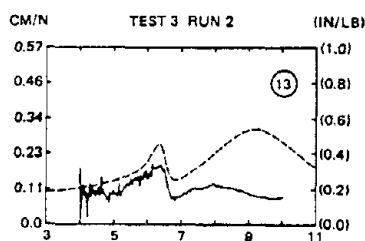
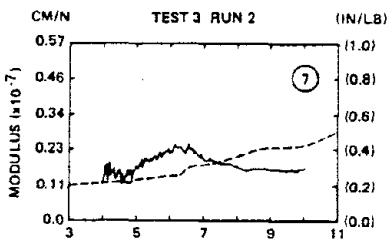
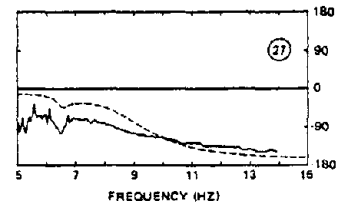
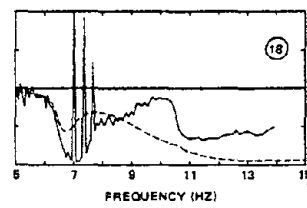
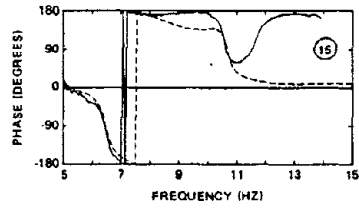
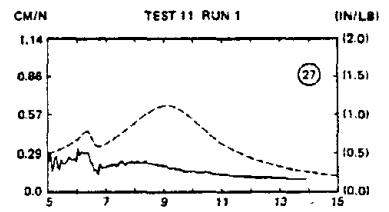
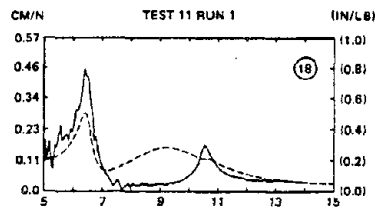
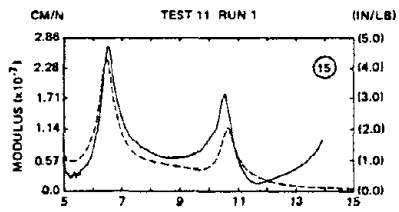


Fig. 9

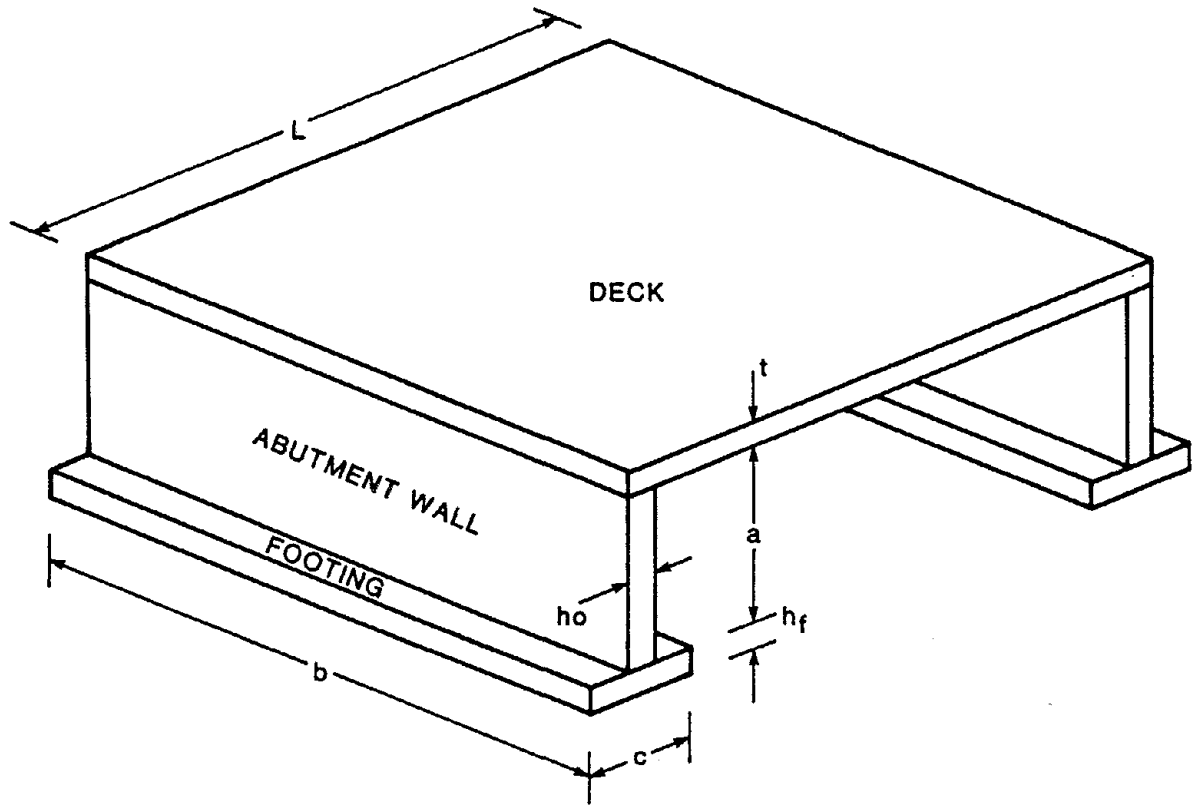


Fig. A-1

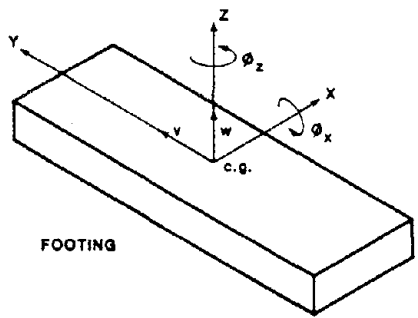
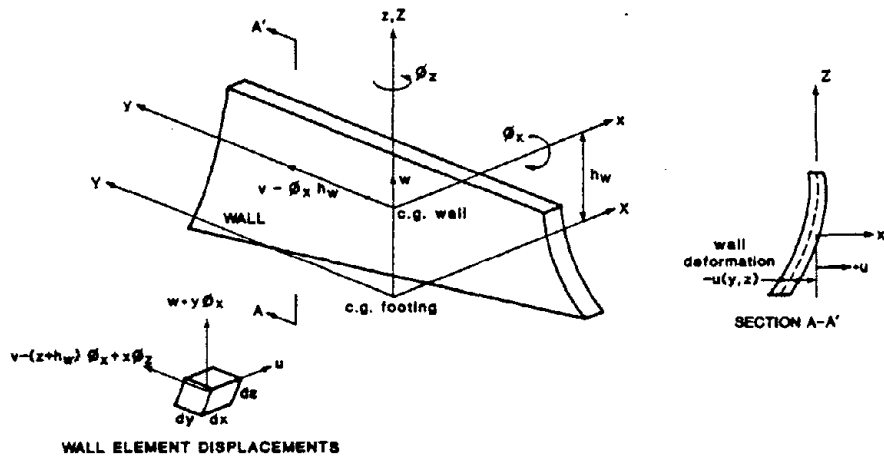
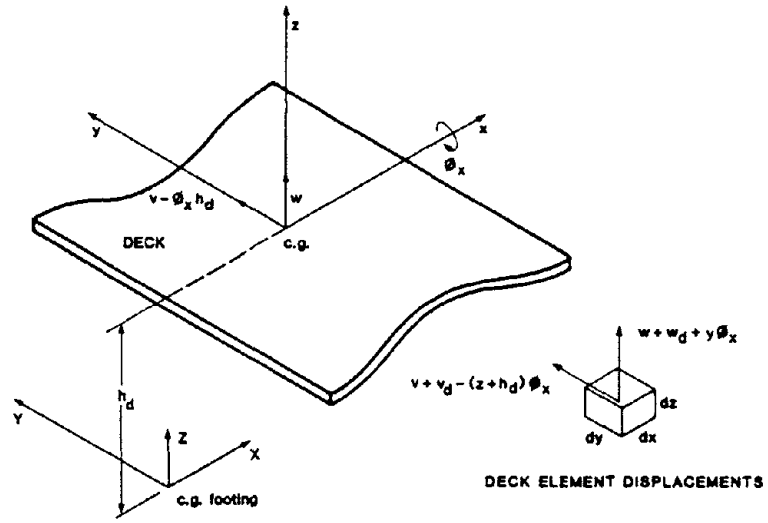


Fig. A-2

CENTRIFUGE TESTING OF A BRIDGE-SOIL MODEL

By Behnam Hushmand,¹ A.M. ASCE, C.B. Crouse,² M.ASCE,
John H. Wood,³ and Geoffrey R. Martin,⁴ M.ASCE

ABSTRACT

Centrifuge experiments, consisting of dynamic quick-release, earthquake simulation, and quasi-static cyclic push-pull tests, were performed on a 1/100 scale model of a single span bridge with monolithic abutments. The abutments were supported on Nevada silica sand, which was also used as the backfill. The responses of the bridge deck and abutment walls, which were measured by strain gauges, accelerometers and displacement and pressure transducers, were generally consistent with the results of field vibration tests performed on a prototype bridge. Measured abutment responses were also consistent with the results of nonlinear, two-dimensional finite element analyses, which were used to predict the neutral and passive static pressure distributions along the height of the abutment wall. Both the experimental and theoretical pressure distributions were largest at the mid-height of the abutment wall and generally smallest near the bottom. The dynamic pressure distributions observed during the quick-release and earthquake-simulation tests were similar in

-
- 1 Sr. Staff Engr., Earth Technology, Long Beach, Calif. 90807.
 - 2 Prin. Engr., Earth Technology, Long Beach, Calif. 90807.
 - 3 Lab. Serv. Engr., Ministry of Works and Development, New Zealand.
 - 4 Vice Pres., Earth Technology, Long Beach, Calif. 90807.

shape to the static distributions. The pressure distributions were different from those measured on simple retaining walls subjected to earthquake-like excitation in the centrifuge. These differences were mainly the result of differences in the boundary conditions between the abutment, which was integrally tied to the deck, and the retaining wall, which was free standing.

INTRODUCTION

The proper modeling of soil-structure interaction of bridges, particularly the interaction between the abutments and backfill soils, is an important aspect of the analysis and design of these structures to resist static and dynamic loads. Experimental testing of actual bridges in the field has provided information on the interaction between the bridge and the surrounding soil(5,6,7). However, some important details of the interaction phenomenon between the abutment and backfill soils, such as the active and passive pressure distributions or the lateral load-deflection behavior, were not obtained from these tests. Using full-scale testing methods to obtain this information is extremely costly and in many circumstances impossible. Conventional reduced scale modeling is often not a viable alternative because of the difficulty in modeling the stress conditions in the soil. These stresses can have a considerable effect on the soil's behavior (and hence the structure's behavior) under both static and dynamic loading.

Therefore, an attractive approach to study the behavior of soil-structure systems such as bridges is to conduct static and dynamic tests on a properly scaled model bridge in a centrifuge. In a centrifuge model, the unit weight of the soil is increased by subjecting the model to a centrifugal acceleration. When modeled to the correct scale under similar boundary conditions, the model experiences the same stresses as in the prototype. Although researchers have applied the technique successfully to various geotechnical problems including the related case of soil-structure interaction behavior of retaining walls⁽¹²⁾, no centrifugal modeling of bridge abutments subjected to static and dynamic loads has been published. This paper reports the results of such tests conducted in the Caltech centrifuge. The model was a single-span bridge with monolithic abutments supported on sand. This bridge was a 1/100 scale model of the Horsethief bridge, whose soil-structure response to forced vibration excitation was examined during a parallel study⁽⁵⁾.

CENTRIFUGE MODEL TESTING

In recent years centrifuge modeling has been recognized as a useful approach to physically model full-scale geotechnical problems. Complex geotechnical problems, such as soil-structure interaction of bridge abutments and foundations can be readily solved by the centrifuge modeling technique. Most soil proper-

ties depend on continuum stresses which are generally gravity-induced. Thus, in order to have the same stress conditions on soil elements at two homologous points in the model and prototype, the unit weight of the model material must be scaled properly to produce the same confining stresses. For a geometrically similar model N times smaller than its prototype, the relationship $\gamma_m = N\gamma_p$ is required where γ_m = the unit weight of the model material representing the soil, and γ_p = the unit weight of the soil in the prototype. This relationship can be achieved either by choosing a model material with a density N times the density of the prototype soil or by increasing the gravitational acceleration on the prototype soil at the model scale.

Soils have extremely complex stress-strain relationships. Under applied loads, they respond in a nonlinear elasto-plastic regime and their behavior may also be anisotropic and dependent on density, water content, stress level, stress path and strain rate. So far, it has been impossible to find a material with: (1) a stress-strain behavior similar to a soil, and (2) a much higher mass density. Therefore, it is more convenient to use prototype soil, but to increase the gravitational acceleration by the lineal scale factor N . Thus, if a 1/100 scale model, made of the same material as the prototype is subjected to a gravitational acceleration 100 times that of the prototype, the confining stres-

ses, and thus the properties and behavior of the model, are the same as in the prototype. A centrifuge is a machine that can provide model gravity to properly reproduce the confining stresses in the prototype(3,13,15). A detailed discussion of static and dynamic centrifuge modeling techniques and derivation of scaling relationships can be found elsewhere(14,15). In the experiments described here, a 1/100 scale model bridge was constructed which approximately simulated the Horsethief highway bridge located approximately 24 km south of Corona, California. This bridge, a single span, reinforced concrete, box-girder structure, was selected for centrifuge modeling because its material and geometric properties, its dynamic behavior, and the in situ characteristics of the surrounding soil were established in a concurrent investigation,(5). Furthermore, the abutment of this bridge is typical of many bridges in the United States, especially California.

In addition to tests at 100g centrifugal acceleration, which simulated the Horsethief bridge, tests were also performed at 50 g, and 87.5 g to simulate other prototype bridges with linear dimensions of 50 and 87.5 times the model's linear dimensions. All tests provided a broad range of information on the behavior of different sizes of prototype bridge-abutment/backfill-soil systems and an extensive data base for the calibration of numerical models.

TEST EQUIPMENT AND PROCEDURE

The testing was conducted with the model A1030 Genisco centrifuge, located in the Civil Engineering Department of the California Institute of Technology. A thorough description of this centrifuge can be found elsewhere⁽¹⁶⁾. The capacity (payload) of the centrifuge is about 44,500 g-N (10,000 g-lbs), which means that at a centrifugal acceleration of 100 g, for example, the maximum weight that the model structure, soil and container can be is about 445 N (100 lbs).

A 1/100 scale model of a bridge similar to the Horsethief bridge was constructed (Figure 1) of aluminum. The mass, moment of inertia, and flexural stiffness values were chosen such that the model properly simulated the Horsethief bridge. The box section of the prototype superstructure was modeled by a ribbed slab milled out of a solid piece of aluminum plate. An exact representation of the box section would have been difficult to make, and it was not considered necessary for the purposes of this study. The flexural stiffness of the model superstructure was verified experimentally by applying a vertical line load at the center of the deck, while it was simply supported at the ends, and measuring displacement of the deck as a function of the applied load.

The weight of the model bridge was 8.9N (2 lb), which implies that the prototype model simulated during the 100g tests weighed 8.9×10^6 N (2,000 kips). Because the model was constructed of aluminum and because of the width limitation of the bucket, this prototype weight was 20 percent less than the weight of the Horsethief bridge, which, for the purposes of this study, is considered to be an insignificant difference.

The size of the centrifuge bucket was 56 cm x 18 cm x 25 cm (22 in x 7 in x 10 in) with a front glass wall at the end of the centrifuge arm. Because of the width limitations of the shaker bucket used to contain the model in the centrifuge, the width of the model was made to coincide with the width of the bucket (18 cm). At 100g, this corresponds to a prototype width of 18 m (59 ft), versus the actual width of 21 m (69 ft) for the Horsethief bridge. Thus, the model was essentially restricted to two dimensional behavior in the vertical and longitudinal horizontal directions. The model bridge-soil system within the bucket is shown in Figure 2. Note that the model approximately simulates the most salient features of the prototype, such as the bridge, abutment-backfill soils, foundation subsoil, the bridge undercrossing road, and side slopes. The chronology of the construction (Figure 3) was as follows. First, dry sand with the required density was placed in the centrifuge bucket to a prede-

terminated depth up to an elevation of the undercrossing road surface. Next, a wooden block built to the shape of the road surface and its side slopes was placed on the soil surface in the center of the bucket along its width. Soil was placed on each side of the wooden block and compacted to the required density up to the elevation of the bridge footings. The wooden block was then removed and the model with its transducers was placed on the soil surface on top of the slopes. Next, soil was placed behind the abutment walls up to the deck surface and compacted to the required uniform density.

The type of soil used was Nevada 120 silica sand (Nevada Fine Sand-NFS). This sand in its well-compacted condition (medium dense to dense) is similar to the prototype cohesionless soil material adjacent to the Horsethief bridge abutment and foundation. Shear-wave velocities in the range of 210 m/sec (690 ft/sec) to 247 m/sec (810 ft/sec) for NFS in its dense condition (dry unit weight of 1.65×10^4 N/m³ (105 pcf)) at a confining pressure of 55 kPa to 83 kPa (8.0 psi to 12.0 psi) were measured in resonant column tests⁽⁹⁾. These confining pressures are expected at a soil depth around 3 m (10 ft).

The response of the bridge model during the testing was measured with 6 miniature pressure transducers (Entran Devices, Inc., Model EPB6-125U-50a), 2 to 4 miniature accelerometers

(Entran Devices, Inc., Model EGA-125f-500d), 6 strain gauges (Micromeritics, Model CEA-13-062UW-350), and one photo diode displacement transducer (United Detector Technology, Inc. Model PIN-SC110D). The locations of the transducers are shown in Figures 1 and 2. Pressure transducers were mounted at different heights at the center of the abutments. Accelerometers were located on the bucket floor, on the roadway under the bridge, and at different locations on the bridge. On each abutment wall and at the center of the bridge deck, two strain gages were mounted to measure the flexural deformation of the abutments and the deck. One displacement transducer was mounted at the center of bridge deck to measure horizontal movement of the bridge. In addition, load cells were used to measure the applied force on the model bridge during quick release and cyclic push-pull tests. Pressure transducers, accelerometers, displacement transducers, and load cells were carefully calibrated before the tests. Because of soil-structure interaction effects between the transducer and the soil, the calibration of pressure transducers to measure absolute pressure is difficult, and consequently, the measured absolute values were not considered reliable⁽⁹⁾. However, relative pressure values and consequently pressure distribution shapes along the height of the abutment wall were reliably measured.

Signals from the transducers were amplified and filtered to eliminate high frequency noise, passed through slip rings, and then recorded digitally by a high speed analog-to-digital converter (ADC) and a microcomputer system.

During some phases of the testing, the containment bucket, which was suspended from a rigid frame, was slowly moved in a direction tangential to the arm of the centrifuge by a servo controlled electro-hydraulic piston⁽⁹⁾. Thus, by restraining the movement of the bridge, static or slow loading tests, and subsequent quick-release tests, were easily performed.

Dynamic and quasi-static tests, consisting of quick release, earthquake simulation and cyclic push-pull, were performed on the model. The quick-release (snap) tests were conducted by applying a tension force to a nylon string. One end of the string was attached to a small block mounted in the center of the bridge deck, and the other end was attached to a stationary frame that held the soil bucket. As described above, movement of the bucket created the tension force in the string. The string was aligned parallel to the centerline of the bridge deck, and the applied tension was measured by a load cell. The quick cutting of the string by a sharp knife released the string tension and set the bridge model into free vibration. The knife was powered by an air piston and was activated by an electric pulse to a solenoid

valve. A diagram of the quick-release mechanism is presented in Figure 4.

Earthquake simulated shaking of the soil bucket and the model bridge was accomplished by an electro-hydraulic system capable of generating random shaking of the bucket in the frequency range of real earthquake-induced vibrations. A microcomputer, MTS controller, and servo-valve controlled the shaking process by sending the earthquake-simulating signal from the computer to the MTS controller and then to the servo-valve that controlled the flow of highly pressurized oil to the piston under the bucket.

During cyclic push-pull tests of the model bridge against the abutment-backfill soil, a horizontal force was applied parallel to the centerline of the bridge deck. The bridge model was fixed to the stationary frame by a stiff rod attached to the bridge deck. The soil container was then moved relative to the stationary frame, which resulted in a push-pull force on the model. The applied force was measured by a load cell on the connecting arm between the rigid frame and model.

RESULTS

Dynamic Tests. Results of the quick-release tests are presented in the form of graphs showing: the load-displacement behavior of the bridge-abutment, backfill-soil system prior to the quick

release; Fourier Amplitude Spectra (FAS) of the free vibration data; and, the dynamic pressure distribution as a function of height along the wall. A typical plot of the load-displacement behavior of the model bridge up to the load at release during a 50 g test is shown in Figure 5. The load-displacement behavior is smoothly nonlinear up to the prototype release load of approximately 375KN (84.3 kips), which was about 34 percent of the prototype bridge weight.

Figure 6 presents selected FAS plots of the transient signals at the prototype frequencies after quick release for three different tests at centrifugal accelerations of 50 g, 87.5 g, and 100 g. The FAS plots are for the translational acceleration and flexural strain in the middle of the bridge deck and the pressure and flexural strain near the center of the right abutment wall. Comparison of the FAS for each test illustrates an obvious similarity and consistency in the number and relative location of each resonant peak. These peaks are definitely associated with the modes of vibration of the bridge-soil system and are not the result of the spurious bucket vibration, which was small. The peaks occur at different frequencies during the 50 g, 87.5 g, and 100 g tests, because each test simulates a different prototype condition. The 50 g tests simulate a smaller bridge with higher flexural rigidity and lower mass, which results in higher natural frequencies compared to those from the 87.5 and 100 g tests.

The following discussion concerns only the interpretation of the modes of vibration observed during the 100 g tests because these tests simulated the Horsethief bridge. Similar interpretations are valid for the results obtained from 50 g and 87.5 g tests. The lightly damped mode observed at 5 Hz in the FAS for the 100 g test results involves considerable flexure of the bridge deck and abutment walls. This frequency is clearly observed in FAS plots of the wall-backfill contact pressure, and the flexural strains in the center of the abutment wall and deck. The mode corresponds to the fundamental bending mode (4.7 Hz) of the Horsethief bridge, which was obtained during the field tests⁽⁵⁾. The lightly damped mode observed at about 9.8 Hz also indicates bending deformation of both the bridge deck and abutment walls. This mode may correspond to the fourth mode of the Horsethief bridge at 10.6 Hz, which involved the fundamental bending mode of the deck in the longitudinal direction and a higher bending mode of the deck and abutment walls in the transverse direction.

The second vibration mode of the Horsethief bridge at 6.4 Hz was the primary twisting mode of the structure, while the third mode at 8.2 Hz involved considerable soil-structure interaction in the transverse direction and was moderately damped. These two modes could not be fully excited in the model tests for two reasons: (1) the pulling force was applied along the centerline

of the bridge in the longitudinal direction; and (2) the test specimen was a two-dimensional approximation of the three dimensional prototype. However, because perfect alignment of the force direction and the two-dimensional modeling of the prototype could not be precisely achieved in such a complex experimental arrangement, the second and third modes of the bridge-soil system may have been excited to some degree. The higher damped mode at 7.2 Hz may represent the primary translational soil-structure interaction mode (8.2 Hz) of the Horesthief bridge. This mode is observed in the FAS plots for the deck acceleration and for the pressure and strain in the wall; it is not observed in the FAS plot for the deck strain. This latter observation is consistent with the results obtained from the field tests which show very little flexural motion (and hence small strain) in the center of the deck. The small peak at a frequency of 5.9 Hz, observed in the FAS plot of the deck and wall strains, may correspond to the savmary twisting mode of the Horsethief bridge deck at 6.4 Hz. The deformation shape of the Horsethief bridge deck in this mode is similar to the deformation shape in the third mode, and consequently, it also has little or no flexural strain in the center of the deck, which is consistent with the data in Figure 6.

Because the number of transducers used in the experiment was not adequate to completely define the mode shapes of the model beyond the first mode, other interpretations of the higher-mode peaks in the FAS cannot be dismissed. However, it is interesting to note that the data are fairly consistent with the field-test results which provides some measure of confidence in the centrifuge modeling.

The dynamic pressure distributions during the quick release tests were generally the same shape along the depth of the abutment. A typical distribution during a 100 g test is shown in Figure 7. Note that the absolute pressure values are approximate because of the calibration problems discussed earlier in the text. However, the relative pressure values are accurate and consequently the pressure distribution configurations are reliable. Note also that the pressure distributions are based on measurements from only three pressure transducers along the depth of the wall, and consequently, these estimated pressure distributions are a rough approximation of the actual distributions. Nonetheless, as shown in Figure 7, and other similar figures, the largest pressure occurs near the mid-depth of the abutment wall. All three pressures along the wall reach their maximum value at the end of the first half cycle of vibration when the displacement of the top of the abutment wall was maximum. Most of

the contribution to the total pressure is due to the effects of gravity. The incremental pressure from the lateral tension load prior to the quick release and the incremental maximum dynamic pressure are much smaller. However, these incremental distributions are similar in shape to the pressure distributions from gravity effects only.

The highest shaking frequencies induced during the earthquake simulations were slightly less than the fundamental frequency of the bridge-soil system. Thus, the natural modes of vibrations were not excited to any significant extent. However, useful information regarding the pressure distribution on the abutment wall was obtained. Figure 8 shows the time-histories of the bucket acceleration, deck displacement, and pressures at the three locations on the abutment wall during a 100 g test. As expected, the time intervals of strong motions and pressure responses coincide. The time during the strong shaking when the pressures were largest is indicated in Figure 8 as a dashed line through the time histories at about 17 sec. The pressure profile at this time, and the static gravity-induced pressure profiles, are shown in Figure 9. These distribution shapes are similar to the ones observed during the quick release tests (Figure 7), except that the incremental maximum dynamic pressures are comparable to the gravity-induced pressures prior to shaking. Also,

the effects of the shaking caused the gravity-induced pressures to increase by about 30 to 50 percent after the shaking ceased. A comparison of Figures 7 and 9 reveals substantial differences in the gravity-induced pressures between the two tests. This difference can only be attributed to the effects of testing on the contact condition between the abutment wall and backfill soil. Presumably, this condition was affected by densification and/or loosening of the soil and possibly undetectable permanent offsets of the bridge during the testing. These observations further underscore the importance of the nonlinear abutment-backfill behavior, which depends not only on the magnitude of the applied load, but also, apparently, on the loading history.

Quasi-Static Cyclic Push-Pull Tests. Results of these tests are represented by load-displacement plots and pressure distribution diagrams for different stages of loading during the 50 g, 87.5 g and 100 g tests.

Figure 10 presents the load-displacement curves for the three tests at the prototype scales. Note that the prototype shapes and material properties are similar but only their dimensions are different. Variations of the abutment-backfill stiffness properties resulting from changes in the prototype size are clearly illustrated in the figure. The initial slopes of the load-displacement curves, which equal the low-strain stiffness between

the abutment and backfill soil, increase as the prototype size increases. This stiffness increase is the result of the increase in confining pressure of the backfill soil. Figure 11 presents the prototype load-displacement behavior of the bridge-soil system under the application of many load cycles during tests at 87.5 g. Figure 11a shows that, under successive constant amplitude cyclic loading, the inelastic deformation and energy dissipation per cycle decrease and finally reach a stable value. The slopes of the cyclic curves, however, do not change considerably (soil stiffness does not change appreciably). The initial load-displacement cycles do not form closed loop cycles, which suggests that the backfill-soil was densifying during the application of a large number of small to medium amplitude load cycles. In Figure 11b, the amplitude of the applied load increases during each successive cycle resulting in an increase in the inelastic deformation and energy loss of the bridge-soil system. This is a common characteristic of load-displacement (stress-strain) behavior of nonlinear inelastic materials.

Figure 12 shows the prototype pressure distribution diagrams, for the 50 g, 87.5 g, and 100 g tests, along the depth of the abutment wall during successive stages of lateral loading against the backfill soil (the pushing quarter cycle of loading). The initial static pressure distributions prior to lateral loading

are also plotted (curves corresponding to $L = 0$). The maximum lateral loads applied during the 50 g, 87.5 g, and 100 g tests were approximately 56%, 34%, and 32% of the respective prototype bridge weights. During lateral loading the pressures consistently reached their maximum values near the center of the wall, a result which is consistent with the pressure distributions measured during the dynamic tests.

FINITE ELEMENT MODELING

One of the objectives of this study was to evaluate the appropriateness of an existing analytical procedure to predict the load-displacement behavior and pressure distribution on bridge abutments during lateral loading. The finite element computer program, DIRTMOD, which was developed from the program DIRT II⁽⁸⁾, was used as the finite-element code for this purpose. DIRTMOD is a nonlinear static finite element code which can include various nonlinear soil models. The variable modulus, effective stress, soil model⁽¹¹⁾ that was selected for this study has been successfully used in the past for modeling sand behavior. More recent, and perhaps improved, models of sand behavior^(1,2,10,18,19) have been developed but they have not been included in the DIRTMOD program. The general features of the variable modulus soil model are: (1) a shear modulus that varies as a function of confining stress, shear-strain amplitude, and

the stress history (loading and unloading), and (2) a bulk modulus that depends on the shear-strain amplitude during loading and is constant during unloading. Parameters for the variable modulus model were estimated from the results of the direct shear and resonant column tests performed on NFS at about the same density of the NFS used in this study⁽⁹⁾. A constant bulk modulus was assumed throughout the nonlinear analyses. The model parameters were changed slightly to obtain a better fit between theoretical and experimental results. The finite element mesh used to simulate the centrifuge tests is shown in Figure 13. A two-dimensional, plane-strain analysis was performed, which was considered to be a realistic representation of the centrifuge tests. Initial runs using a linearly elastic soil model were performed to study the effects of: (1) different boundary conditions at the interface between the soil and bucket end walls, and (2) different interface conditions between the backfill soil and bridge abutment and between the footing and supporting soil. Figure 14a shows the variations in the total pressure distributions on an abutment wall when only gravity loads are acting and when bonded and frictionless contact conditions are assumed at the interface between the soil and bucket wall. Although appreciable differences between the two pressure distributions are observed near the top half of the wall, the shapes of both distributions are similar. The negative pressures indicating

tension at the interface between the abutment and adjacent soil elements result from the assumption of a perfectly bonded contact between these elements for these runs. The percentage difference between the two pressures decreases when large compressive lateral loads are applied.

The effects on the pressure distribution from using three different element types to model the interface conditions between adjacent abutment and backfill elements, were also examined. These elements are: (1) contact element - free (frictionless) condition, (2) contact element - bonded condition, and (3) spring element. Both contact elements can model separation of the two contact surfaces in the direction normal to the plane of contact. In the tangential direction a free or bonded condition is assumed. Figure 14b presents the effects of abutment-soil interface conditions on the contact pressure distribution. The effects of the interface conditions are minor except near the top of the abutment walls. However, the overall lateral stiffness of the system is affected, which is apparent by comparing the loads (corresponding to the different interface conditions) that are required to produce the same deck displacement (see insert box in Figure 14b). The uncertainty in the stiffness could have been reduced if a more realistic contact element, capable of modeling the frictional behavior at the abutment-soil interface, had been available in the DIRTMOD program.

The boundary conditions employed in the subsequent nonlinear analyses of the bridge-soil system were: (1) a bonded contact condition between the soil and bucket walls, and (2) spring elements for the soil-abutment and soil-footing interfaces. From the standpoint of predicting pressure-distribution shapes, the choice of the interface elements was not critical. Spring elements were selected because the use of the contact elements introduced some problems in the convergence of the solution. Typical pressure distribution diagrams on abutment walls at different stages of loading (pushing monotonically against the backfill) are shown in Figure 15. Also shown is the Rankine static pressure distribution for a rigid wall. The calculations were performed at model scale and simulated the 50 g tests. A pronounced similarity exists between the shapes of the predicted and measured pressure distributions (compare Figure 15 with Figures 7, 9, and 12).

A final series of calculations was performed to determine whether the load-displacement curves obtained during the cyclic tests at the three different centrifugal accelerations could be predicted by the finite element method using the variable modulus model. Figure 16 presents the comparisons between the predictions and observations at the model scales. Excellent agreement is observed between the predicted and experimental results up to

loads equal to approximately 30 percent of the model bridge weight, which is equal to about 445 N (100 lb), 779 N (175 lb), or 890 N (200 lb) at 50g, 87.5g, or 100g, respectively. Initial slopes of the load-displacement curves (small displacement stiffnesses) are also in good agreement. The fact that the finite element model approximately predicts the results of the tests at all three model scales, suggests that the model can be used to successfully predict the behavior of any size prototype in the small to moderate ranges of loads and displacements. However, large displacement nonlinear behavior of the bridge-soil-abutment system is poorly predicted. A better prediction for the large displacement behavior of the bridge-soil system can be obtained by choosing a new set of model parameters for the soil at these displacements. However, the good agreement previously achieved for small displacement behavior of the bridge model will be sacrificed to some extent. The major reasons for the inability of the finite element model to predict the test results over a wide displacement range were: (1) the soil model did not adequately simulate the volumetric behavior of the sand because the bulk modulus did not vary with confining pressure; (2) variation of bulk modulus with strain amplitude was not considered; (3) the structural fabric and density of the backfill soil changed during cyclic push-pull tests at different g levels; (4) the stress history of the soil could not be modeled in the analyses; and (5)

the interface conditions between soil, bucket walls, and bridge abutments and footings could not be modeled correctly.

CONCLUSIONS

The feasibility of conducting centrifuge tests to determine the behavior of a bridge-soil model was demonstrated during the investigation. The overall dynamic response of the system was generally consistent with the results of vibration tests performed on the prototype Horsethief bridge. During cyclic lateral loading of the bridge abutment in which the maximum force in each cycle was constant, the stiffness of the abutment-soil system increased slightly and the hysteretic energy loss per cycle decreased considerably. This behavior is probably the result of the progressive densification of soil adjacent to the abutment wall during each cycle of loading. When the load was progressively increased with each cycle, the inelastic deformation and the energy loss per cycle increased. These results are consistent with the results of other laboratory soil tests used to determine the strain-dependent stiffness properties of soils below the strains at which gross failure or significant stiffness degradation of the specimen occurs.

From the standpoint of design of bridge abutments, one of the significant results of this study was the identification of the

gross shape of the pressure distributions along the depth of the abutment wall during dynamic and static loading. During both types of tests the pressures were consistently greater near the middle of the wall. The pressure profiles predicted from a static finite element program, DIRTMOD, were consistent with these observations. These results differ from those of Ortiz, et al⁽¹²⁾, who performed dynamic centrifuge tests on a cantilever retaining wall. Their results consistently showed that pressure distributions gradually increased from the top to the bottom of the wall. The differences in pressure distributions obtained from tests on two similar structures (bridge abutment and retaining wall) arise mainly from differences in the geometry between the two models and its influence on the behavior. Probably the most significant difference is the constraint or boundary condition at the top of each structure. The retaining wall is free standing, whereas, the abutment is tied monolithically with the bridge deck. Thus, in addition to the forces exerted by the soil, the abutment experiences shearing and lateral forces and bending moments produced by the lateral movement and vertical deformation of the bridge deck. The significant differences observed in these two related tests emphasizes the attention to details that must be given in model testing to properly represent the behavior of prototype or full-scale structures.

Numerical prediction of the load-displacement behavior of the bridge-soil system was in fair agreement with the test results. In the future, however, a better model for cohesionless soils, calibrated against the centrifuge test results, should be developed and used to calculate the abutment-backfill stiffness properties for use in the seismic analysis and design of monolithic bridge abutments.

ACKNOWLEDGEMENTS

This study was supported by the National Science Foundation under grant ECE-8316976. The suggestions and assistance from Professor Ronald F. Scott and John Lee of the California Institute of Technology were beneficial during the centrifuge testing. John Lee built and instrumented the model bridge. Their support is gratefully acknowledged.

Appendix I. - REFERENCES

1. Aboim, C. A., and Roth, W. H., "Bounding - Surface Plasticity Theory Applied to Cyclic Loading of Sand," International Symposium on Numerical Models in Geomechanics, Zurich, Switzerland, Sept. 13 - 17, 1982.
2. Bardet, J. P., "Application of Plasticity Theory to Soil Behavior: A New Sand Model," Ph.D. Thesis, California Institute of Technology, 1983.
3. Bucky, P. B., "Use of Models for the Study of Mining Problems," American Institute of Mining and Metallurgical Engineers Tech. Pub. No. 425, 1931, pp. 3-28.
4. Crouse, C. B., Hushmand, B., Liang, G. C., Martin, G., and Wood, J., "Dynamic Response of Bridge-Abutment-Backfill Systems," Proceedings Joint U.S. New Zealand Workshop on Seismic Resistance of Highway Bridges, San Diego, Calif., 1985.
5. Crouse, C. B., Hushmand, B., and Martin, G.R., "Dynamic Soil-Structure Interaction of a Single Span Bridge, submitted to Journal of Earthquake Engineering and Structural Dynamics, 1986.
6. Douglas, B. M., and Reid, W. H., "Dynamic Tests and System Identification of Bridges," Journal of Structural Engineering Division, ASCE, Vol. 108, 1982, pp. 2295-2312.
7. Douglas, B. M., and Richardson, J. A., "Maximum Amplitude Dynamic Tests of a Highway Bridge," Proceedings of Eighth World Conference on Earthquake Engineering, Vol. VI, July, 1984, San Francisco, Calif., pp. 889-896.
8. Hughes, T. J. R., and Prevost, J. H., "DIRT II: A Nonlinear Quasi-Static Finite-Element Analysis Program," California Institute of Technology, 1977.
9. Hushmand, B., "Experimental Studies of Dynamic Response of Foundations," Ph.D. Thesis, California Institute of Technology, 1983.
10. Lade, P. V., "Elasto-Plastic Stress-Strain Theory for Cohesionless Soil with Curved Yield Surfaces," International Journal of Soils and Structures, 1977, Vol. 13, pp. 1019-1035.

11. Nelson, I., and Baron, M. L., "Application of Variable Moduli Models to Soil Behavior," International Journal of Solids and Structures, March, 1970, Vol. 5, pp. 399-417.
12. Ortiz, L. A., Scott, R. F., and Lee, J., "Dynamic Centrifuge Testing of a Cantilever Retaining Wall," Journal of Earthquake Engineering and Structural Dynamics, Vol. 11, 1983, pp. 251-268.
13. Pokrovsky, G. I., and Fyodorov, I. S., "Centrifugal Model Testing in the Construction Industry," (in Russian) Publishing House of Literature for the Construction Industry, Moscow, 1968.
14. Rowe, P. W., "Application of Centrifugal Models to Geotechnical Structures," Proceedings of Symposium on Geotechnical Structures, University of New South Wales, Australia, 1975.
15. Scott, R. F., and Morgan, N. R., "Feasibility and Desirability of Constructing a Very Large Centrifuge for Geotechnical Studies," Report 760-170, California Institute of Technology and Jet Propulsion Laboratory, March, 1977.
16. Scott, R. F., Ting, J. M., and Lee, J., "Comparison of Centrifuge and Full Scale Dynamic Pile Tests," International Conference on Soil Dynamics and Earthquake Engineering, Southampton, UK, July, 1982.
17. Schofield, A. N., "Dynamic and Earthquake Geotechnical Centrifuge Modeling," Proceedings of International Conference on Recent Advances in Geotechnical Engineering and Soil Dynamics, St. Louis, Missouri, 1981, pp. 1-18.
18. Valanis, K. C., and Read, H. E., "A New Endochronic Plasticity Model for Soils," Soil Mechanics - Transient and Cyclic Loads, Edited by G. N. Pande and O. C. Zienkiewicz, John Wiley and Sons, Ltd., 1982, pp. 375-417.
19. Wu, H. C., and Wang, T. P., "Endochronic Theory for the Mechanical Behavior of Cohesionless Soil Under Static Loading," Report G189-80-001, Div. of Materials Engineering, Univ. of Iowa, 1980.

Appendix II. - NOTATION

The following symbols are used in this paper:

g = gravitational acceleration;

H = abutment height;

L = lateral load;

N = scaling factor; or, is the abbreviation for Newtons;

P = lateral soil pressure on abutment;

Y = depth of point on abutment beneath ground surface;

γ = unit weight of prototype soil;

γ_p = unit weight of prototype material;

γ_m = unit weight of model material; and,

ω = rotational speed of centrifuge.

FIGURE CAPTIONS

- FIG. 1. Model of Horsethief Bridge Used in Centrifuge Tests
- FIG. 2. Bridge-Soil Model in Centrifuge Bucket
- FIG. 3. Construction of Bridge-Soil Model: (a) Foundation Soil with Side Slopes; (b) Placement of Bridge Model; (c) Finished Model with Backfill Soil
- FIG. 4. Idealized View of Experimental Arrangement for Quick Release Tests
- FIG. 5. Prototype Force-Displacement Curve of Bridge Deck during Loading Prior to Quick Release Test
- FIG. 6. Fourier Amplitude Spectra of Signals Generated during Quick Release Tests at Prototype Frequency Scales
- FIG. 7. Prototype Pressure Distributions on Abutment before, during, and after Quick Release Test
- FIG. 8. Prototype Time Histories Generated during Earthquake Simulation Test
- FIG. 9. Prototype Pressure Distributions on Abutment before, during, and after Earthquake Simulation Test
- FIG. 10. Comparison of Prototype Force-Displacement Curves
- FIG. 11. Prototype Force-Displacement Curves during Cyclic Load Tests at 87.5 g : (a) Constant Maximum Force; (b) Progressively Increasing Maximum Force
- FIG. 12. Prototype Pressure Distributions on Abutment during Lateral Loading
- FIG. 13. Finite Element Model of Bridge-Soil System
- FIG. 14. Pressure Distribution on Abutment Computed from Finite Element Model Assuming Different Interface Conditions Between: (a) Soil and Bucket; and (b) Abutment and Backfill
- FIG. 15. Pressure Distribution and Deformation Shape of Abutment Computed from Finite Element Model Subjected to Lateral Loads (L)
- FIG. 16. Comparison of Experimental and Predicted Force-Displacement Curves at Model Scale

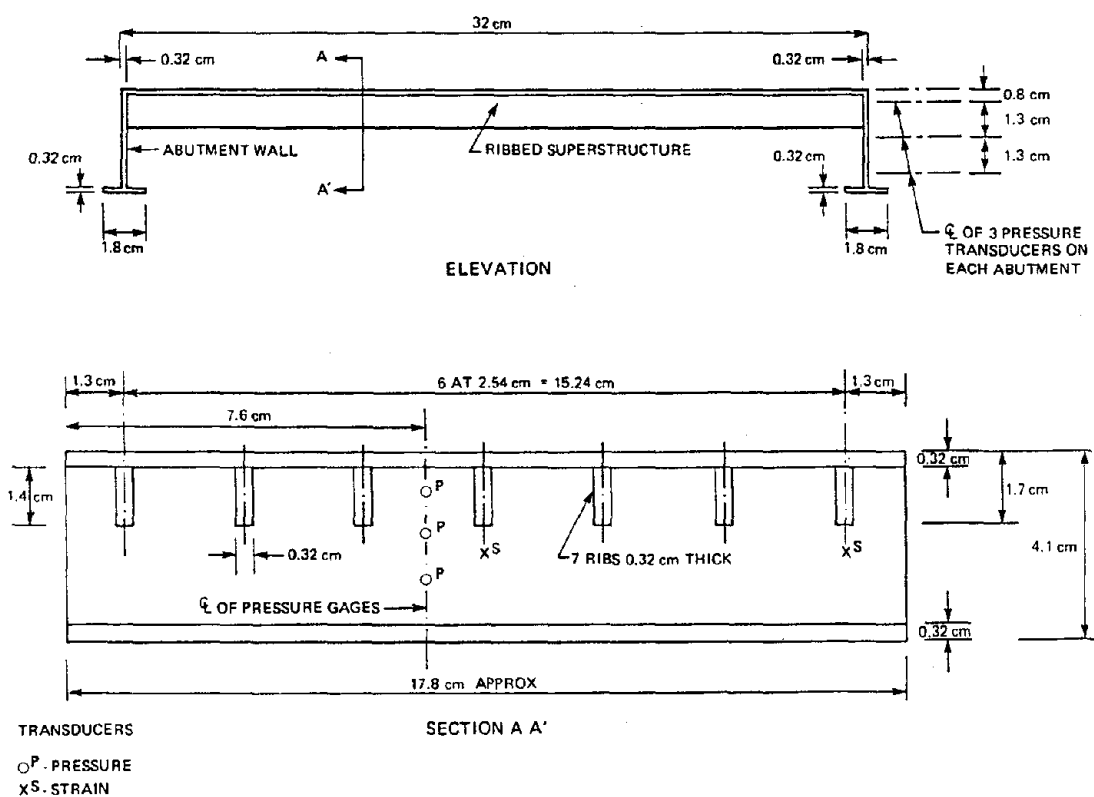
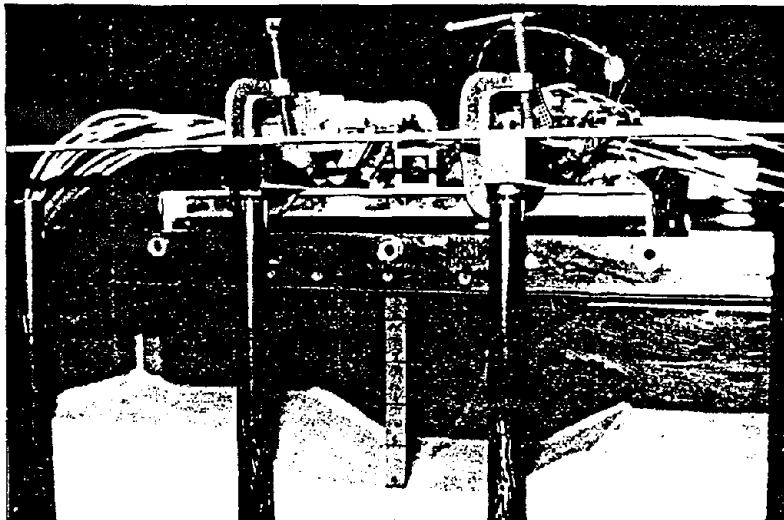


FIG. 1

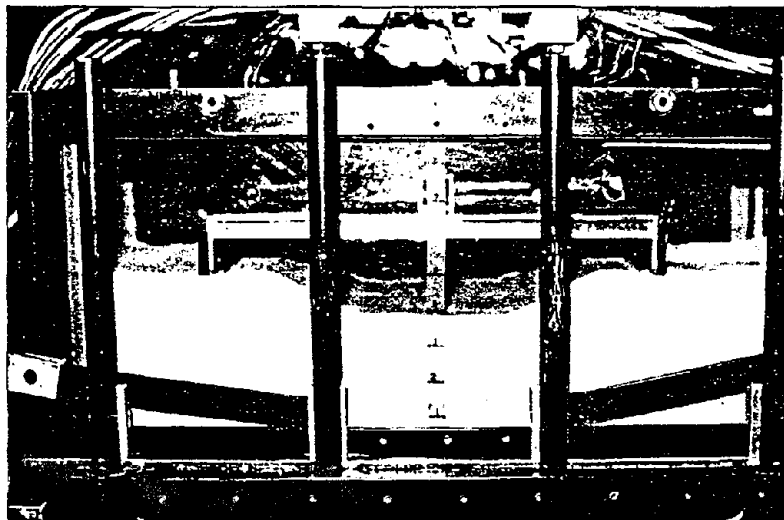
Reproduced from
best available copy.



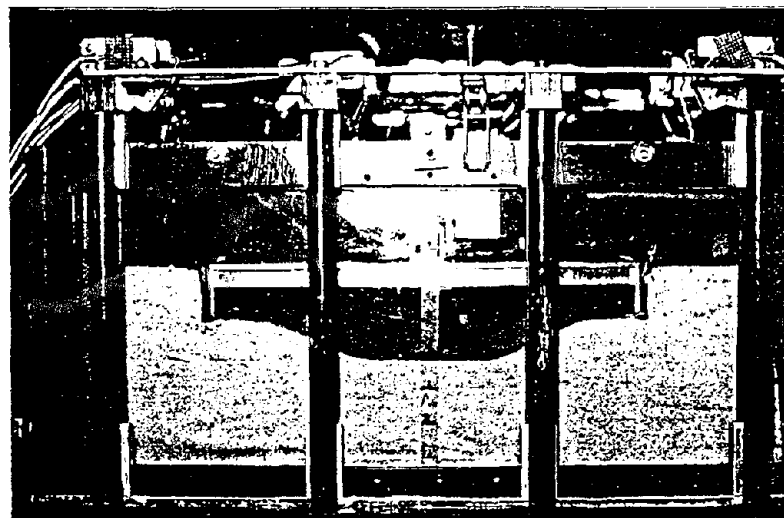
(a)

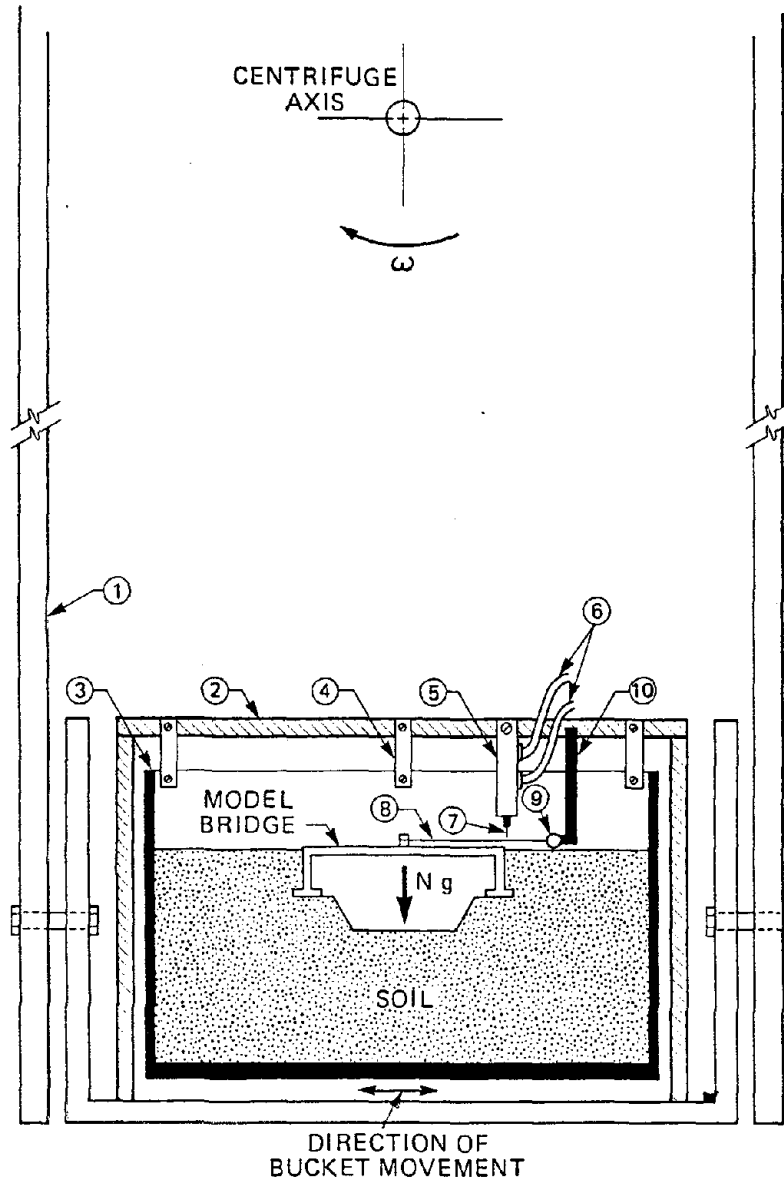


(b)



(c)





- ① CENTRIFUGE ARM
- ② STATIONARY FRAME
- ③ MOVING SUSPENDED CONTAINER
- ④ SUSPENSION RODS
- ⑤ AIR POWERED KNIFE
- ⑥ AIR TUBES
- ⑦ BLADE
- ⑧ NYLON STRING
- ⑨ LOAD CELL
- ⑩ STIFF ROD

FIG. 4

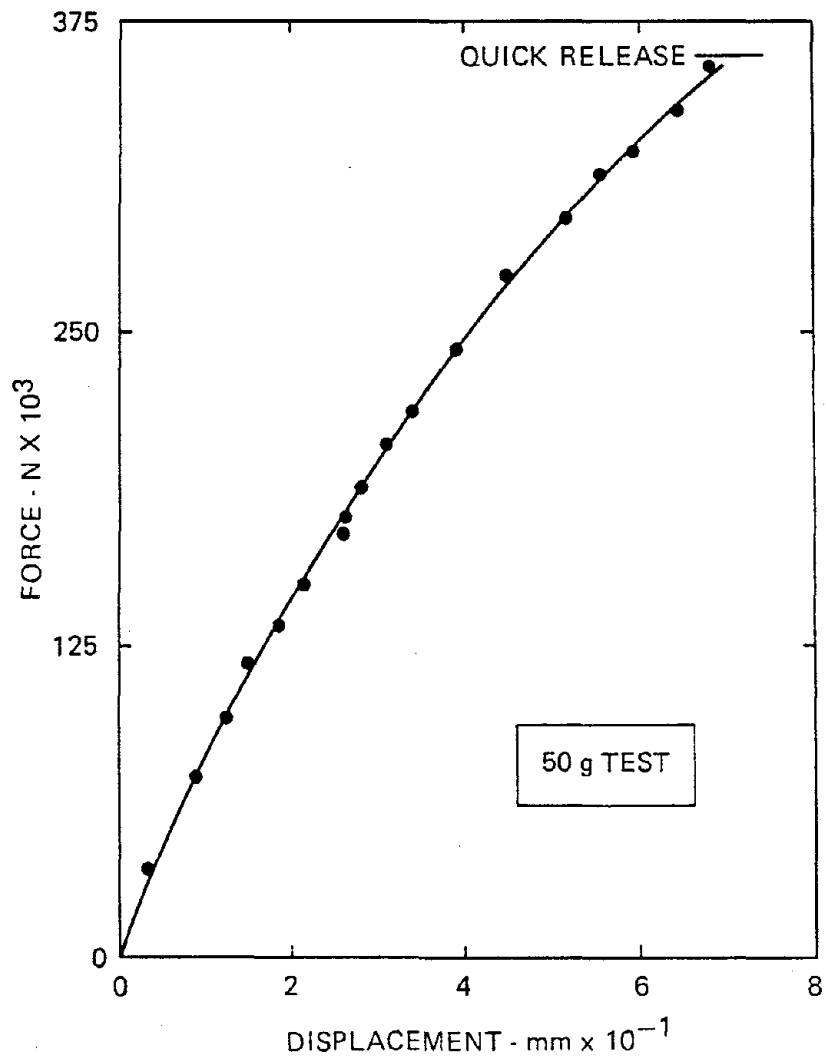
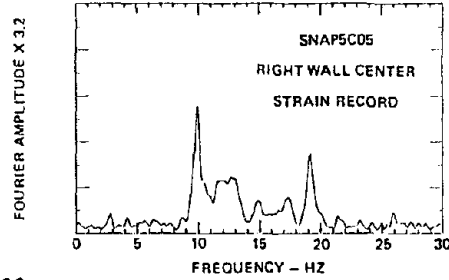
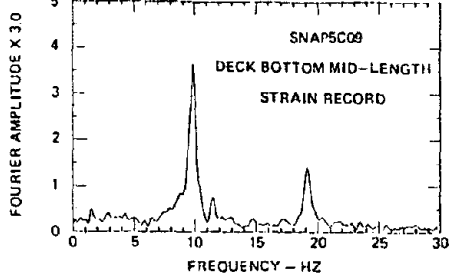
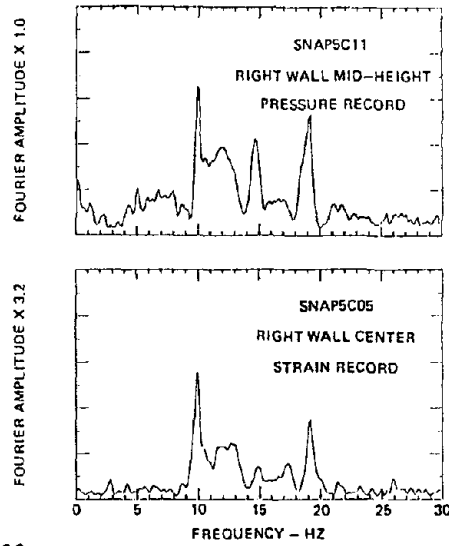
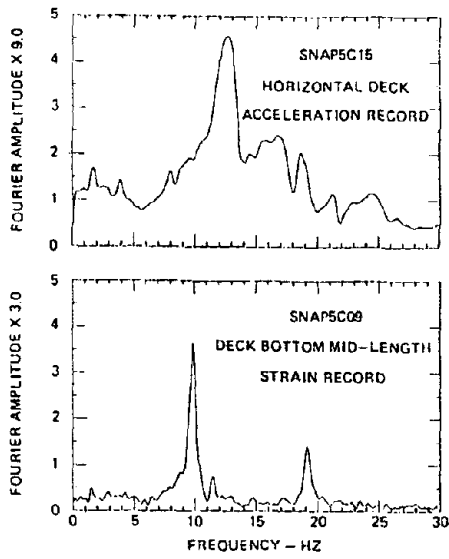
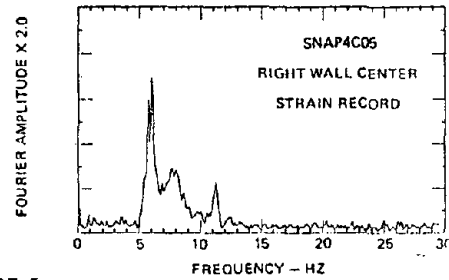
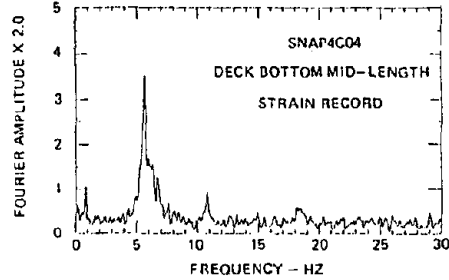
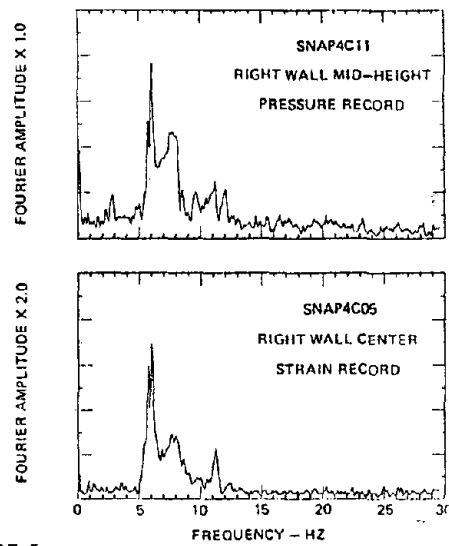
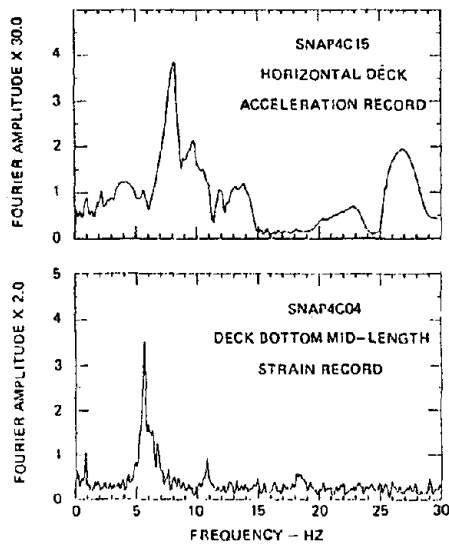


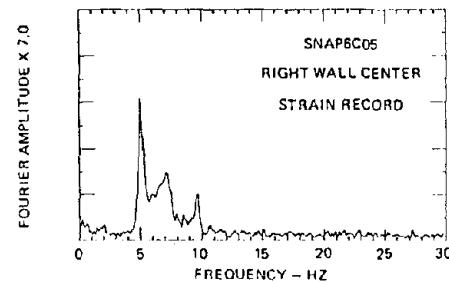
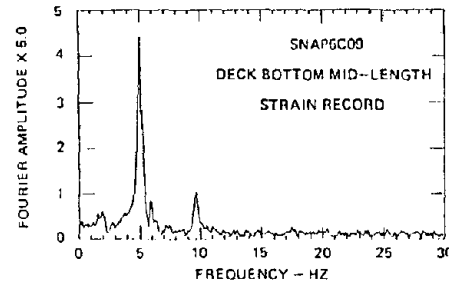
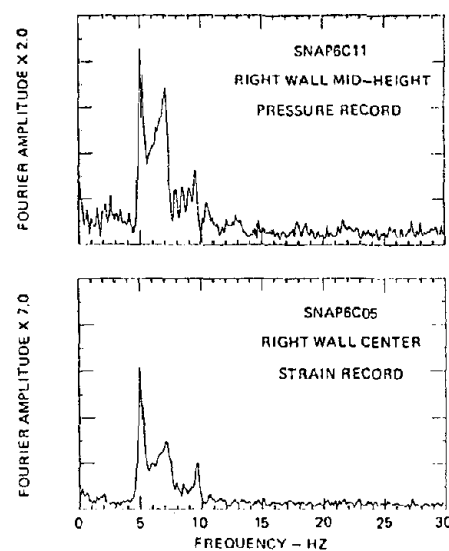
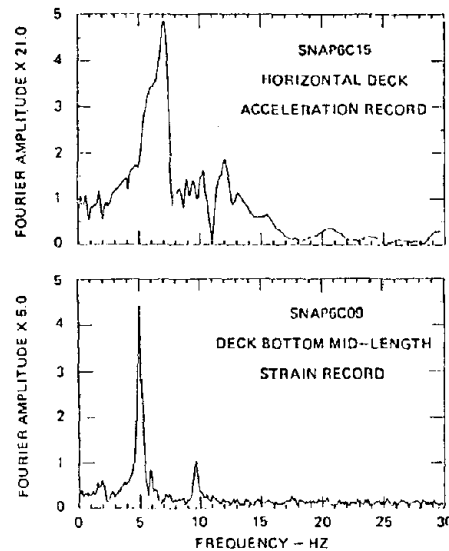
FIG. 5



(a) 50 g



(b) 87.5 g



(c) 100 g

FIG. 6

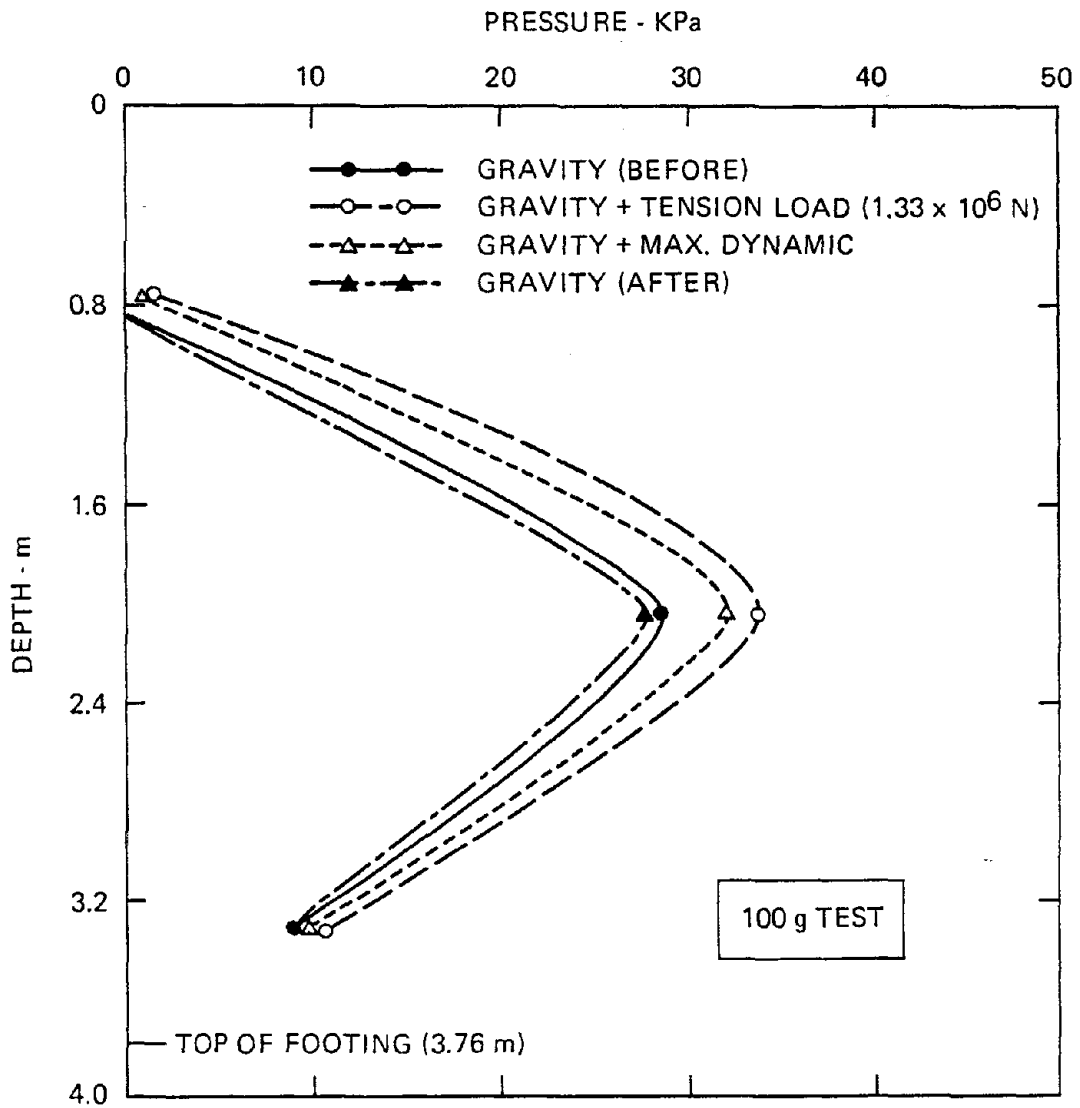


FIG. 7

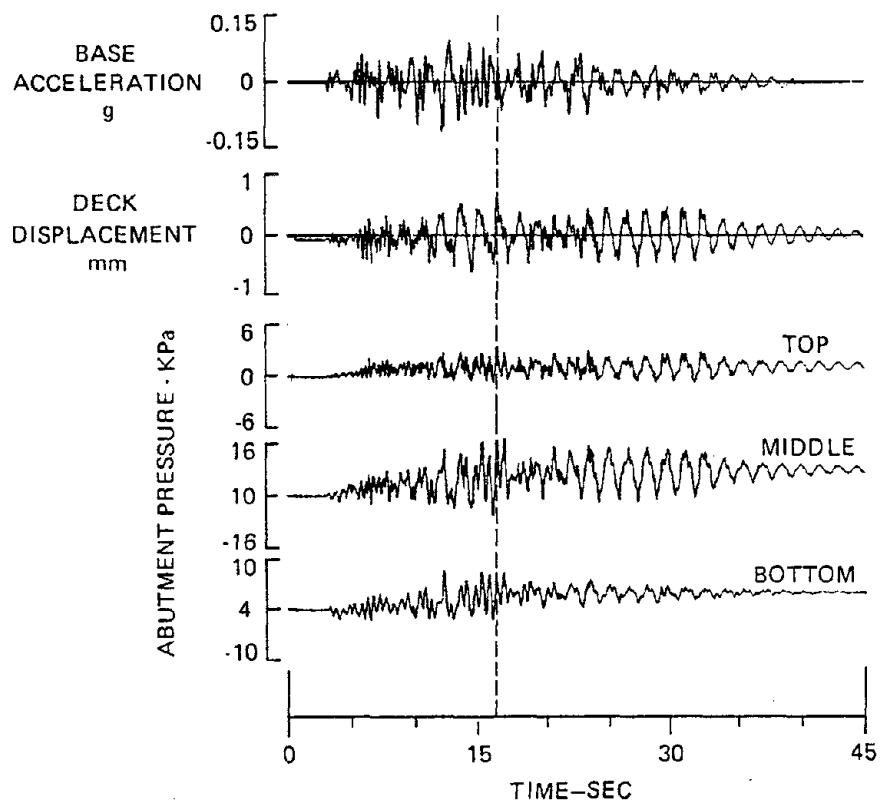


FIG. 8

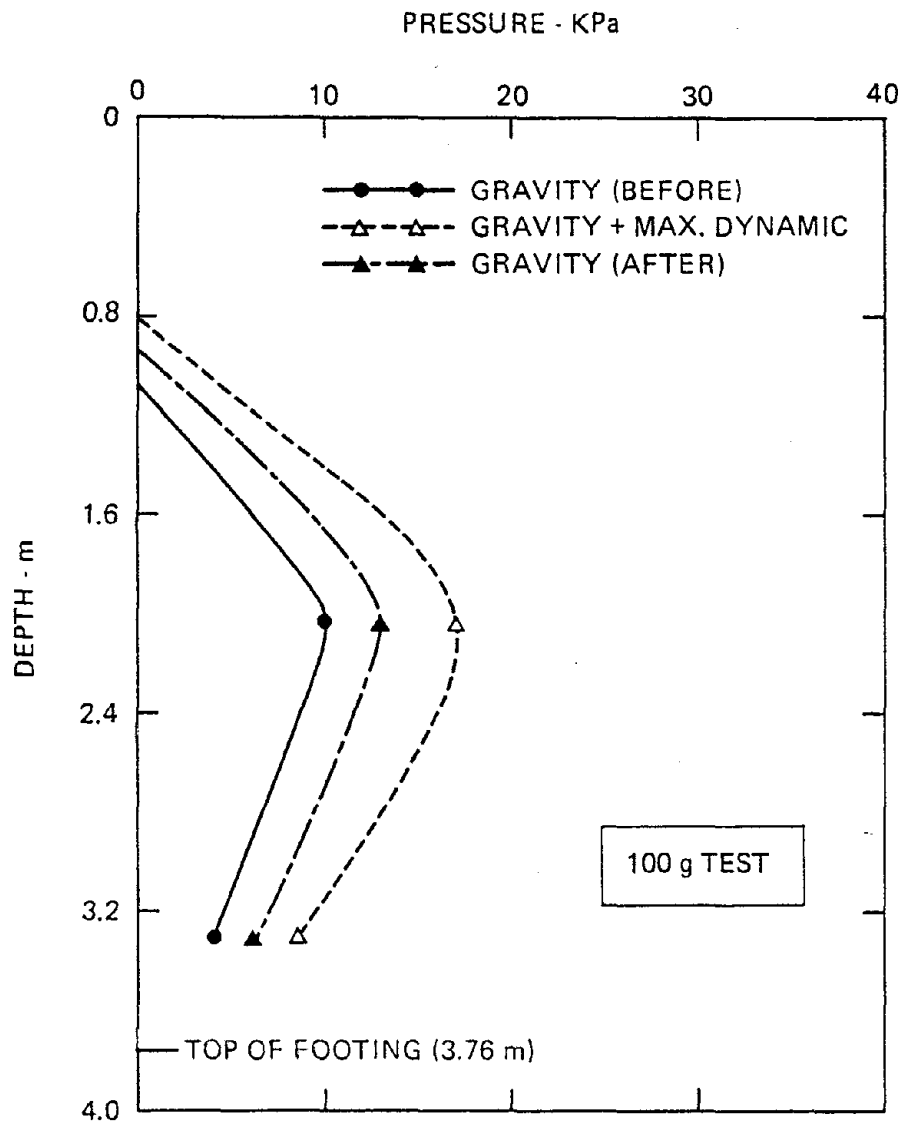


FIG. 9

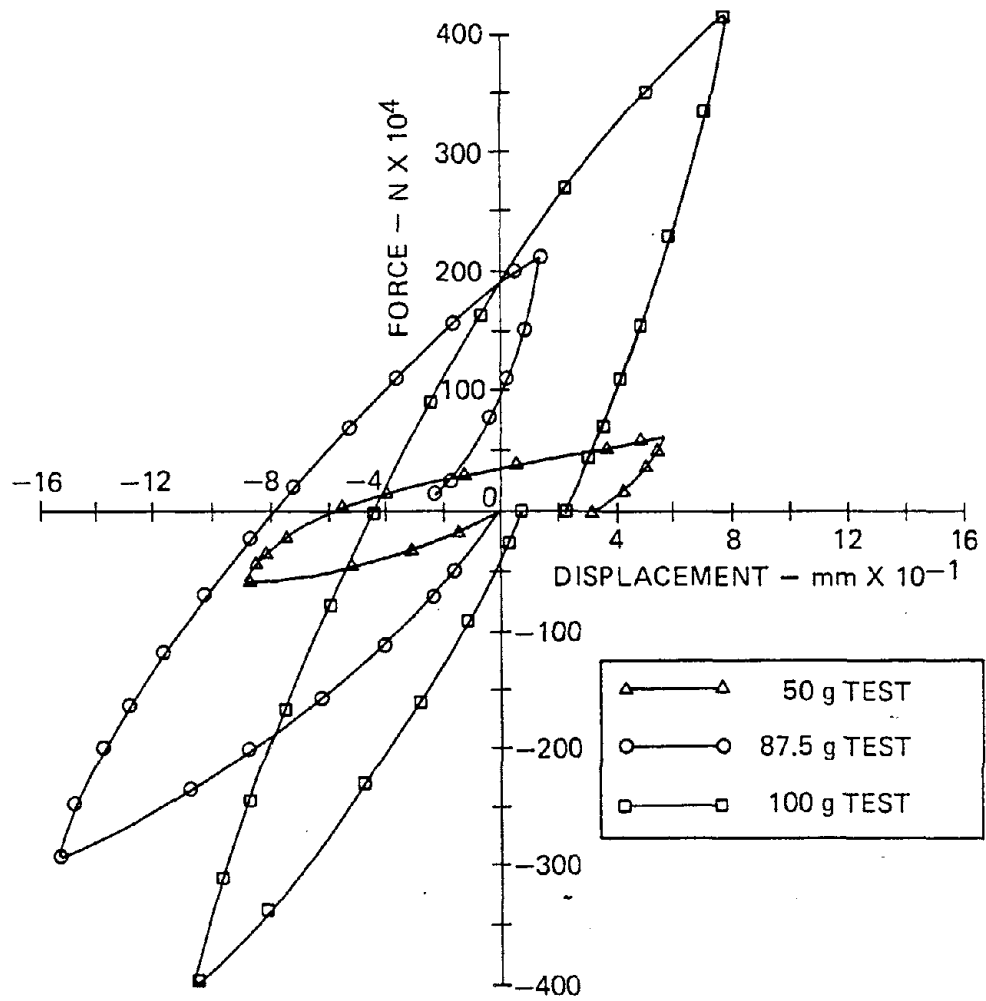


FIG. 10

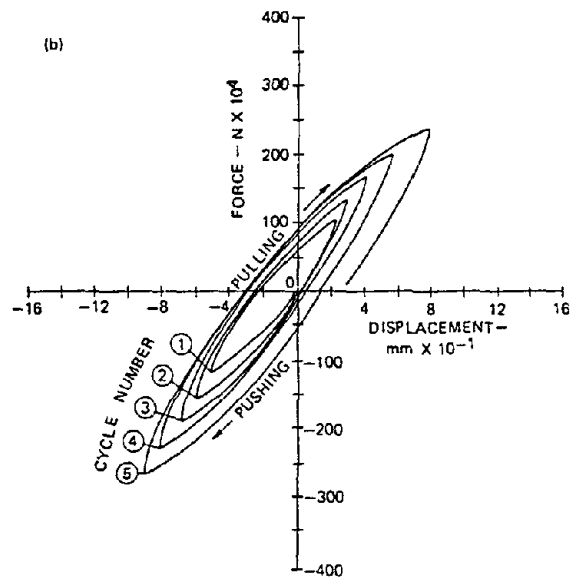
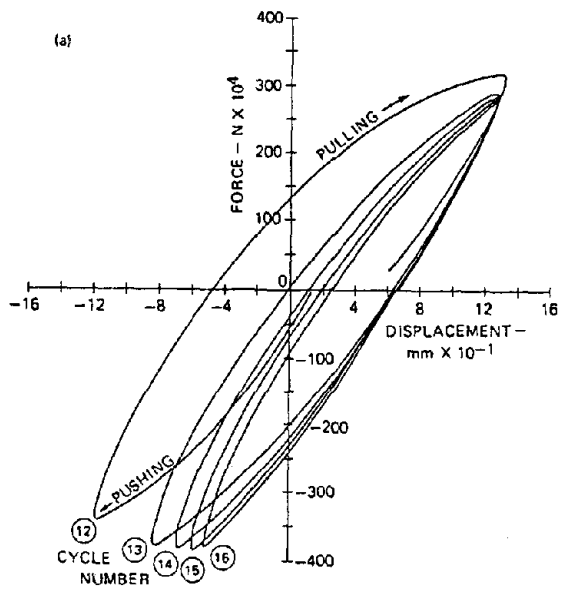


FIG. 11

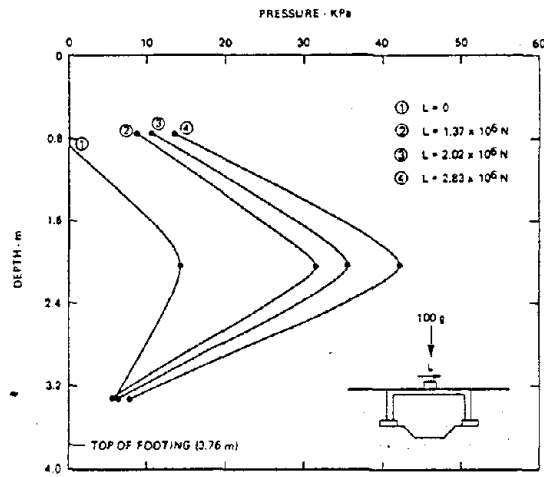
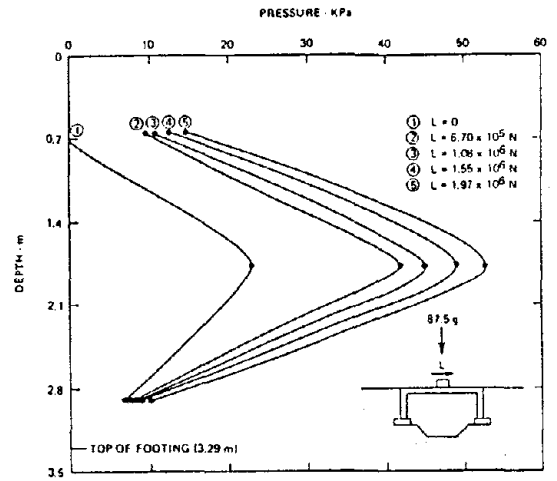
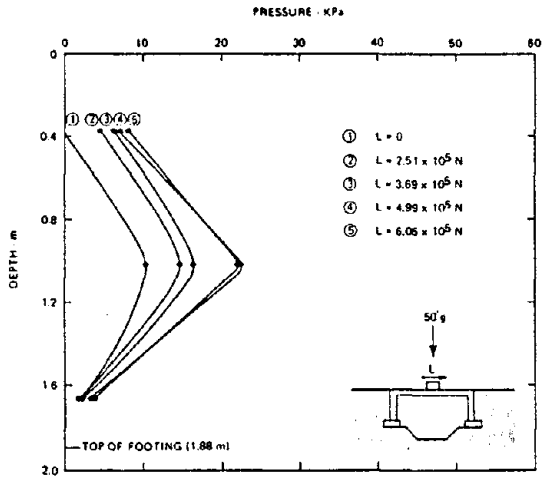


FIG. 12

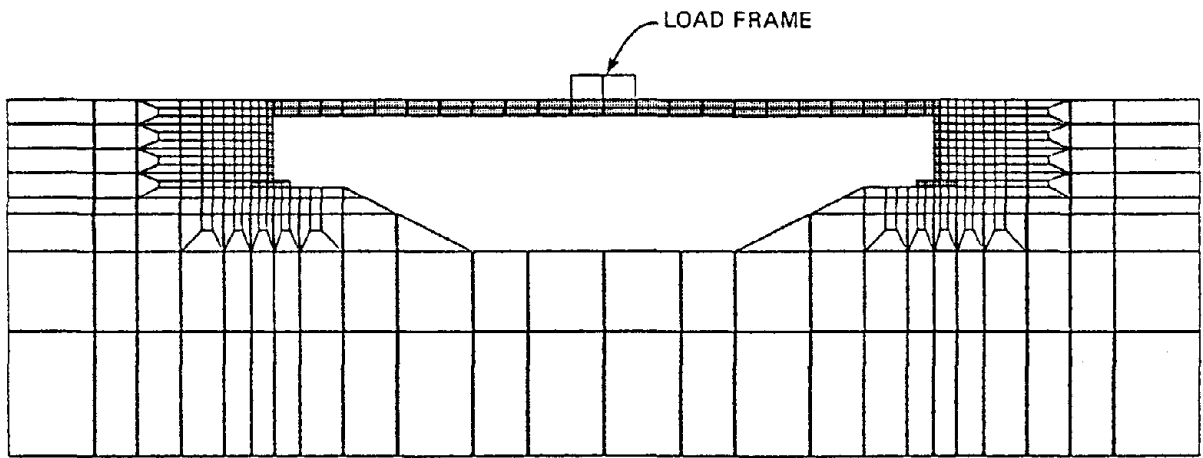


FIG. 13

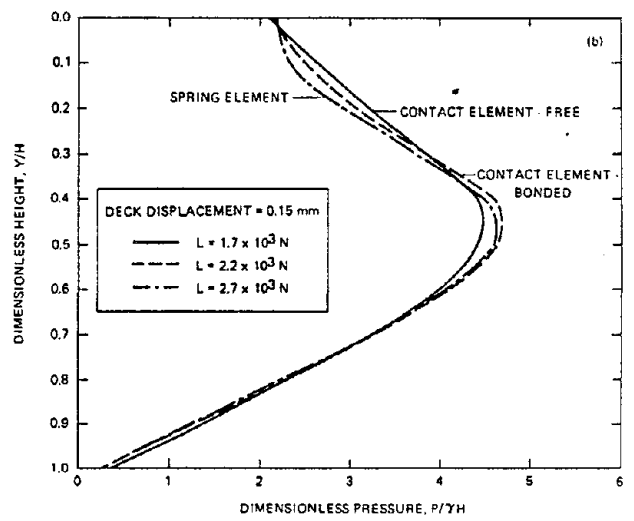
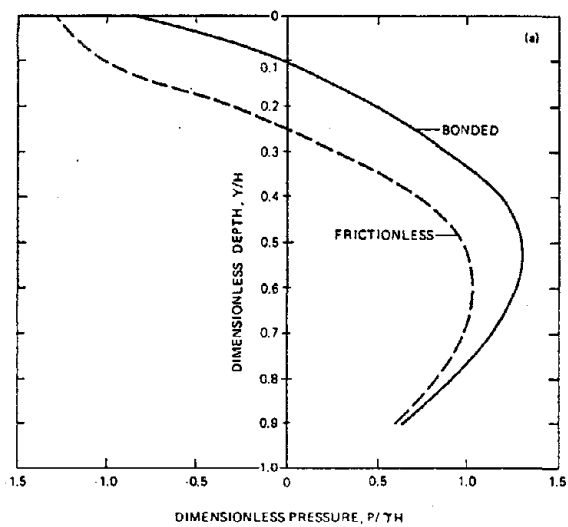


FIG. 14

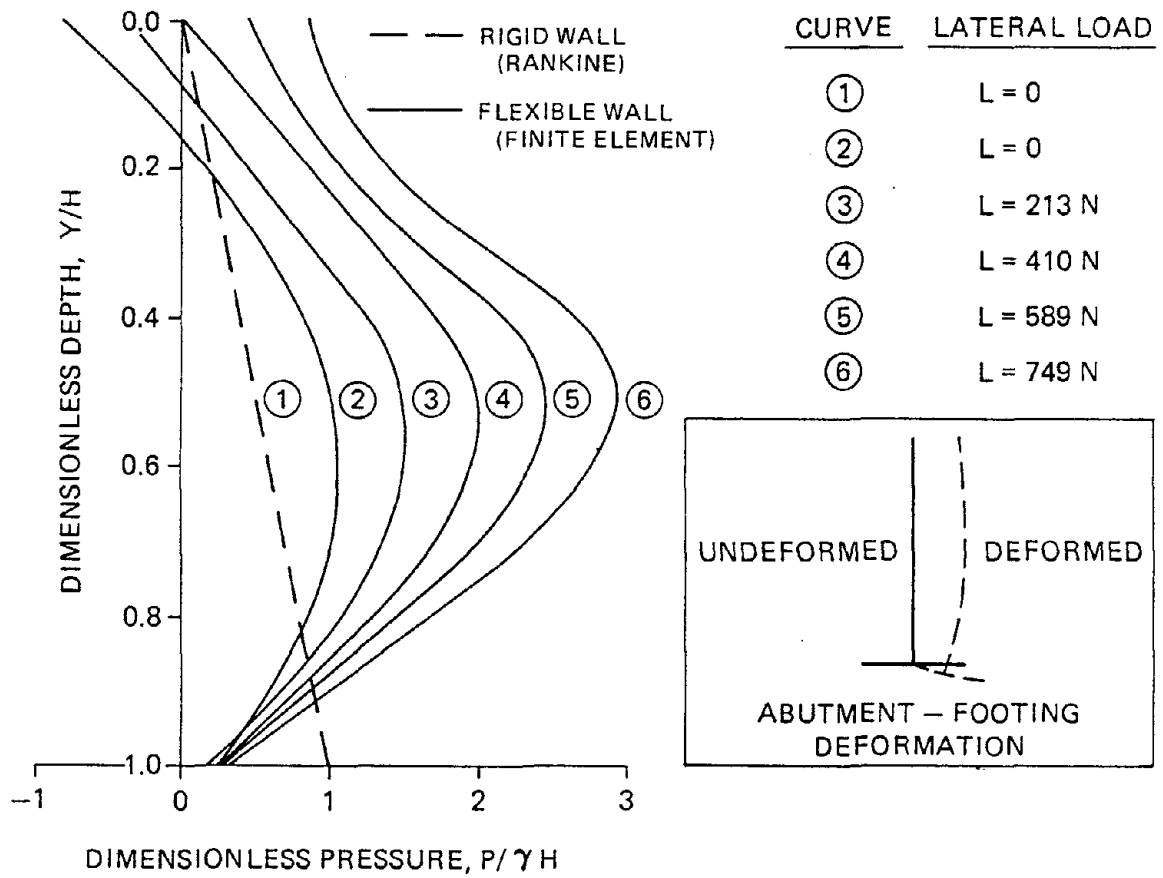
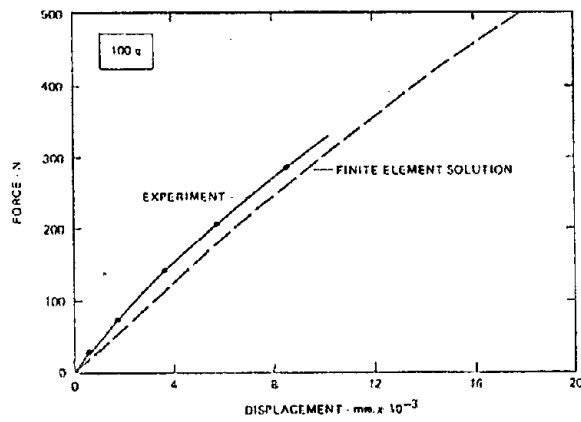
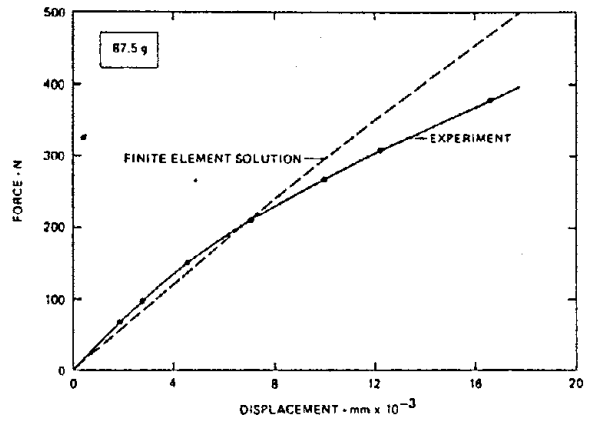
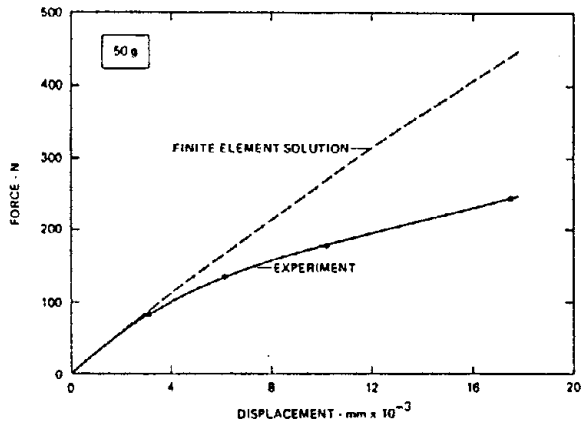


FIG. 15



102
FIG. 16